AUTOMATIC AND ELASTIC REGISTRATION FOR BIOMEDICAL IMAGES

Xiu Ying WANG

A thesis submitted in fulfillment of
the requirements for the degree of
Doctor of Philosophy

The University of Sydney

August 2005

ABSTRACT

With the advances in medical imaging technologies, the diverse imaging modalities are playing an increasingly important role in improving the quality and efficiency of healthcare. Clinical practice often involves collecting and integrating considerable amounts of multimodality medical imaging data over time intervals to improve the optimization and precision of clinical decision and to achieve better, faster, and more cost-effective healthcare. However, how to fully make use of the widely available multimodal images of the human body to provide the connection of structural-anatomical knowledge with functional-physiological knowledge and assist in making image data more usable for clinical training and surgery simulation and planning is an important and challenging issue. Registration of medical images is a significant step in combining the most meaningful information and facilitating the smart use of the embedded information and knowledge.

Accurate and efficient biomedical image registration can lead to additional and complementary information not apparent in the isolated images and provide clinical professionals with the sufficient information for diagnostic and medical decision making. Biomedical image registration is an important technique for presenting relevant clinical information to clinicians at the point of care, and therefore can improve the quality of care, patient safety, and healthcare benefits. Accurate diagnostic and clinical decision making can be achieved after automatic image registration to localize and identify anatomy and lesions. Biomedical image registration also plays an important role in monitoring treatment by allowing comparison of tumor size and location during treatment over time.

Because of its importance and significance in both clinical applications and research, biomedical registration has been extensively studied for decades and great progresses (especially for brain image registration) have been achieved. Intensity-based registration can fully make use of image information and has potential to achieve automatic registration. However, the computational complexity of category of registration is very high. Feature-based registration has advantage of efficient computation, which may require subjective and manual feature selection, and hence may lead to less accurate result.

To address the existing issues in biomedical image registration area, this thesis focuses on the research and exploration of automatic and elastic biomedical image registration with high computation efficiency and accuracy. Several new elastic registration algorithms, including intensity-based registration methods, feature-based registration techniques, hybrid registration, and hierarchical registration, have been investigated and presented in this thesis.

Firstly, an elastic automatic registration method has been proposed to improve registration accuracy with comparable computational efficiency with its corresponding intensity-based initial affine estimation approach.

Secondly, to explore and combine the merits of the intensity-based algorithms and the landmark-based approaches, two hybrid registration methods have been proposed. In these two methods, two different automatic landmark selection methods have been used.

Thirdly, even though the accurate and efficient registration of abdominal images is highly desired in nuclear medicine, research, and clinical practice, abdominal image registration is a more complex and challenging task because of the non-rigid and involuntary motion caused by breath and heartbeat, and elastic deformation of organ structure and volume makes the undertaking even more difficult. In our research, an efficient, automatic, abdominal image registration method is proposed. The proposed approach has been validated by the experiments with PET (Positron Emission

Tomography) and CT (Computed Tomography) abdominal images of both intra-subject and inter-subject, monomodal and multimodal images.

Fourthly, to accelerate registration speed and produce a good registration performance, steerable wavelet based hierarchical registration algorithms using image intensity or coefficient has been explored. Besides, the application of medical image registration methods in bioinformatics has been investigated and the medical image registration method has been extended to protein gel image registration.

Finally, an efficient non-iterative registration based on wavelet has been presented. On the basis of automatically selected affine-invariance features, the proposed method can avoid inherent barrier of fast wavelets' lack of translation- and rotation-invariance, and be able to register images automatically. The computational complexity can be reduced dramatically by directly deriving affine parameters from the mean squared errors (MSE). This innovative method can be able to register images at "real-time", and would be a solution to practical clinical applications.

Keywords: Biomedical imaging, medical image registration, rigid registration, non-rigid registration, intensity similarity measures, feature-based registration, block matching, iterative method, wavelets, active contour

PUBLICATIONS

- **JOURNAL PAPERS AND BOOK CHAPTER**

1. X. Wang, D. Feng, "Automatic Elastic Medical Image Registration Based on Image Intensity", International Journal of Image and Graphic (IJIG), World Scientific, Vol.5, No.2, pp.351-369, April 2005.
2. X. Wang, D. Feng, "Biomedical Image Registration for Diagnostic Decision Making and Treatment Monitoring", Chapter 9 in R. K. Bali (Ed.) "Clinical Knowledge Management: Opportunities and Challenges", pp.159-181, Idea Group Publishing, April 2005.
3. X. WANG, D. FENG, "Active Contour Based Efficient Registration for Biomedical Brain Images", Journal of Cerebral Blood Flow & Metabolism, Vol.25 (Suppl), pS623, 2005.
4. X. Wang, D. Feng, "An efficient wavelet-based biomedical registration for abdominal images", Journal of Nuclear Medicine, Vol.46, P161p, 2005.
5. X. Wang, Y. Zhou, H. Hong "Automatic Mono-modality Medical Image Registration", Journal of Natural Science of Heilongjiang University, Vol.21, No.1, pp55-57, 2004.
6. X. Wang Y. Zhou, H. Hong, "Elastic Registration Algorithm for 2-D Medical Images", Journal of Jilin University, Vol.21 pp.73-80, 2003.

- **CONFERENCE PAPERS**

7. X. Wang, D. Feng, and J. Jin, "Elastic Medical Image Registration Based on Image Intensity", Proc. Visual Information Processing Workshop (VIP2001), Vol.11, pp.139-142. Sydney Australia, 5 Dec 2001.

8. X. Wang, D. Feng, "Two-step Elastic Medical Image Registration Based on Image Intensity", Proc. 2nd International Conference on Image and Graphics (ICIG 2002), SPIE Vol.4875, pp.458-463. Hefei, China, 16-18 August 2002.

9. X. Wang, D. Feng, H. Hong, "Novel Elastic Registration for 2-D Medical and Gel Protein Images", Australian Computer Science Communications, Vol. 25, No. 4, Conferences in Research and Practice in Information Technology, Vol.19, and Proceedings of the 1st Asia-Pacific Bioinformatics Conference (APBC2003), pp. 223-226, 4-7 Feb 2003, Adelaide, Australia.

10. X. Wang, D. Feng, H. Hong, and Z. R. Chi, "Novel Automatic Registration for Medical Image", the 5th IFAC Symposium on Modeling and Control in Biomedical Systems (IFAC2003), pp.99-103, Melbourne, Australia, 21-23 August 2003.

11. Xiuying Wang, Dagan David Feng: Hierarchical elastic registration of human brain images based on wavelet decomposition. 2004 International Symposium on Intelligent Multimedia, Video and Speech Processing, IEEE, Kenneth K. M. Lam, pp 731-734. 2004. ISBN 0-7803-8687-6.

12. Wai Law, Dagan David Feng, Koon Pong Wong, Xiuying Wang: An automated elastic image registration method for CT and MR brain images. 2004 International

Symposium on Intelligent Multimedia, Video and Speech Processing, IEEE, Kenneth K. M. Lam, pp 350-353. 2004. ISBN 0-7803-8687-6.

13. Xiuying Wang, David Dagan Feng: Automatic hybrid registration for 2-dimensional ct abdominal images. Third International Conference on Image and Graphics, IEEE Computer Society, David Zhang, pp 208-211. 2004. ISBN 0-7695-2244-0.

14. Xiuying Wang, David Dagan Feng: Hybrid registration for two-dimensional gel protein images. Third Asia-Pacific Bioinformatics Conference, Imperial College Press, Yi-Ping Phoebe Chen and Limsoon Wong, I, pp 201-210. 2005. ISBN 1-86094-477-9.

15. H.T. Su, D. Feng, X.Y. Wang, "Face Recognition Using Hybrid Feature", Proc. International Conference on Machine Learning and Cybernetics, (ICMLC2003), pp. 3045-3049, Xi'an, China, Nov2-5, 2003.

16. H. Su, D. Feng, R. Zhao, and X. Wang, "Face recognition Method Using Mutual Information and Hybrid Feature", 5th International Conference on Computational Intelligence and Multimedia Applications (ICCIMA03), pp.436-440, Xi'an, China, Sep 27-30, 2003.

17. J. Zheng, D. Feng, W. Sui, Y. Zhang, X. Wang, "The Accurate Extraction & Tracking of Moving Objects for Video Surveillance", Proc. International Conference on Machine Learning and Cybernetics, IEEE 2002, Vol.4, pp. 1909-1913.

ACKNOWLEDGEMENTS

Firstly, I would like to express my deep appreciation for my supervisor, Professor David Feng, for his professional and inspiring supervision. His broad knowledge, affluent research experience, and brilliant research insights into the future ICT developments and trends give my research a very helpful guidance. Furthermore, his academic integrity and excellence set a role model for his students, from which, I will be benefited for my future career development.

Besides, I am grateful to Dr. Tom Cai for his helps and supports in my research and work during my thesis preparation. Thanks to Ms. Cherry Ballangan, Ms. Law Wai, and Dr. Kong Pong Wong for their collaboration and contribution. Appreciations to School of Information Technologies for the supports and research facilities, and thanks to Royal Prince Alfred Hospital and Hong Kong Sanatorium & Hospital for the courtesy of data source. Many thanks to the colleagues in Biomedical and Multimedia Information Technology (BMIT) research group for providing a very pleasant and stimulating research environment.

Finally, I appreciate my mother for her support. I also would like to thank my husband for his understanding and encouragement.

LIST OF FIGURES

LIST OF TABLES

CONTENT

CHAPTER 1 INTRODUCTION

To improve the optimization and precision of clinical decision and to achieve better, faster, and more cost-effective healthcare, a considerable amount of multimodality medical imaging data over time intervals need to be collected and analyzed in clinical practice. Information from multiple medical imaging modalities is usually of a complementary nature, for example, anatomical modalities, mainly depicting morphology, while functional modalities, primarily revealing information on the biochemistry of the underlying anatomy. Therefore, how to fully make use of the widely available multimodal medical images to provide an effective mechanism to integrate the relevant information and knowledge in clinical diagnosis, operation planning, and image guided surgery is an essential issue. Registration of medical images is a significant step in extracting and facilitating the smart use of the most meaningful embedded information and knowledge. Biomedical image registration can assist observation of the changes of anatomical structures and pathological tissues, and provide correlations between the function and morphology of human body.

Because of its critical role in both research and clinical practice, biomedical image registration has been studied extensively for decades and numerous registration algorithms have been proposed. Monomodality image registration is essential for follow-up treatment and disease monitoring, while multimodality image registration provides complementary and additional information for early detection of disease, clinical decision-making, surgical planning, and treatment assessment. Rigid registration is often used to correct translation and rotation displacement, but it is not sufficient for correcting the complex, non-linear distortions, which may result from such factors as differences between the imaging modalities, the temporal displacements due to disease progression and surgical intervention, and individual variations. Non-rigid biomedical image registration remains an active and challenging area for both brain and other deformable organs.

Although the more advanced imaging system, the PET scanner containing a CT scanner, has been developed, with ever-increasing growth of medical datasets with higher resolution, higher dimensionality, and wider range of scanned areas, the demand for automatic registration approaches with both high precision, computational efficiency, and validity, which can be used in clinical practice, will be increased.

This thesis targets at investigating and developing efficient, accurate, and automatic registration algorithms for biomedical images. The thesis is divided into 10 chapters.

Research background, which mainly covers biomedical imaging techniques and major applications of biomedical image registration, is given in chapter 2.

Biomedical image registration fundamentals, implementation issues, and major registration methodologies have been reviewed in chapter 3. Besides, the main problems related to the existing registration approaches and the corresponding possible solutions have been presented in this chapter.

On the basis of raw image intensity, a two-step elastic registration method of high registration accuracy and efficiency has been proposed in chapter 4.

To correct both rigid and elastic deformations across medical images, two automatic hybrid registration algorithms, which are able to properly combine the intensity-based algorithms with automatic landmark-based methods, have been presented in chapter 5.

Abdominal image registration is a more challenging and complex issue than brain image registration. An efficient and automatic registration method has been described to correct non-rigid deformations in chapter 6.

Hierarchical image registration has the properties of both computational efficiency and accuracy, and is a possible solution to clinical applications. One main concern in this kind of registration is how to build a proper registration pyramid. Due to their capability of distinguishing image data into different frequencies and preserving information at multiple resolutions, Wavelet techniques are an optimal option for constructing registration pyramids and have been introduced in chapter 7.

In chapter 8, steerable wavelet based multiresoltion registration method has been explored by using the image intensity (or coefficient) information. However, this intensity/coefficient based method can only register affine distortions, and to correct more complex displacements, further refinement is needed on the basis of feature-based methods. The proposed hybrid and hierarchical medical image registration method has been extended to bioinformatics area to register gel-protein images.

MultiResolution Analysis (MRA) technique provides a solution to fast discrete wavelet transformations, however, fast wavelets lack of translation- and rotation-invariance, which is the basic requirement in image registration. The lack of affine-invariance obviously blocks wavelets' applications in medical image registration area. To make use of the merits of wavelets and at same time to avoid their inherent obstacle, a feature-based automatic registration has been proposed in chapter 9. Instead of using traditional time-consuming optimization algorithms, this method provides a very efficient registration scheme by deriving transformation parameters directly from the mean squared error (MSE).

Finally, conclusion, a few of future research perspectives, and our future work concerns are included in chapter 10.

CHAPTER 2 BACKFROUND

2.1 Biomedical Imaging Techniques

In last a few decades, significant progresses have been made in medical imaging technologies. Medical imaging modalities can be divided into two major categories: anatomical modalities and functional modalities. Anatomical modalities, mainly depicting morphology, include X-ray, computed tomography (CT), magnetic resonance imaging (MRI), and ultrasound (US). Functional modalities, primarily describing information on the biochemistry of the underlying anatomy, include single photon emission computed tomography (SPECT), and positron emission tomography (PET).

CT scans measure photon linear attenuation of a tissue relative to water. These scans produce high-resolution anatomic images because of the high contrast between soft tissue and skeletal structures. In radiotherapy, CT scans are essential in supplying an accurate map of radiation-attenuation coefficients so that dose distributions can be calculated. However, in CT scans, it is difficult to localize critical central nervous system (CNS) structures that must be avoided during radiation therapy.

MRI scans acquire highly detailed anatomic information. Magnetic pulse sequences highlight the different amounts of water (hydrogen protons) contained in anatomical structures and fluids. MRI can also provide functional information with the use of paramagnetic tracers to selectively increase contrast and by measuring blood flow and water diffusion.

PET provides metabolic images of functional parameters, such as blood flow and glucose consumption, by measuring the distribution of radioactive tracers. The anatomic information provided by a PET image is inherently limited by its resolution, its dependence on the radioactive tracer used, and the variability of brain activity. This limited anatomic information makes it difficult to find the contours of structures accurately, especially when the size of the structure is close to the resolution of the PET scanner.

SPECT studies also facilitate the calculation of functional parameters by measuring the distribution of radioisotopes. A considerable advantage of SPECT is its ability to use the conventional nuclear medicine camera since these cameras are widely used in conventional nuclear medicine imaging. SPECT, however, provides little anatomic information and its spatial resolution is low.

Nowadays, these diverse imaging modalities are playing a more and more important role in improving the quality and efficiency of healthcare. Medical images facilitate the understanding of anatomy and function, and are critical to improve human life quality. For example, the functional imaging techniques can be used to image physiological and biochemical processes in different organs, such as brain, lung, liver, bone, thyroid, heart and kidney (Figure 2-1). In such clinical settings, PET aids clinicians in choosing the most appropriate treatment and monitoring the patients' response to these therapies.

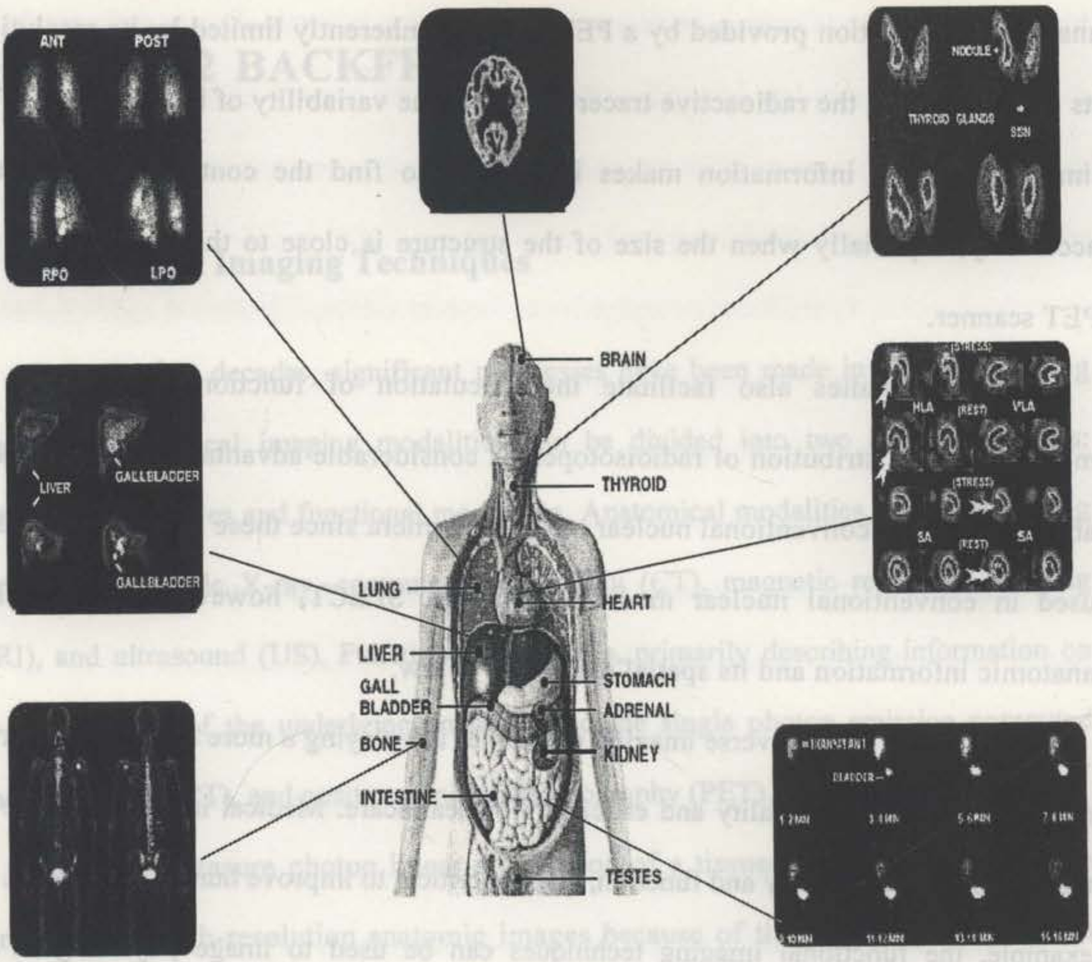

Figure 2-1 Positron Emission Tomography (PET)

(Courtesy of Hong Kong Sanatorium & Hospital)

2.2 Applications of Biomedical Image Registration

Since image data from multiple medical imaging sources reflect information from different aspects, proper extraction and registration of the embedded information and knowledge is essential in the healthcare decision making process and in clinical practice. The combination of more advanced and user-friendly medical image databases is making medical imaging results more accessible to clinical professionals. However, how to fully make use of the widely available multimodal images of the human body to provide the connection of structural-anatomical knowledge with functional-physiological knowledge and assist in making image data more usable for clinical training and surgery simulation and planning is an important and challenging issue. Registration of medical images aims to solve this problem and is a significant step in extracting the most meaningful information to facilitate the smart use of this information.

Accurate and efficient biomedical image registration can lead to additional clinical information not available in the isolated images and provide clinical professionals with the sufficient information for diagnostic and medical decision making. For example, through the proper registration of functional information provided in PET with anatomical background of CT scanning, physiological functional regions can be located more precisely (Figure 2-2) and surgeon can optimize the operation with minimal damage to the health organs. Such functional-to-anatomical data registration is very useful for clinical diagnosis and surgical operation, especially for telesurgery.

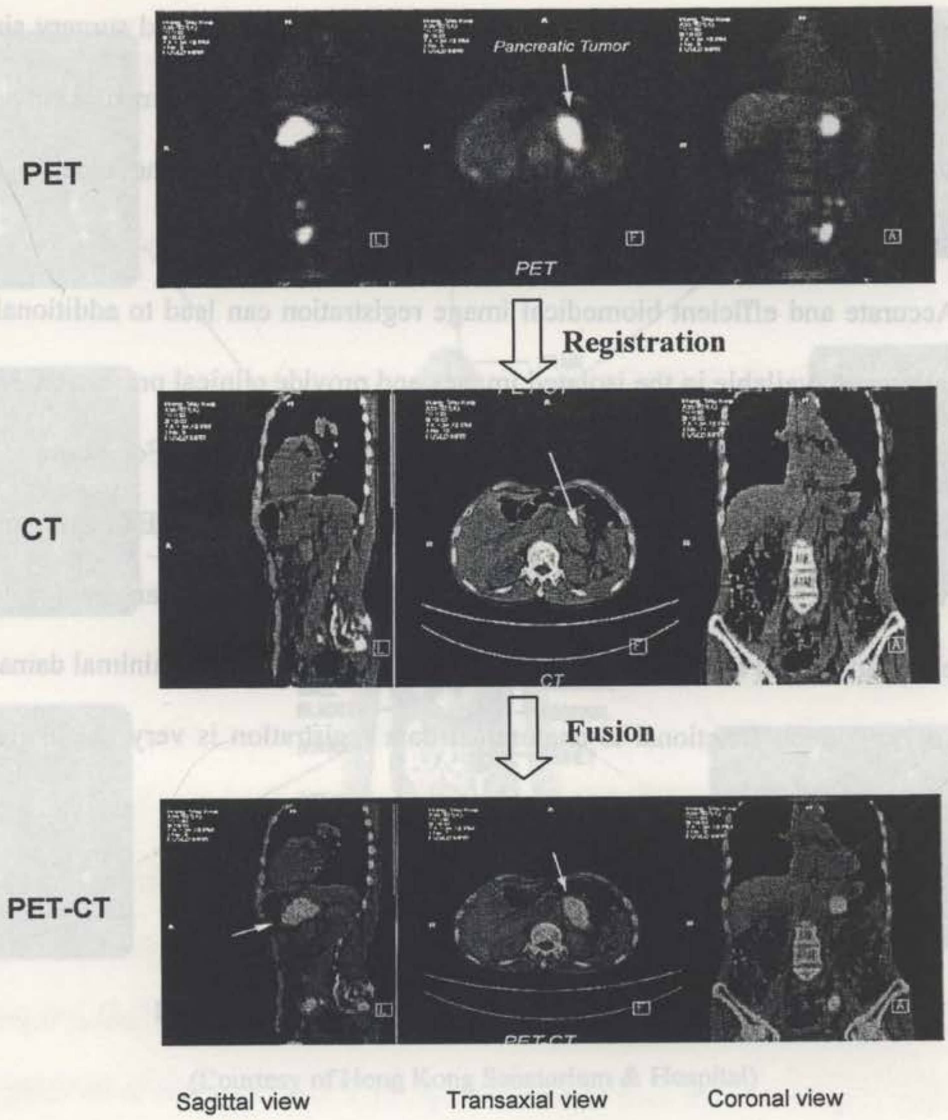

Figure 2-2 Registration of PET Imaging Scan with Anatomic Maps
(Courtesy of Hong Kong Sanatorium & Hospital)

2.2.1 Clinical and Surgical Applications

Biomedical image registration is an important technique for presenting relevant clinical information to clinicians at the point of care, and can improve the quality of care, patient safety, and healthcare benefits. Registration algorithms provide new possibilities for the analysis and visualization of multimodal image datasets. Using these algorithms, image data from multiple imaging modalities can be matched and presented in a common coordinate system, and hence, anatomical and functional image information can be visualized simultaneously. Biomedical image registration assists the observation of the changes of anatomical structures and pathological tissues, and correlations between the function and morphology of human body as well. By using registration techniques, a complete analysis and insight into the patient data over times or across medical imaging modalities can be obtained, and as a result, an improved medical diagnosis and patient treatment can be achieved.

Based on the data sources of medical images to be registered, medical image registration can be divided into monomodality registration and multimodality registration. Both of these two categories of registration are important for clinical research and practice. By quantitative comparison of images taken at different times, monomodality medical image registration provides an essential mechanism for clinical evaluation of disease progress, treatment assessment, and detection of anatomical or functional changes. By combining the complementary information from different imaging techniques, multimodality medical image registration is important to minimally invasive procedures, image guided neurosurgery planning, and radiotherapy treatment planning, e.g., [WON 1995] and [HAJ 1995]. Multimodal image registration methods play a central role in therapeutic systems, e.g., [HIL 1998], [ROS 1998], [HIL 2000], and [LEE 2003]. For example, the registration of functional images with anatomical images helps early diagnosis and better localization of pathological areas.

Applications of biomedical image registration include radiation therapy, interventional radiology, diagnostic and clinical decision making, image-guided surgery, procedure planning and simulation, treatment and disease progression monitoring, and minimally invasive procedures. Besides, image registration is widely used in biomedical imaging, which includes methods developed for automated image labeling and pathology detection in individuals and groups. Registration algorithms can reveal patterns of anatomic variability in human populations, and can be used to create disease-specific, population-based atlases.

Many surgical procedures require highly precise 3D localization to extract deeply buried targeted tissue while minimizing collateral damage to adjacent structures [GRI 1995]. Image-guided surgery (Figure 2-3) emerged to meet this end. In surgical practice, surgeons usually examine 2-D anatomical images (MRI or CT) and then mentally transfer the information to the patient. Thus, there is a clear need for registration technique which can assist the surgeons to directly visualize important structures to guide the surgical procedure.

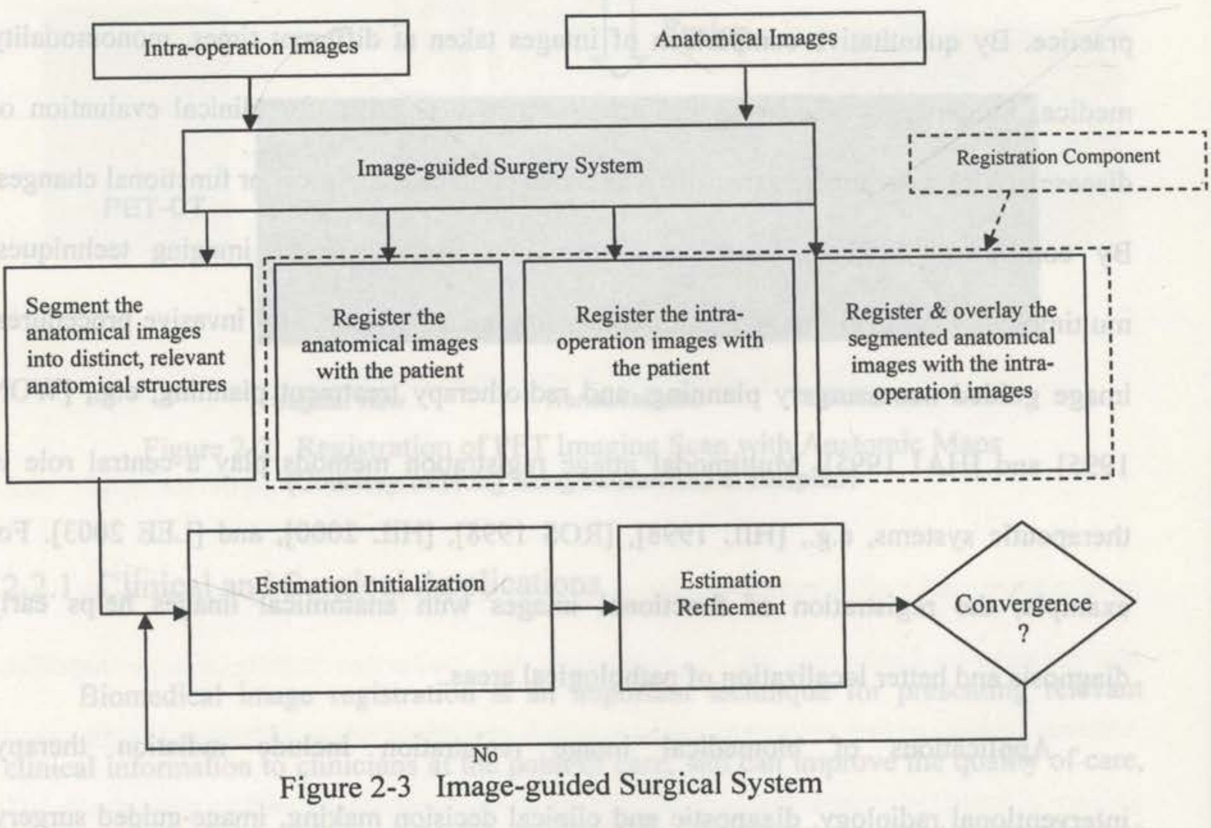

Figure 2-3 Image-guided Surgical System

Biomedical image registration is important for telemedicine, which is the integration of telecommunication technologies, information technologies, human-machine interface technologies, and medical care technologies, when distance separates the participants. For example, biomedical image registration is an important component in teleradiology, which is a primary image-related application. In the case of health care, a telemedicine system should be able to register multiple sources of patient data, diagnostic images, and integrate other information to enhance health care delivery across space and time.

2.2.2 Biomedical Registration for Different Organs

Medical image registration has been applied to the diagnosis of breast cancer, cardiac studies, wrist and other injuries, and different neurological disorders including brain tumors.

2.2.2.1 Brain Image Registration

Brain image registration is the most intensively studied subject in the biomedical image registration field. Numerous rigid and non-rigid registration algorithms for monomodal and multimodal images have been proposed. Feature-based biomedical image registration includes, for examples, crest-line-based registration ([GUÉ 1992]; [GUÉ 1993]; [AYA 1993]; [THI 1996] etc), chamfer-matching-based registration ([Van 1994]; [XIA 1995]), head-hat surface matching technique ([PEL 1989]), and iterative closest point (ICP) algorithm ([BES 1992]). Intensity-based head image registration algorithms include: minimization of variation ratios ([WOO 1993]; [HIL 1993]), correlation-based registration ([COL 1994]), and mutual information registration ([COL 1995]) etc. Figure 2-4 summarizes some main methodologies of brain medical image registration.

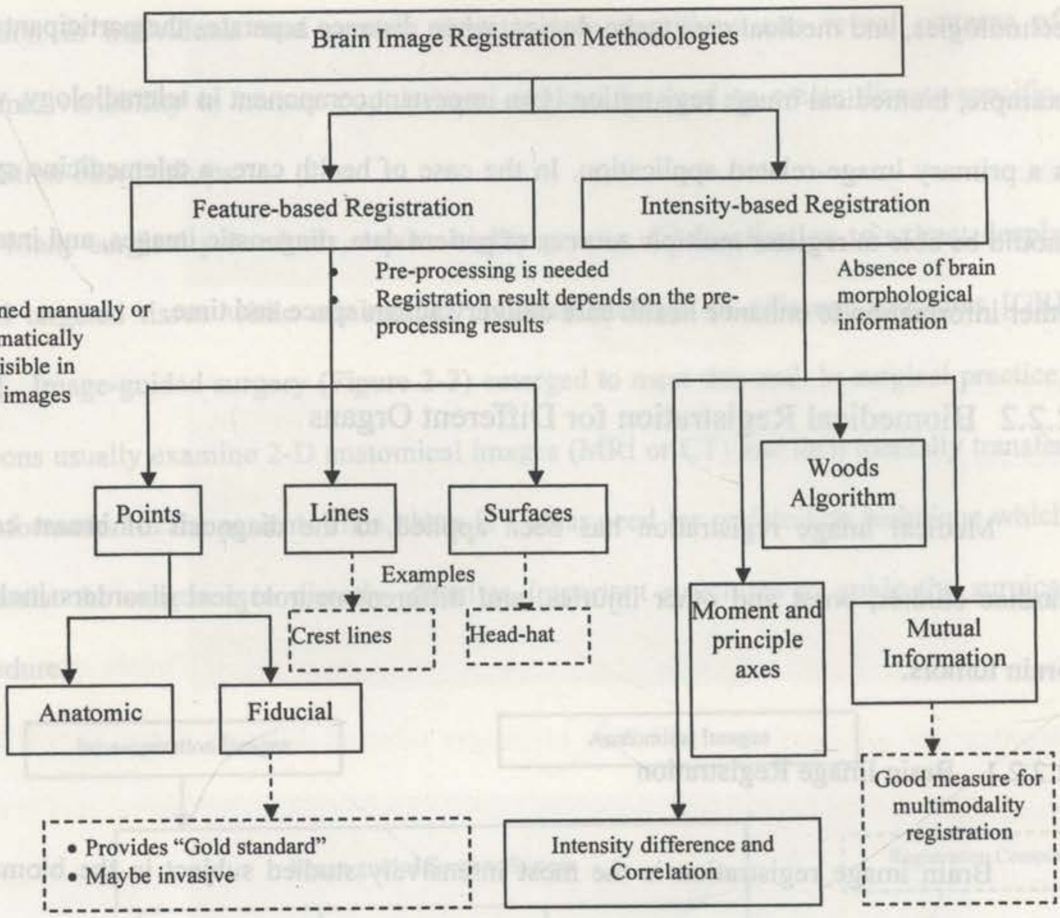

Figure 2-4 Brain Image Registration Techniques

2.2.2.2 Cardiac Image Registration

The registration of cardiac images from multiple imaging modalities is a preliminary step to combine anatomic and functional information. The integration of the complementary data provides a more comprehensive analysis of the cardiac functions and pathologies, and additional useful information for physiologic understanding and diagnosis.

Because of The non-rigid and mixed motion of the heart and the thorax structures, the cardiac image registration is more complex than brain image registration. Researchers have proposed numerous registration approaches for cardiac images, e.g., [PAL 1995], [THI 1998], and [DEY 1999], [MCL 2002]. Mäkelä et al. [MÄK 2002] published a good review of cardiac image registration methods. However, cardiac image registration remains a challenge because of a number of problems related to the existing registration methods. For example, point-based registration approaches for the heart are not always accurate because of the lack of accurate anatomical landmark points in the cardiac; using heart surfaces can result in better registration of the region of interest, but the registration result is highly dependent on the surfaces selected and the imaging modalities involved. In intensity-based cardiac image registration, the use of image intensity difference and correlation methods relies on the assumption that pixel values in the registered images are strongly correlated. However, the assumption is usually not true, especially in multimodal registration.

The cardiac image registration methods can be divided into feature-based methods and intensity-based methods (Figure 2-5).

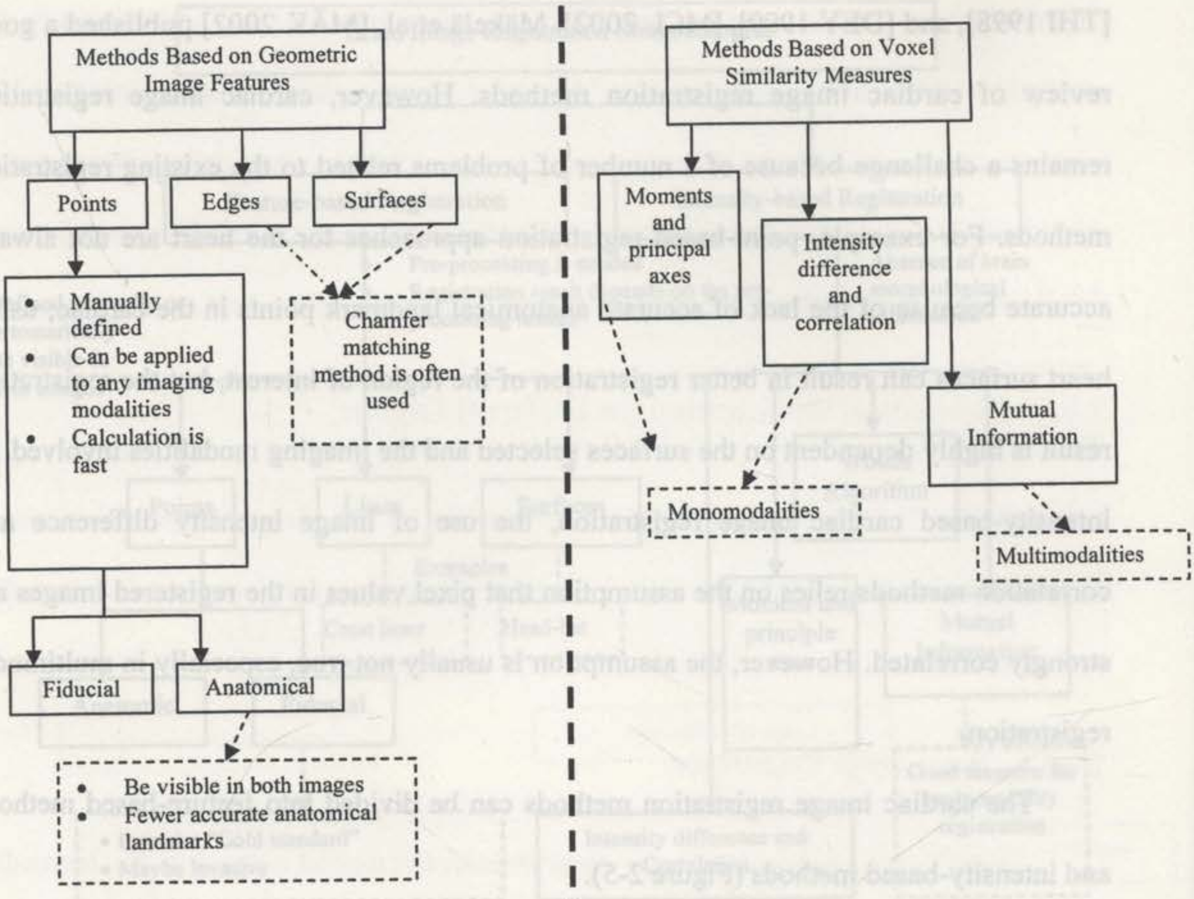

Figure 2-5 Cardiac Image Registration Methods Classification

2.3 Summary

The chapter introduces different biomedical imaging techniques, and biomedical image registration is introduced as a means of integrating and providing complementary and additional information from multiple medical images simultaneously to facilitate diagnostic decision making and treatment monitoring. The registration applications in clinical context, which includes clinical and surgical applications and registration of different organs, are presented.

CHAPTER 3 LITERATURE REVIEW

As a fundamental task in image processing, the process of registration aims to match two data sets that may differ in time of acquisition, imaging sensors, or viewpoints. The problem of registration arises whenever images acquired from different sensors, at different times, or from different subjects need to be combined or compared for analysis or visualization. Biomedical image registration is the primary tool for comparing two or more medical images to discover the differences in the images or to combine information from multimodality medical images to reveal knowledge not accessible from individual images.

3.1 Technological Fundamentals of Biomedical Image Registration

3.1.1 Biomedical Image Registration Definition and Procedure

The main task of medical image registration is to determine a mapping to relate the pixels of one image to the corresponding pixels of a second image with respect to both space and intensity [BRO 1992].

$$I_2 = g(I_1(f(x,y,z))) \qquad \text{Equation 3-1}$$

where: I_2 and I_1 are 3-D images, indexed by (x,y,z); $f:(x,y,z) \rightarrow (x',y',z')$ is a spatial transformation which transfers image I_1 to the coordinate system of image I_2; g is One-dimensional intensity transformation.

Generally, the basic registration procedure can be divided into four steps (Figure 3-1): firstly, the preprocessing step, e.g., used to clean the noise of each individual image to be registered; secondly, the decision of similarity measurement; thirdly, optimization process of registration transformation; finally, correspondence between the image data sets achieved.

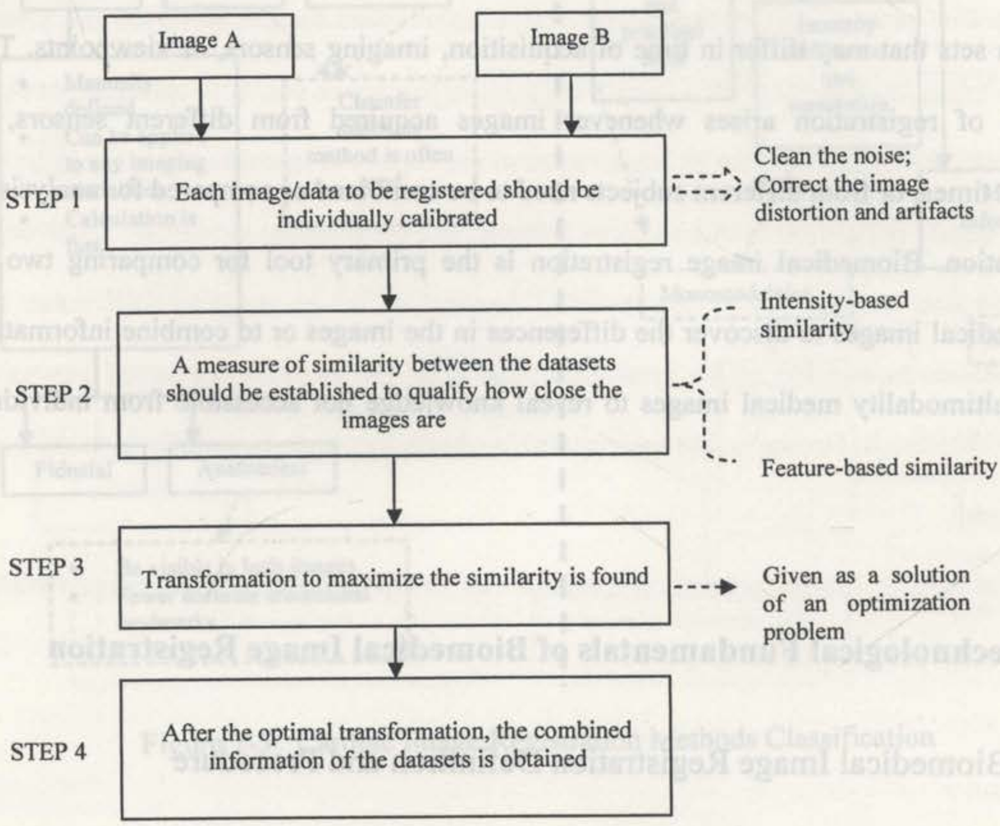

Figure 3-1 Biomedical Image Registration Procedure

3.1.2 Medical Image Distortions and Biomedical Registration Transformations

Biomedical image distortions must be taken into consideration when two sets of medical images are to be registered. There are many factors that can result in medical image distortions, for example, different underlying physics of imaging sensors, inter-subject differences, voluntary and involuntary movements of the subject during imaging. These distortions impose many challenges for biomedical image registration because image characteristics and distortions determine the registration transformations. For more details on medical imaging deformation characteristics and registration transformations, please refer to [BAN 2000], [FIT 2000], [TUR 2000], and [HIL 2001].

In medical image registration, a transformation which maps datasets obtained from different times, different viewpoints, and different sensors, must be determined. Depending on the characteristics of the differences between the medical images to be registered, generally, the registration transformations can be divided into rigid and non-rigid transformations. The rigid transformations can be used to cope with rotation and translation differences between the images. But usually, patient postures, tissue structures, and the shapes of the organs cannot always remain the same when they are imaged with different imaging devices or at different times, therefore, elastic or non-rigid registrations are required to deal with these differences between the images [ROH 2000].

3.1.2.1 Rigid Distortion and Transformation

Rigid distortion caused by translation and rotation is the simplest distortion. Because of the rigid structure of the skull, the distortions of the brain images are often assumed as rigid. When the brain image registration is carried out, the rigid transformation, which preserves the lengths and angle measures, is often used to correct these translation and rotation displacements.

In rigid transformation, the straightness of lines and the distances between points are preserved and the rigid transformation only includes translations and rotations. For example, a transformation is said to be rigid if it preserves relative distances, i.e., if p and q are transformed to p' and q', then the distance from p to q is the same as that from p' to q'.

All the rigid transformations will be considered as affine. The transformation

$f : p \rightarrow p'$ is calculated in terms of coordinate vectors x and x' according to:

$$x' = Ax + v \qquad \text{Equation 3-2}$$

Where: A is a matrix and v a vector. The matrix A is called the linear component, and v the translation component of the transformation. The properties of rigid transformation:

1. A rigid transformation preserves angles as well as distances.

   If p , q and r are three points transformed to p' , q' and r' , then the angle θ between segments pq and pr is the same as the angle θ' between $p'q'$ and $p'r'$.

2. The composition of rigid transformations is rigid.
3. A rigid transformation has an inverse which is rigid as well.

An affine transformation will be rigid when its linear component is rigid, since a translation will certainly not distort lengths.

3.1.2.2 Affine Distortion and Transformation

Affine distortion is caused by translation, rotation, scaling and skewing of the coordinate space. For example, if the gradients of magnetic resonance imaging are miscalibrated, the scaling errors will present in the MRI images. A tilted gantry in CT would introduce skewing distortions into images. Affine transformation, which is a composition of rotations, translations, scalings, and shears (Table 3-1), and maps parallel lines into parallel lines, can be used to correct these deformations. Geometric contraction, expansion, dilation, reflection, rotation, shear, similarity transformations, spiral similarities, and translation are all affine transformations, and so as their combinations.

Affine Transformation	Illustration	Transformation Matrix	
Translation	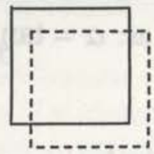	$\mathbf{q} = \begin{bmatrix} q_1 \\ q_2 \end{bmatrix}$	q_1 and q_2 specify the displacement along the x axis and the y axis respectively.
Rotation	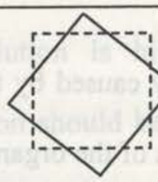	$A = \begin{bmatrix} \cos\alpha & \sin\alpha \\ -\sin\alpha & \cos\alpha \end{bmatrix}$	α is the angle of rotation.
Shear	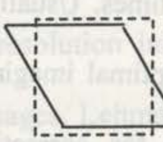	$A = \begin{bmatrix} 1 & a_{12} \\ a_{21} & 1 \end{bmatrix}$	a_{12} and a_{21} specify the shear factor along the x axis and the y axis respectively.
Scale		$A = \begin{bmatrix} a_{11} & 0 \\ 0 & a_{22} \end{bmatrix}$	a_{12} and a_{21} specify the scale factor along the x axis and the y axis respectively.

Table 3-1 Affine Transformation

An affine transformation that combines rotation, scaling, and translation can be expressed as:

$$\begin{bmatrix} x' \\ y' \end{bmatrix} = s \begin{bmatrix} \cos\alpha & \sin\alpha \\ -\sin\alpha & \cos\alpha \end{bmatrix} \begin{bmatrix} x - x_0 \\ y - y_0 \end{bmatrix} = s \begin{bmatrix} \cos\alpha(x - x_0) + \sin\alpha(y - y_0) \\ -\sin\alpha(x - x_0) + \cos\alpha(y - y_0) \end{bmatrix}$$

Equation 3-3

Separate the equation, we can get:

$$x' = (s\cos\alpha)x + (s\sin\alpha)y - s(x_0\cos\alpha + y_0\sin\alpha)$$

$$y' = (-s\sin\alpha)x + (s\cos\alpha)y - s(x_0\sin\alpha - y_0\cos\alpha)$$

Equation 3-4

and

$$x' = ax - by + c$$

$$y' = bx + ay + d$$

Equation 3-5

where: $a = s\cos\alpha$ and $b = -s\sin\alpha$. The scale parameter can be defined as: $s \equiv \sqrt{a^2 + b^2}$; and the rotation parameter can be define as: $\alpha = \tan^{-1}(-\frac{b}{a})$.

3.1.2.3 Non-rigid Distortion and Registration

Non-rigid medical image deformations are mainly caused by the dramatic changes of the subject positions, tissue structures, and the shapes of the organs when the subject is imaged with different imaging devices or at different times. Usually, different imaging devices require the subject to pose differently to get optimal imaging results, therefore, rigid and affine transformations are not sufficient for correcting these non-rigid deformations. The involuntary motions of the lung and the heart lead to elastic deformations which cannot be registered using rigid and affine transformations as well. Although the skull is often assumed to be a rigid structure, because of changes of, for example, a tumor, or the differences between pre-operation and post-operation, the brain structure cannot always be considered as the same over time [HIL 2001].

Non-linear or elastic image registration is an active research area, which is important for correcting the anatomic deformations or changes over time, or matching the images from different subjects. In elastic transformations, the straightness of lines cannot be preserved and the transformations can be arbitrarily complex.

The elastic medical image registration was first introduced by Bajcsy [BAJ 1989]. As a challenging and active research topic, elastic medical image registration has attracted extensive attentions of researchers and a number of novel methods have been proposed, e.g., a block matching strategy was used by Lin et al., 1994, and a flexible fluid model was proposed by [CHR 1996].

3.2 Implementation Issues

3.2.1 Interpolation

Interpolation is required when an image needs to undergo transformations. Usually, the intra-slice resolution is higher than the inter-slice resolution, and hence, the interpolation operation should be carried out to compensate for this difference. Because images from different imaging modalities have different resolution, in a multimodal image registration, lower resolution images are often interpolated to the sample space of the higher resolution images. Lehmann, Gönner, and Spitzer [LEH 1999] presented a survey of interpolation methods in medical image processing.

In biomedical image registration, the most frequently used interpolation methods include nearest neighbor, linear, bilinear, trilinear, cubic, bicubic, tricubic, quadrilinear, cubic spline, sinc function, and cubic convolution interpolation. The more complex the interpolation methods, the more surrounding points concerned, and the slower the registration speed. For example, the nearest point interpolation uses only a single point, while the trilinear interpolation method takes 8 points into account, and tricubic interpolation needs 64 points. In order to speed up the registration procedure, low cost interpolation techniques are often preferred. Because of its good trade-off between accuracy and computational complexity, the bilinear interpolation is the most commonly used method ([ZIT 2003]). According to the research of [THÉ[1] 2000], in cardiac and thorax image registration, trilinear interpolation can help to achieve good registration performance.

3.2.2 Optimization

Optimization algorithm, serving as a searching strategy, is required by most of registration procedures. There are several optimization algorithms often used in the biomedical image registration. The exhaustive searching method has been used by [Van 1995] and [MAI 1996]. However, because of its high computational complexity, the exhaustive method for searching for the global optimization is not an efficient choice. Powell algorithm by Powell (1964) and Simplex method by Nelder and Mead (1965) are more efficient than the exhaustive searching strategy in finding an optimum solution.

The Powell algorithm has been used frequently as an optimization strategy for biomedical image registration, e.g., [COL 1995], [MAE 1997], and [DEY 1999]. The Powell algorithm performs a succession of one-dimensional optimizations, finding in turn the best solution along each freedom degree, and then returning to the first degree of freedom. The algorithm stops when it is unable to find a new solution with a significant improvement to the current solution.

The Downhill-Simplex algorithm has been used by, for example, [HIL 1993], [VAN 1994]. Rohlfing and Maurer (2003) adopted a variant of the Downhill-Simplex algorithm restricted to the direction of the steepest ascent. Downhill-Simplex has the characteristics of:

1. Finding the minimum of a function with more than one independent variables;
2. Requiring only function evaluations, not derivatives;
3. Especially efficient for the function evaluations that can be computed easily.

In order to search a vast number of parameters, which represent the complex deformation fields, multi-resolution optimization algorithms have been adopted by researchers in the biomedical image registration community, for example, [PAL 1995] and [PEN 1998]. Initially, the registration is performed at coarse spatial scales, then to the finer ones. These multi-resolution or coarse-to-fine optimization algorithms can accelerate computation and help to escape from the local minima.

3.2.3 Performance Validation of Biomedical Image Registration

For all types of registration, assessment of the registration accuracy is very important. A medical image registration method cannot be accepted as a clinical tool to assist the patient management until it has been proved to be accurate enough. Important criteria for assessing the performance of registration schemes are accuracy, robustness, usability, and computational complexity. Researchers have been developing novel and practical validation techniques, for example, [HEL 2001] proposed a hierarchical estimation method for 3-D registration, and [SCH 2003] proposed a validation of nonrigid image registration using finite-element methods. [WAN 2001] proposed a novel automatic method to estimate confidence intervals of the resulting registration parameters and allow the precision of registration results to be objectively assessed for 2-D and 3-D medical images. [FIT 2000], [WOO 2000], [HIL 2001], [MÄK 2002], and [ZIT 2003] presented good discussions and summaries about performance validation methods for medical image registration.

Validation of registration accuracy is a difficult task because of the lack of the ground truth. Objective performance validation still remains a challenge in the field of biomedical image registration.

Fiducial landmarks, which can predict the expected error distribution, have been devised to assess the registration accuracy. To a certain extent, assessment using fiducial landmarks provides a "gold standard" for medical image registration. However, the fiducial landmarks can either suffer from the movement of skin mobility or are highly invasive. Also, these validation measures cannot be applied retrospectively.

Phantom studies are important for the estimation of the registration accuracy because the data and displacement information is fully known beforehand. Phantom-based validations provide measures for mean transformation errors and computational complexity for different methods, and they are especially useful for estimating the accuracy of intra-modality registration methods.

Visual inspection, which provides a qualitative assessment, is the most intuitive method for evaluation of the registration accuracy. This assessment method may involve the inspection of subtraction images, contour overlays, or viewing anatomical landmarks. It has been used widely in both rigid and non-rigid registration assessment, but it may be considered as a subjective and insufficient approach.

The measurement of the consistency of transformations has been proposed to serve as accuracy qualification method by, e.g., [WOO 1998], [HOL 2000], and [CHR 2001]. Given three images of the same subject, A, B, and C, there are three transformations $T_{A\rightarrow B}$, $T_{B\rightarrow C}$, and $T_{C\rightarrow A}$. Applying these three transformations in turn to complete a circuit should result in the identical transformation for a perfect registration. Consistency measures have been used for monomodality, rigid registration.

3.3 Major Biomedical Image Registration Methodologies

Because of its crucial role in improving healthcare quality, medical image registration has been studied extensively for decades, which has resulted in a bulk of reviews, surveys, and books, e.g., [BRO 1992], [MAU 1993], [VAN 1993], [MAI 1998], [LES 1999], [ROH 2000], [HIL 2001], [MÄK 2002], [BAN 2000], and [FIT 2000]. According to the registration feature space, principally, medical image registration can be distinguished into intensity-based registration and feature-based registration [BRO 1992].

3.3.1 Intensity-Based Medical Image Registration

As one principal medical image registration methodology, intensity-based registration has attracted significant attention in the research community, e.g., [ALP 1990], [WOO 1993], [HIL 1993], [COL 1995], [VIO 1995], and [CHR 1996]. As a result, numerous registration approaches have been proposed and used, for example, correlation based methods, Fourier-based approaches, the moment and principal axes methods [ALP 1990], minimizing variance of intensity ratios ([WOO 1993], [HIL 1993]), and mutual information methods ([COL 1995] and [VIO 1995]). Directly exploiting the image intensities, the intensity-based registration algorithms have the advantages of no segmentation required and few user interactions involved, and most importantly, these methods have potential to achieve fully automated registration. However, this category of schemes does not make use of a priori knowledge of the organ structure and the registration computation is not efficient. In order to improve the registration performance, speed, accuracy, and at same time avoiding the local minima, hierarchical medical image registration has been proposed, e.g., [VAN 1999], [THE 2000], and [PLU 2001].

Intensity-based medical image registration fully and directly exploits the image raw intensities and an explicit segmentation of the images is not required. There are several well-established intensity-based similarity measures used in the biomedical image registration area.

3.3.1.1 Similarity Measures by Minimizing the Intensity Differences

Minimizing the intensity difference methods include the Sum of Squared Differences (SSD) and the Sum of Absolute Differences (SAD), which exhibit a minimum in the case of perfect matching, e.g., [HOH 1993] and [CHR 1996].

$$SSD = \sum_{i}^{N}(I_R(i) - T(I_S(i)))^2 \qquad \text{Equation 3-6}$$

$$SAD = \frac{1}{N}\sum_{i}^{N}\left|I_R(i) - T(I_S(i))\right| \qquad \text{Equation 3-7}$$

Where $I_R(i)$ is the intensity value at position i of reference image R and $I_S(i)$ is the corresponding intensity value in study image S; T is geometric transformation.

SSD and SAD can work well with the ideal datasets, for example, only a small fraction of intensity changes between the images to be registered. Although they are efficient to calculate, these methods are sensitive to intensity changes. This unpleasant feature of these methods limits their application to monomodality image registration only.

3.3.1.2 Correlation Techniques

Correlation methods attempt to determine the best registration by maximizing the similarity between images of the same object that differ primarily because of different acquisition conditions and also possibly because of small object changes. A parameterized geometrical transformation, to be applied to one of the images to correct for variations in acquisition conditions, is firstly selected. The parameters of this transformation are then estimated by optimizing a similarity criterion between one image and the other transformed image.

Correlation based registration techniques were proposed to aim at multimodal biomedical image registration, e.g., [MAI 1996] and [VAN 1995]. The cross-correlation technique has also been used for rigid motion correction of SPECT cardiac images, e.g., [O'CO 1998], and [MÄK 2002]. However, because usually the geometric deformations of the image modalities are not likely to be linear, these correlation methods, which require a linear dependence between the intensity of the images, cannot achieve reliable registration results. The normalized cross correlation is defined as:

$$CR = \frac{\sum_i (I_R(i) - \bar{I}_R)(I_S(i) - \bar{I}_S)}{\sqrt{\sum_i (I_R(i) - \bar{I}_R)^2}\sqrt{\sum_i (I_S(i) - \bar{I}_S)^2}} \qquad \text{Equation 3-8}$$

where $I_R(i)$ is the intensity value at position i of reference image R and $I_S(i)$ is the corresponding intensity value in study image S; $\bar{I}_R$ and $\bar{I}_S$ are the mean intensity value of reference and study image respectively.

3.3.1.3 Information Theoretic Techniques

Information theoretic techniques play an important role in multimodality medical image registration. The Shannon entropy is widely used as a measure of information in many branches of engineering. It was originally developed as a part of information theory in the 1940s and describes the average information supplied by a set of symbols $X = \{x\}$ whose probabilities are given by $\{p(x)\}$.

1. The binary entropy function

The entropy of a random variable X is

$$H = -\sum_x p(x) \log p(x) \qquad \text{Equation 3-9}$$

Suppose X is a binary random variable,

$$X = \begin{cases} 1 & \text{with probability p} \\ 0 & \text{with probability 1 - p} \end{cases}$$

Then the entropy of X is:

$$H(X) = -p \log p - (1-p)\log(1-p) \qquad \text{Equation 3-10}$$

If all symbols have equal probability, then entropy will be at maximum. If one symbol has a probability of 1 and all others have a probability of zero, then the entropy will have a minimum.

2. **Joint entropy**

The joint entropy $H(X,Y)$ of pairs of random variables (X,Y) is defined as:

$$H(X,Y) = -\sum_{x\in X}\sum_{y\in Y} p(x,y)\log p(x,y)$$

Or:

$$H(X,Y) = -E\log p(X,Y) \qquad \text{Equation 3-11}$$

3. **The conditional entropy**

The conditional entropy $H(Y\mid X)$ is defined as:

$$H(Y\mid X) = \sum_{x\in X}\sum_{y\in Y} p(x,y)\log p(y\mid x) = -E_{p(x,y)}\log p(y\mid x) \qquad \text{Equation 3-12}$$

The definition can also be expressed as:

$$H(Y\mid X) = -\sum_{x\in X} p(x)\sum_{y\in Y} p(y\mid x)\log p(y\mid x) = -\sum_{x\in X} p(x)H(Y\mid X=x)$$

Equation 3-13

4. **Theorem:**

The entropy about both X and Y is equal to the entropy about X plus the conditional entropy about Y given X is known.

$$H(X,Y) = H(X) + H(Y\mid X) \qquad \text{Equation 3-14}$$

- Proof:

$$
\begin{aligned}
H(X,Y) &= -\sum_{x\in X}\sum_{y\in Y} p(x,y)\log p(x,y) \\
&= -\sum_{x}\sum_{y} p(x,y)\log p(x)p(y\mid x) \\
&= -\sum_{x}\sum_{y} p(x,y) - \sum\sum p(x,y)\log p(y\mid x) \\
&= \sum_{x} \mathrm{p(x)} - \sum_{x}\sum_{y} p(x,y)\log(y\mid x) \\
&= \mathrm{H(X)} + \mathrm{H(Y\mid X)}
\end{aligned}
$$

In image registration area, when the images are correctly aligned, the joint histograms have tight clusters and the joint entropy is minimized. These clusters disperse as the images become less well registered, and correspondingly, the joint entropy is increased, [COL 1995]. [ZHU 2002] proposed cross-entropy optimization based volume image registration method. Because minimizing the entropy does not require that the histograms are unimodal, the joint entropy is generally applicable to multimodality registration and segmentation of images is not needed.

3.3.2 Feature-Based Medical Image Registration

The other principal medical image registration category is based on corresponding features that can be extracted manually or automatically. The feature-based medical image registration methods can be classified into point-based approaches, e.g., [BOO 1992], [BES 1992], [FIT 1998], curve-based algorithms, e.g., [MAI 1996], [SUB 1998], and surface-based methods, e.g., [CHE 1987], [BOR 1988], and [PEL 1989] , [THO 1996] and [AUD 2000]. One main advantage of feature-based registration is that the transformation can be stated in analytic form, which leads to efficient computational schemes. However, in the feature-based registration methodologies, a preprocessing step of detecting the features is needed and the registration results are highly dependent on the result of this preprocessing. Because registration algorithms using landmarks often require users to specify corresponding landmarks from the two images manually or semi-automatically, such methods cannot always provide very accurate registration. Figure 3-3 illustrates the feature-based registration procedure.

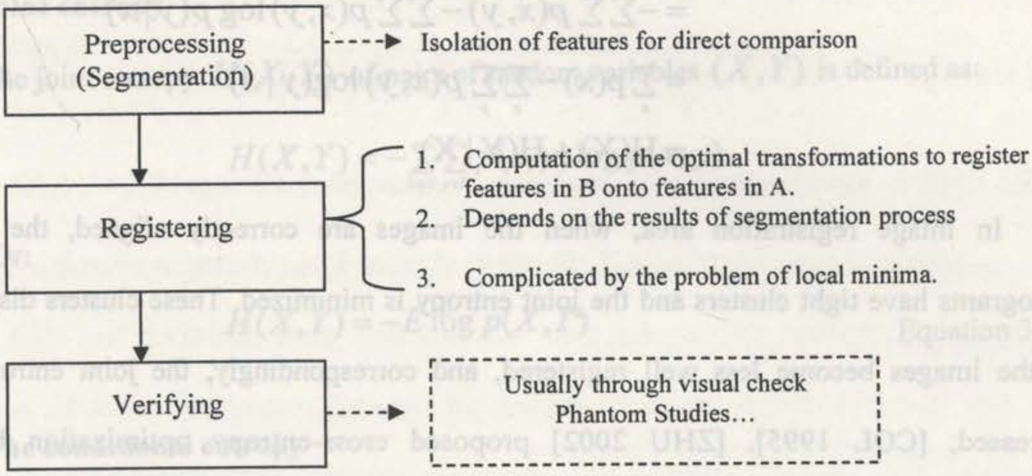

Figure 3-2 Feature-based Registration Procedure

3.3.2.1 Point-Based Registration

Point-based registration involves identifying corresponding points in the images to be registered, registering the points, and inferring the image transformation.

The corresponding points are also called homologous landmarks to emphasize that they should present the same feature in the different images. These points can either be anatomical features that can be identified in images, or markers attached to the patient which can be identified in both images modalities. For example, [CHR 1996] and [THI 1996] proposed medical image registration methods based on anatomical landmarks, while [MAU 1995] and [EDW 1995] used registration algorithm based on extrinsic landmarks. When points are available, Thin-Plate Splines (TPS) which produce a smoothly interpolated spatial mapping, are often used to determine the transformation for 2-D medical image registration, e.g., [BOO 1989], [ROH 1998].

Anatomical landmark based registration methods have the drawback of user interaction being required. Registration algorithms based on extrinsic landmarks which maybe invasive or non-invasive, are comparatively easy to implement, fast, and can be automated, but they may have drawbacks of invasiveness and less accurate results. [FIT 1998] presented accuracy assessment methods for rigid-body, point-based registration.

As a successful example, iterative closest points (ICP) method proposed by [BES 1992], maybe the most widely used medical image registration approach in medical imaging applications, e.g., [HIL 2001], [MAU 1998]. The algorithm has two stages and iterations. The first stage involves identifying the closest model points for each data point, and the second stage involves finding the least square transformation relating to these point sets. The algorithm then re-determines the closest point set and continues until it finds the local minimum match between the two surfaces.

3.3.2.2 Boundary- or Surface-Based Methods

Boundaries and surfaces are distinct features in medical image registration due to various segmentation algorithms which can successfully locate such features. Surface-based registration methods can be rigid and deformable. In rigid surface-based registration methods, the same anatomical structure surfaces are extracted from the images and used as input for the registration procedure.

The Head-and-Hat algorithm, proposed by [CHE 1987] and [PEL 1989], is one successful surface fitting technique for multimodal image registration. In this method, two equivalent surfaces are identified in the images. The first surface extracted from the higher-resolution images, is represented as a stack of discs, and is referred to as "head". The second surface, referred to as "hat", is represented as a list of unconnected 3D points. The registration is determined by iteratively transforming the hat surface with respect to the head surface, until the closest fit of the hat onto the head is found. Because the segmentation task is comparatively easy, and the computational cost is relatively low, this method remains popular. However, this method is prone to error for convoluted surfaces.

In deformable surface-based registration methods, the extracted surfaces or curves from one image is elastically deformed to fit the second image. The deformable curves are known as snakes or active contours which help to fit contours or surfaces to image data. Snakes operate by simulating a controllable elastic material, much like a thin, flexible sheet. We can initially position the model by using information from anatomical atlases; then, the model is allowed to relax to a stationary position. This minimum energy position seeks to find the best position to trade off internal and external forces. The internal forces are due to the elastic nature of the material and the external forces stem from sharp boundaries in image intensity. Important deformable surface-based registration approaches include the snake model proposed by [KAS 1988], the elastic matching approach proposed by [BAJ 1989], and the finite-element model technique proposed by [TER 1991], etc.

Deformable surface-based registration is suited for intersubject and atlas registration. A drawback of these methods is that a good initial pre-registration is required to achieve a proper convergence. For recent surveys, please refer to [MAI 1998], [AUD 2000], [HIL 2001], and [ZIT 2003].

Although biomedical image registration has been intensively investigated and enormous advances in imaging techniques have been achieved, the ever-increasing growth of imaging data and their applications in medical and clinical environments ensure the existence of future challenges in more precise and efficient biomedical image registration.

3.4 Problems Related to the Current Registration Methods

There are several problems with the current registration methods and algorithms:

(1) Problem 1: Computational complexity may be high.

The traditional image registration methods that find the peak of the spatial cross-correlation or the sum of squared differences require exclusive transformations of one set of the images. When the degrees of freedom of transformations are increased, this procedure can be expensive and impractical.

(2) Problem 2: Convergence may fall into local minimum.

Optimization approaches are susceptible to convergence on local minima when optimizing over highly non-convex objective function, as is generally the case in registration.

The registration problem is complicated by a number of factors that must be handled by proposed solution. These factors include:

(1) Different coordinate frames in datasets being registered, resulting in possibly large initial pose offsets;

(2) Sensor distortions are different across images;

(3) Different spatial resolution;

(4) Different structural coverage—the images may not cover the same physical volumes;

(5) Tissue may be displaced, articulated, or deformed in one of the images relative to the other.

3.5 The Proposed Solutions and Aims

The proposed solution to these problems consists of a hierarchical approach in which refinements are made along two dimensions.

(1) Measurement resolution

In order to achieve the ideal registration result, we attempt to adopt coarse-to-fine method, in which coarse metrics are designed to pull in solutions across large pose offsets while not adversely impacted by outliers, missing surface patches, or spatial perturbations. Once close to final solution, fine metrics are designed to accurately localize the pose which minimizes a more sensitive distance measure takes between the surfaces.

(2) Pose complexity

To deal with the problems related with pose complexity, we should convert rigid transformation to deformable transformation in registering the images.

Our registration methods should achieve the following aims:

(1) Automated Processing: Minimize manual intervention for ease-of-use and high accuracy.

One of the key aspects of medical image registration is the need for automated registration processing. This issue is not only including efficiency concerns, but also accuracy consideration.

(2) Robust performance: Minimize the impact of data deviations. The result should achieve good precision.

3.6 Summary

This chapter has focused on the fundamental theories of biomedical image registration and major methodologies and contributions of this area. We summarize our understanding of main methods and technologies, current issues, and to provide the connection between different biomedical image registration methods in this chapter. Furthermore, discussions on the problems related to the current registration schemes and the possible solutions have been presented.

CHAPTER 4 AUTOMATIC ELASTIC MEDICAL IMAGE REGISTRATION BASED ON IMAGE INTENSITY

Automatic registration has advantage of avoiding subjective errors and less accurate results because of human intervention. While rigid transformations (rotation and translation) are sufficient in most applications, there are many other applications (e.g. anatomic standardization and intersubject registration), where nonrigid (or elastic) transformations are required to establish spatial correspondence between images.

In this chapter, an automatic elastic medical image registration approach is proposed on the basis of image intensity. The algorithm is divided into two steps. In Step one, global affine registration is firstly used to establish an initial guess and the resulting images can be assumed to have only small local elastic deformations. The mapped images are then used as inputs in Step two, during which, the study image is modeled as elastic sheet by being divided into sub-images. Moving the individual sub-image in the reference image, the local displacement vectors are found and the global elastic transformation is achieved by assimilating the local transformations into a continuous transformation. The proposed elastic registration algorithm is illustrated in Figure 4-1.

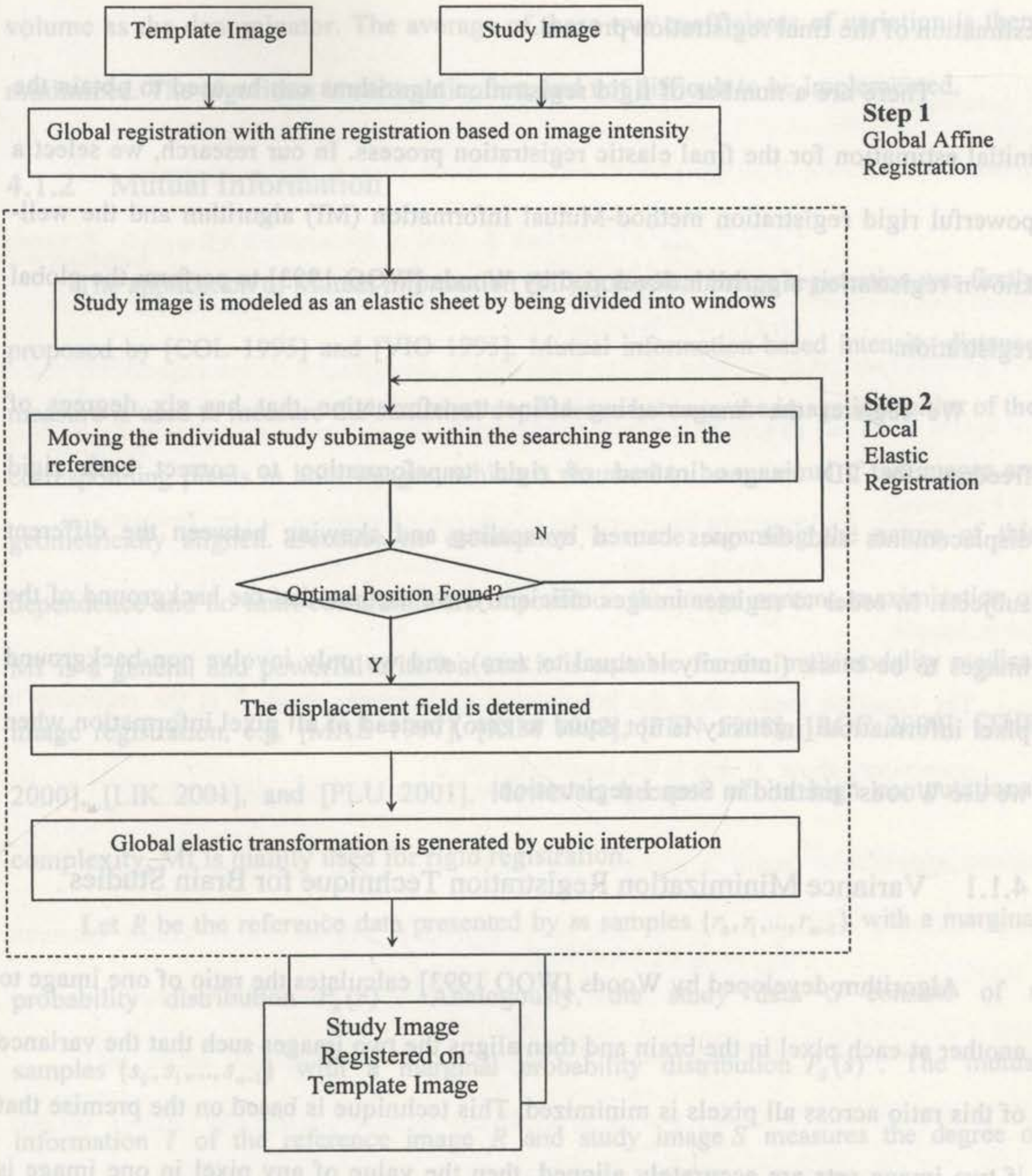

Figure 4-1 Illustration of the Elastic Registration Algorithm

4.1 Step One: Global Registration

An initial rigid registration can be used to correct global displacements, provide initial estimation, and accelerate more complex elastic registration procedure. Because of the rigid structure of the brain skull, the affine registration is a good initial estimation of the final registration process.

There are a number of rigid registration algorithms can be used to obtain the initial estimation for the final elastic registration process. In our research, we select a powerful rigid registration method-Mutual Information (MI) algorithm and the well-known registration algorithm developed by Woods [WOO 1993] to perform the global registration.

We register the images using affine transformation that has six degrees of freedom for 2D images instead of rigid transformation to correct both rigid displacements and the ones caused by scaling and skewing between the different subjects. In order to register images efficiently, we assume that the background of the images to be black (intensity is equal to zero), and we only involve non-background pixel information (intensity is not equal to zero) instead of all pixel information when we use Woods' method in Step 1 registration.

4.1.1 Variance Minimization Registration Technique for Brain Studies

Algorithm developed by Woods [WOO 1993] calculates the ratio of one image to another at each pixel in the brain and then aligns the two images such that the variance of this ratio across all pixels is minimized. This technique is based on the premise that if two image sets are accurately aligned, then the value of any pixel in one image is related to the value of its corresponding pixel in the other image by a single factor α. If the images are misaligned, α is no longer constant across the volume but varies from pixel to pixel. The algorithm aligns the two volumes such that the coefficient of variation of the ratio volumes is minimized through an iterative method. To avoid bias, two ratio volumes are calculated. The first ratio volume is computed where the first input volume serves as the denominator; the second ratio volume uses the second input volume as the denominator. The average of these two coefficients of variation is then minimized. The algorithm is automatic, fast, and not difficult to be implemented.

4.1.2 Mutual Information

The application of Mutual information (MI) in medical image registration was firstly proposed by [COL 1995] and [VIO 1995]. Mutual information-based intensity distance measure is used to measure the statistical dependence between the image intensities of the corresponding pixels in both images, which is assumed to be maximal if the images are geometrically aligned. Because no assumption is made regarding the nature of this dependence and no limit constraints are imposed on the image content, maximization of MI is a general and powerful criterion and it is suitable for the multimodality medical image registration, e.g. [MAE 1997], [KIM 1997], [PEN 1998], [ROC 2000], [THE 2000], [LIK 2001], and [PLU 2001]. However, because of its high computational complexity, MI is mainly used for rigid registration.

Let R be the reference data presented by m samples $\{r_0, r_1, ..., r_{m-1}\}$ with a marginal probability distribution $P_R(r)$. Analogously, the study data S consists of n samples $\{s_0, s_1, ..., s_{n-1}\}$ with a marginal probability distribution $P_S(s)$. The mutual information I of the reference image R and study image S measures the degree of dependence of R and S by measuring distance between the joint distribution $P_{RS}(r,s)$ and the distribution associated to $P_R(r)$ and $P_S(s)$. MI can be defined as:

$$I_{R,S} = \sum_{(r,s)} P_{RS}(r,s) \log\left(\frac{P_{RS}(r,s)}{P_R(r)P_S(s)}\right)$$ Equation 4-1

If R and S are independent, $P_{RS}(r,s) = P_R(r)P_s(s)$ (definition of independence), then $I_{RS} = 0$, which means: if R and S are independent random variables then S cannot estimate any information about R.

With $H(R)$ and $H(s)$ being the entropy of R and S, respectively, $H(R,S)$ is their joint entropy.

$$H(R) = -\sum_{r} P_R(r) \log P_R(r) \quad \text{Equation 4-2}$$

$$H(S) = -\sum_{s} P_S(s) \log P_S(s) \quad \text{Equation 4-3}$$

$$H(R,S) = -\sum_{r,s} P_{RS}(r,s) \log P_{RS}(r,s) \quad \text{Equation 4-4}$$

- Theorem: An important interpretation of mutual information can be expresses as:

$$I_{RS} = H(R) - H(R \mid S) \quad \text{Equation 4-5}$$

The equation means that the information that S tells about R is the reduction in uncertainty about R due to the knowledge of S.

- Proof:

$$\begin{aligned} I_{R,S} &= \sum_{(r,s)} P_{RS}(r,s) \log\left(\frac{P_{RS}(r,s)}{P_R(r) P_S(s)}\right) \\ &= \sum_{r,s} P_{RS}(r,s) \log \frac{P(r \mid s)}{P_R(r)} \\ &= -\sum_{r,s} P_{RS}(r,s) \log P(r) + \sum_{r,s} P_{RS}(r,s) \log P(r \mid s) \\ &= H(R) - H(R \mid S) \end{aligned}$$

- Property of Symmetry:

$$I_{RS} = H(S) - H(S \mid R) = I_{SR} \quad \text{Equation 4-6}$$

This symmetry property means that R tells as much information about S as S tells about R. Because of $H(R,S) = H(R) + H(S \mid R)$, MI is related to entropy by the equation:

$$I_{RS} = H(R) + H(S) - H(R,S) \quad \text{Equation 4-7}$$

The information that R tells about S is the uncertainty in R plus the uncertainty about S minus the uncertainty in both R and S.

Under the assumption that the mutual information of the two images is maximum when the images are in registration, registration can be performed by maximizing the mutual information as a function of a geometric transformation T of the study image S:

$$S_T = T(S) \quad \text{Equation 4-8}$$

$$I_{R,S_T} = \sum_{(r,T(s))} P_{R,S_T}(r,T(s)) \log\left(\frac{P_{RS_T}(r,T(s))}{P_R(r)P_{S_T}(T(s))}\right) \quad \text{Equation 4-9}$$

$$T_{reg} = \arg\max_T (I_{R,S_T}) \quad \text{Equation 4-10}$$

T_{reg} is the transformation that will bring the images into registration.

Mutual information registration does not assume a linear relationship among intensity values of the images to be registered and is one of the few intensity-based measures that are well suited to the multimodality image registration.

This affine registration step is carried out using Powell's optimization method ([POW 1964]). We assume that on the basis of such a global affine registration, the images are registered up to small local elastic deformations.

4.2 Step Two: Local Elastic Registration

After affine registration step, rotation, translation, and scaling differences between the images can be corrected. However, usually, patient pastures, tissue structures, and the shapes of the organs cannot always keep the same when they are imaged with different imaging devices or at different times, therefore, elastic or non-rigid registrations are required to cope with these differences between the images, [ROH 2000].

In this step, the matched images are used as inputs and the study image is modeled as an elastic sheet by being divided into equal sized windows which number is less than the number of pixels. A local transformation is found in each individual window and the global elastic transformation is achieved by assimilating all of the local transformations into a continuous transformation.

4.2.1 Finding the Best Position for Each Individual Study Subimage

The study image is modeled as an elastic sheet by being divided into some number of square windows. By iteratively moving the individual study window on the reference image within a searching range (in our method, we define the size of the searching range the same as the size of each individual study window), we can optimize the local similarity and get the best position for each individual study subimage.

We use the sum of squared distance (SSD) as the objective criterion whose role is to measure the similarity of the study image with respect to the reference image. Suppose that $I_{swi}(x,y)$ and $I_{rwi}(x,y)$ are the *ith* subimages of study image and its corresponding same size neighborhood in the reference image respectively. Taking a warping function T, we can get a warped version of the sub-image of the study image $I_{wswi}(x,y)$.

$$I_{wswi}(x,y) = I_{swi}(T(x,y)). \qquad \text{Equation 4-11}$$

We want to find a warping function T (to simplify and speed up the algorithm, we limit the warping function to translation within each sub-image searching range) such that the warped study subimages are as close as possible to the corresponding reference subimages, in the sense of the sum of squared distance (SSD):

$$E = \sum e^2 = \sum_{(x,y)\in I} \left(I_{wswi}(x,y) - I_{rwi}(x,y)\right)^2 . \qquad \text{Equation 4-12}$$

4.2.2 Determination of the Local Displacement Field

The displacement vectors for the pixels in each individual subimage are determined by the position differences between the original and the new subimage pixels. Let V_i^t be the pixel position of the subimage (window) i at iteration t. The warping function T^t of the iteration t transforms V_i^t into V_i^{t+1}.

$$V_i^{t+1} = T^t(V_i^t). \qquad \text{Equation 4-13}$$

The local displacement field in the window i is determined by:

$$D_i = \{V_i^{t+1} - V_i^t\} = \{T^t(V_i^t) - V_i^t\}. \qquad \text{Equation 4-14}$$

Defining a displacement vector for each pixel and a displacement field for each window enable us to handle subtle image deformations.

The local displacement fields found are translated into global elastic transformation by cubic interpolation. The elastic registration is achieved by applying the global elastic transformation to the study image.

4.3 Validation

In this section, some experimental results achieved by our two-step elastic registration approach will be presented to validate the proposed algorithm. Because no gold standard is available for measuring the performance of registration algorithms, in our paper, the registration results are tested by subtracting the registered images and visually investigating the difference image. The more the corresponding parts overlap, the more successful the registration is.

4.3.1 Experimental Data Preparation

I. Designate an image I_r as the reference image;

II. Create the study image I_s by

a. Firstly, elastically deform I_r using polynomial warping:

$$x' = a(x, y) = \sum_{i=0}^{N-1}\sum_{j=0}^{N-1} p_{ij} x^j y^i.$$

$$y' = b(x, y) = \sum_{i=0}^{N-1}\sum_{j=0}^{N-1} q_{ij} x^j y^i.$$

b. Secondly, rotate the image by 5 degrees;

c. Finally, translate the image by $(dx, dy) = (5, 5)$.

III. Register the images using the proposed algorithm.

4.3.2 Experimental Validation Using Simulated Data

4.3.2.1 Experiments Using Simulated Data

We use Phantom images that represent the most important features of human brain in this series of experiments. In the experiments using Woods' algorithm as Step 1 registration approach, we register the images with windows of 8*8 pixels in Step 2 registration. In the experiments using MI method as affine registration algorithm, we register the images with windows of 4*4 pixels in the elastic registration process.

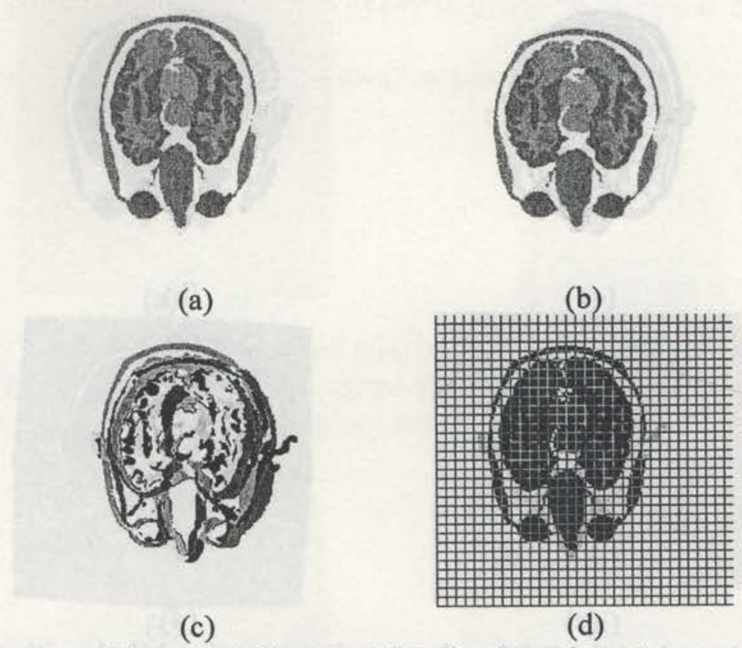

Figure 4-2 Phantom Data for Experiments
(a) is the reference image; (b) is the study image; (c) is the difference image between the reference image and the study image before the registration; (d) is the study image with grids (windows) overlaid

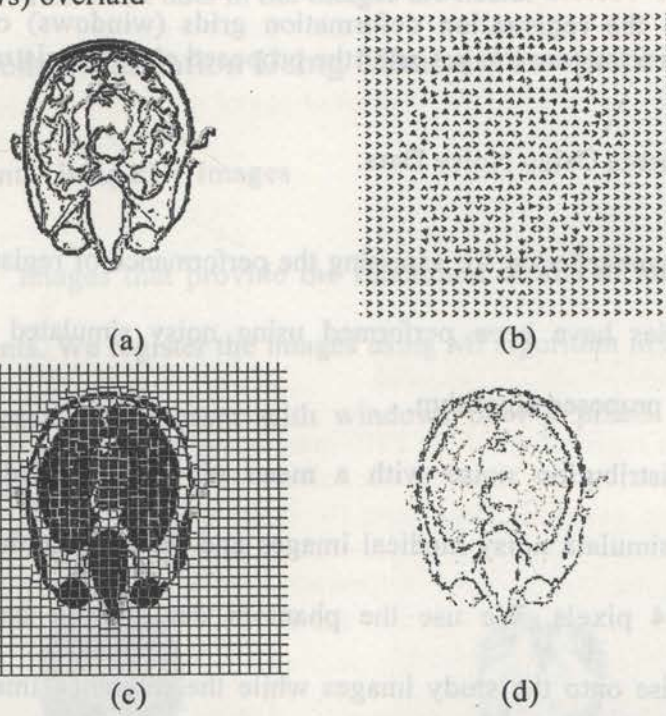

Figure 4-3 Elastic registration of the phantom images using Woods' algorithm in Step 1
(a) is the difference image between the reference and the corrected study image after Step 1 registration using the algorithm of Woods; (b) is the global displacement field shown by the displacement vectors that are denoted by arrows; (c) is the result of Step 2 registration with the registration deformation grids (windows) overlaid; (d) is the difference between the two images after the proposed elastic registration.

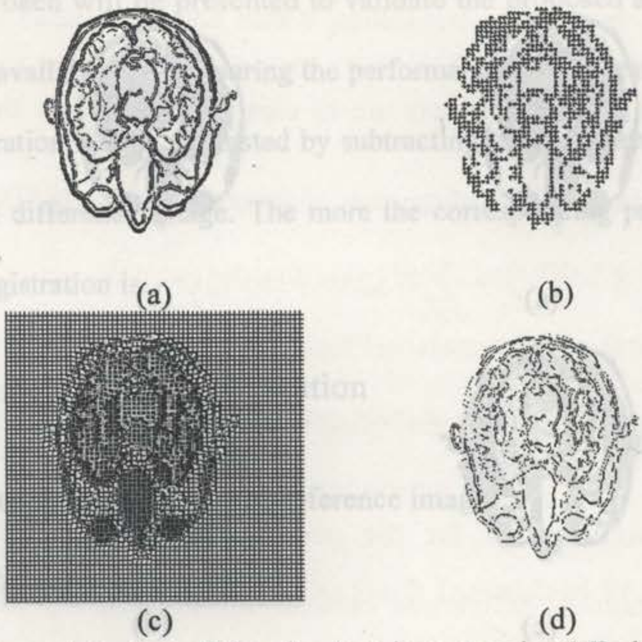

Figure 4-4 Elastic registration of the phantom images using MI algorithm in Step 1
(a) is the difference image between the reference and the corrected study image after Step 1 registration using MI algorithm; (b) is the global displacement field shown by the displacement vectors that are denoted by arrows; (c) is the result of Step 2 registration with the registration deformation grids (windows) overlaid; (d) is the difference between the two images after the proposed elastic registration.

4.3.2.2 Experiments Using Noisy Data

One important criterion for assessing the performance of registration algorithms is robustness. Studies have been performed using noisy simulated data to assess the robustness of the proposed algorithm.

Poisson distribution noise with a mean of 1.5 is added to images in our experiments to simulate noisy medical images and we register the two images using windows of 4*4 pixels. We use the phantom data in our experiments and just superimpose noise onto the study images while the reference images are kept clean. Experiment results in Figure 4-5 show that the noise does not affect the registration results significantly, because the six registration parameters are not changed when the noise is added.

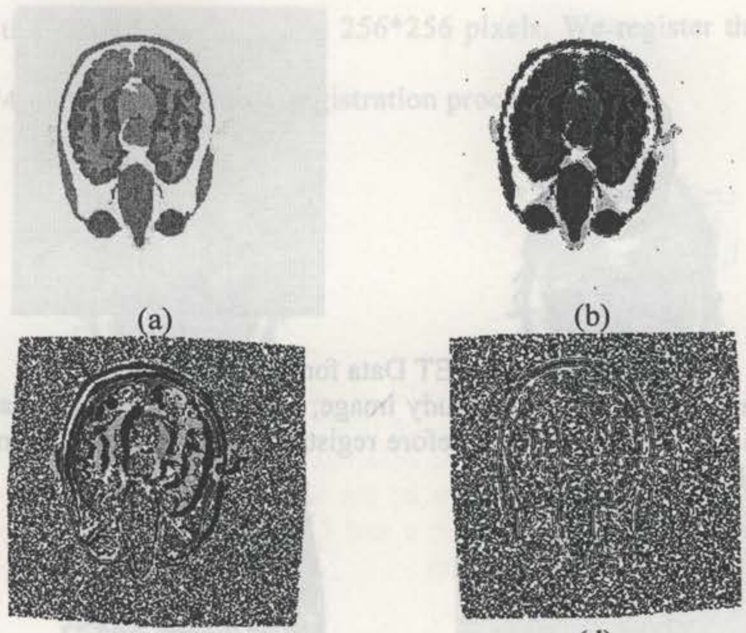

(a) (b)

(c) (d)

Figure 4-5 Noisy simulated data for Experiments
(a) is the reference image; (b) is the noisy deformed study image; (c) is the difference image between the two images before the registration; (d) is the difference after the elastic registration. The black dots in the images are noise.

4.3.3 Experimental Validation Using Clinical Tomographic Data

4.3.3.1 Experiments Using PET Images

We use PET images that provide the functional details of human brain in this series of experiments. We register the images using MI algorithm in Step 1 registration and correct the local displacement with windows of 4*4 pixels in Step 2 of the registration process.

(a) (b)

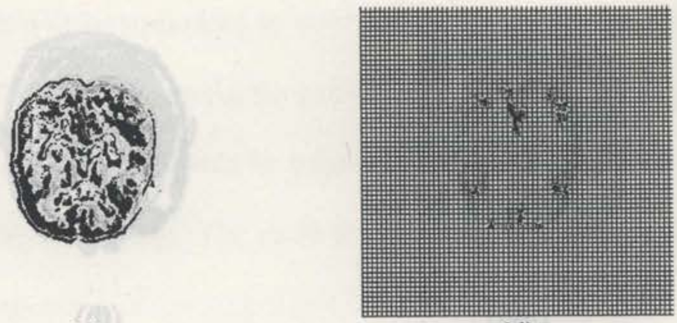

(c) (d)

Figure 4-6 PET Data for Experiments

(a) is the reference image; (b) is the study image; (c) is the difference image between the reference image and the study image before registration; (d) is the study image with grids (windows) overlaid.

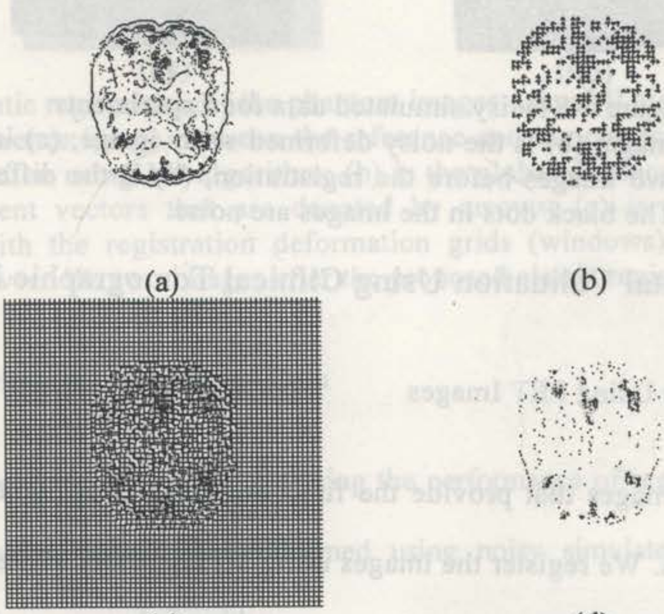

(a) (b)

(c) (d)

Figure 4-7 Elastic registration of the PET images using MI algorithm in Step 1

(a) is the difference image between the reference and the corrected study image after Step 1 registration using MI algorithm; (b) is the global displacement field shown by the displacement vectors that are denoted by arrows; (c) is the result of Step 2 registration with the registration deformation grids (windows) overlaid; (d) is the difference between the two images after the elastic registration.

4.3.3.2 Experiments Using MR Images

In this series of experiments we adapt the experimental procedure slightly in the sense that I_r is now MR proton-density images of head at a magnetic field strength of

1.5 Tesla and the size of the images is 256*256 pixels. We register the images using windows of 4*4 pixels in the elastic registration process.

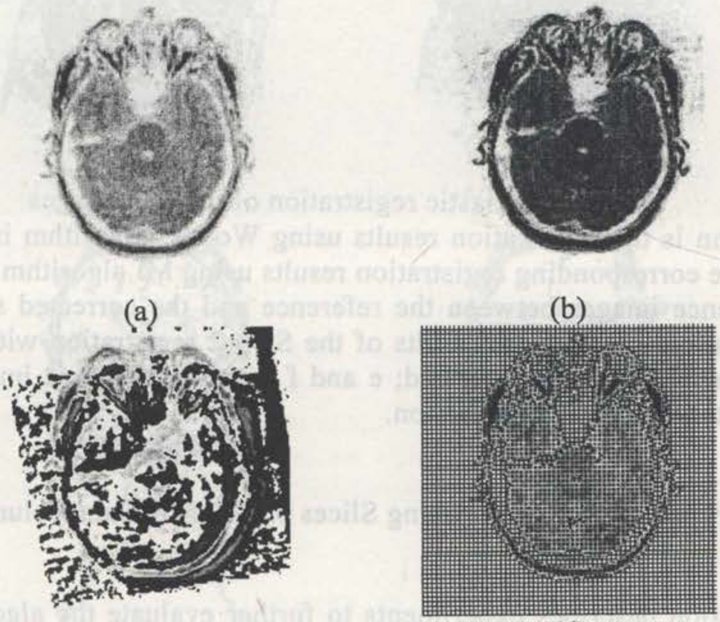

Figure 4-8 MR Data for Experiments

(a) is the reference image; (b) is the study image; (c) is the difference image between the reference image and the study image before the registration; (d) is the study image with grids (windows) overlaid

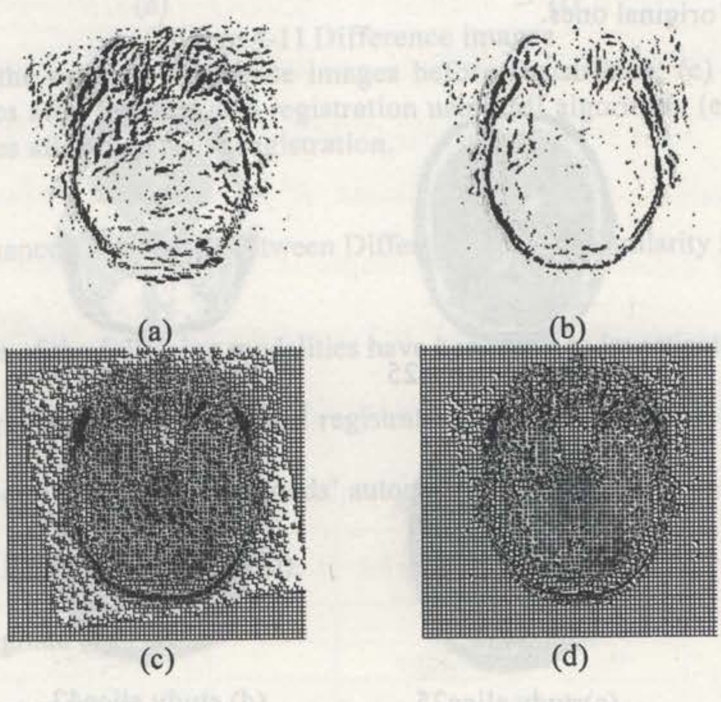

(e) (f)

Figure 4-9 Elastic registration of the MR images

The left column is the registration results using Woods' algorithm in Step 1, and the right row is the corresponding registration results using MI algorithm in Step1. a and b are the difference images between the reference and the corrected study image after Step 1 registration; c and d are results of the Step 2 registration with the registration deformation grids (windows) overlaid; e and f are the difference images between the two images after the elastic registration.

4.3.3.3 Experimental Validation Using Slices of 3-D MR Data Volume

This section describes experiments to further evaluate the algorithm's accuracy and performance. Transverse slices of 3-D MR volume (256*256*46) of same subject are registered. The quality of the registration is assed by comparing the transformed slices with the original ones.

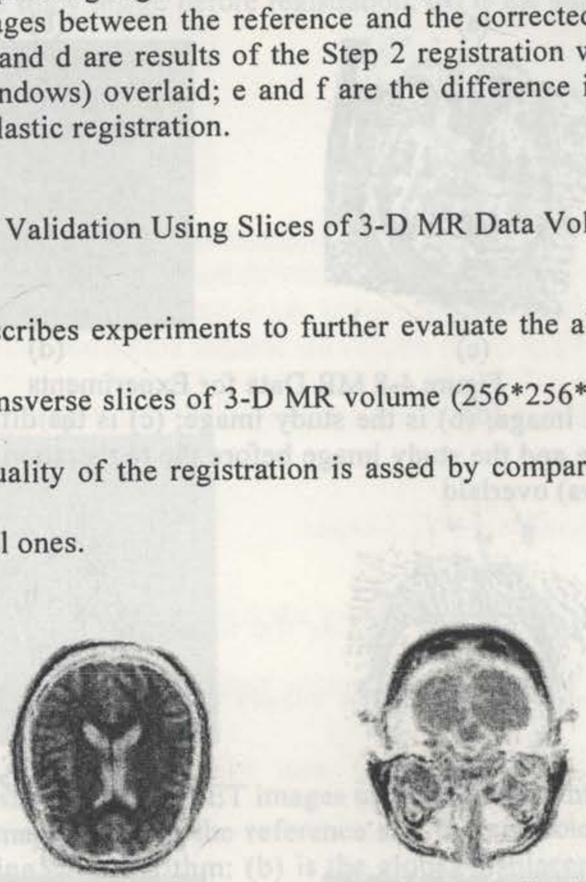

(a) reference slice25 (b) reference slice42

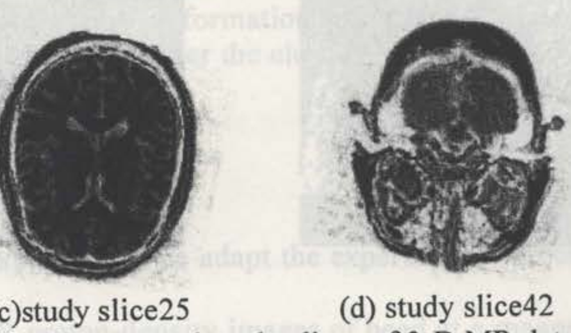

(c)study slice25 (d) study slice42

Figure 4-10 Reference and study slices of 3-D MR data volume

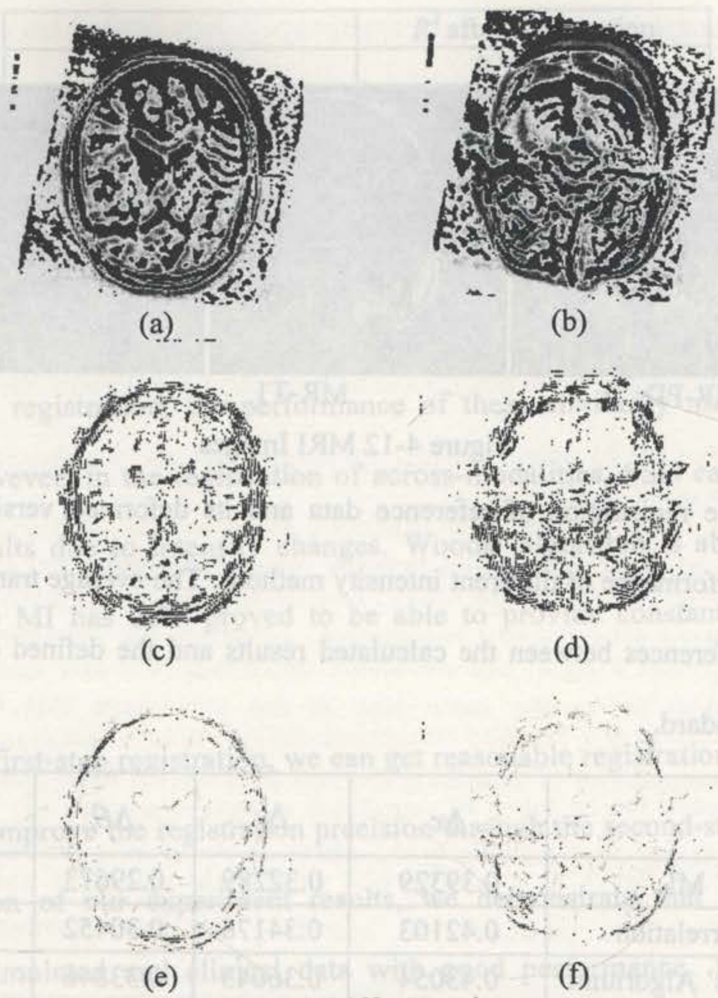

Figure 4-11 Difference images

(a) and (b) are the original difference images before registration; (c) and (d) are the difference images after the first step registration using MI algorithm; (e) and (f) are the difference images after the elastic registration.

4.3.3.4 Performance Comparison between Different Intensity-Similarity Methods

The images of the following modalities have been used to investigate the registration performance of different intensity-based registration methods including maximization of MI, correlation coefficient method, Woods' automatic method.

- MR, Proton Density weighted (PD)
- MR, T1 weighted (T1)
- MR, T2 weighted (T2)

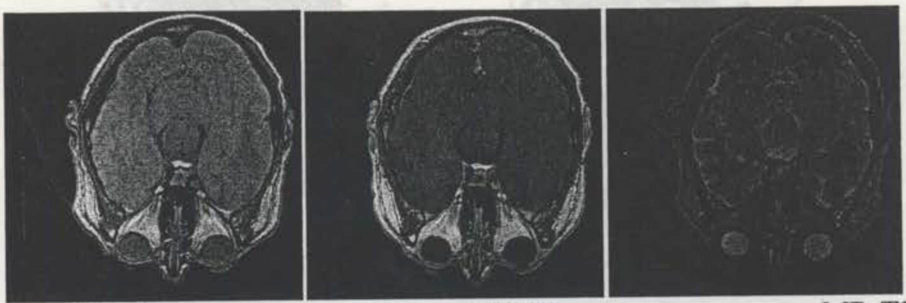

Figure 4-12 MRI Images

Firstly, the registration of reference data and its deformed versions are used to compare the performance of different intensity methods. The average translation, rotation, and scaling differences between the calculated results and the defined ones are used as comparison standard.

	Δx	Δy	$\Delta\theta$	Δs
MI	0.39329	0.32289	0.29673	0.0045
Correlation	0.42103	0.34176	0.30452	0.0069
Woods' Algorithm	0.43054	0.36043	0.33846	0.0085
SSD	0.46027	0.35014	0.37573	0.0091

Table 4-1 Performance Comparison Using Phantom Data

The squared correlation coefficient R^2 is calculated before and after the registration of different MR modal images to test the registration performance of different approaches. The average R^2 before registration of the 3-D MR-T1 and MR-PD slices is 0.900640; the average R^2 before registration of the 3-D MR-T2 and MR-PD slices is 0.900236.

	R^2 after registration
MI	0.936498
Correlation	0.902362
Woods' Algorithm	0.901329
SSD	0.900867

Table 4-2 Performance Comparison of the Registration between MR-T1 and MR-PD

	R^2 after registration
MI	0.925371
Correlation	0.902874
Woods' Algorithm	0.902665
SSD	0.892437

Table 4-3 Performance Comparison of the Registration between MR-T2 and MR-PD

From the experimental results of Table 4-1 to Table 4-3, we find out that for the Phantom image registration, the performance of these similarity measurements is not significant. However, in the registration of across-modalities, SSD cannot provide good registration results due to intensity changes. Woods' algorithm is able to find optimal solutions, while MI has been proved to be able to provide constant good registration results.

After the first-step registration, we can get reasonable registration results. However, we can further improve the registration precision through the second-step registration. By visual inspection of our experiment results, we demonstrate that our algorithm can register both simulated and clinical data with good performance. The algorithm also works well with noisy data and no noise filtering process is needed before the registration procedure being carried out, which shows its robustness against noise.

4.4 Discussion

Computational complexity is one of the important criteria for assessing the performance of registration schemes. In this section, the computational complexity of our algorithm will be analyzed roughly to demonstrate its superior performance of the computational cost.

The computational complexity of the registration process can be estimated by counting an approximate number of arithmetic operations needed for the first-step and the second-step registration using the algorithm proposed in this paper. Because in the first global affine registration step, we mainly adopt the rapid algorithm developed by Woods and the Mutual Information (MI) algorithm, we will concentrate on analyzing the computational cost of the second elastic registration step.

Suppose we work with images containing $r * c = n$ pixels and we divide the images into $\frac{r * c}{m * m}$ subimages ($1 \le m * m \prec n$) of size $m * m$ pixels. Because we are working on the basis of assumption that the images are registered up to small local elastic deformations after the first registration, we define the searching range for each individual window to be the same size as the sub-image that is $m * m$ pixels. Computational complexity of searching the best position for each individual subimage is determined mainly by Equation 4-12, which is about m^2, and iterative times are about $c_c * m^2$ (c_c is a constant), so, searching the best position for individual subimage costs about $c_c * m^2 * m^2$ operations. There are $\frac{r * c}{m * m}$ images, so the local elastic registration computational complexity is $o(\frac{r * c}{m * m} * c_c * m^4) = o(nm^2)$.

The algorithm was implemented on an IBM personal computer (Intel Pentium 4, 1600MHz). The computation time required for our 2-D elastic registrations using Woods' algorithm as the first step of the registration is about 120 seconds, while using MI method as the first step of the registration, we need about 440 seconds to perform our registration process. In our second step registration, we just need about 10 seconds that vary according to the selected size of the windows (subimages).

From the analysis and experimental results, we demonstrate our elastic algorithm has almost as good computational performance as the selected affine registration algorithm of Woods and MI method, and it is a potential solution to the real clinical registration.

In order to find out its influence on registration results, we alter the subimage size during the implementation of our series of experiments. By choosing the smallest size of 1*1 pixel for each subimage in our registration experiments, we found out that the image spatial connectivity would be violated, which would result in incorrect registration. The mismatch is mainly due to the reason that the spatial context of each pixel has not been taken into account. The use of larger subimage size enables us to solve the spatial connectivity problem mentioned above to a certain extent because we are taking more spatial information into consideration. However, too large a subimage size cannot always result in accurate elastic registration results because it is easily being trapped in local minima if the subimage size is too large. In order to get accurate registration results, we select subimage size from 4*4 pixels to 8*8 pixels in our series of experiments.

We intended to make a further improvement to our algorithm by repeating the two-step registration process. However, since exhaustive searching did not significantly increase the accuracy of our registration results, and also due to its higher computational cost by the iteration process, as a result, the extra iterative registration process is unnecessary.

4.5 Summary

We have described an elastic medical image registration algorithm where the images are firstly registered using global affine transformation and then through the second elastic registration step, the local elastic deformations are matched.

The approach has four main advantages: the first attractive feature of this registration approach is that it can register the medical images with high performance; the second attractive feature is that it is an automatic algorithm, using the raw intensity as feature space, the algorithm requires no human intervention and can perform registration automatically; thirdly, by analyzing its computational complexity, we proved that our algorithm can register images more rapidly; finally, it is robust against noise.

The algorithm has been validated by simulated data, noisy data and clinical tomographic image data. It has been demonstrated that our algorithm has high precision in coping with both rigid and local elastic deformations and superior computational efficiency.

CHAPTER 5 AUTOMATIC HYBRID REGISTRATION FOR MEDICAL IMAGES

Study of anatomic structure and physiology of internal organs is often aided by different imaging modalities that highlight different aspects of the organs or structures. Both intra-subject registration and inter-subject registration has been the subject of extensive study in medical imaging literatures. These registration methods seek to optimize values of a cost function which defines the similarity measures between the images. The similarity measures can be the sum of squares of the distances between certain homogeneous features or gray values in the two image sets to be registered.

The challenges created by inter-subject variations in the organ structures promote researchers to explore the hybrid approaches for biomedical image registration. Hybrid registration approaches, combining the intensity-based algorithms with landmark-based methods and making use of the merits of both these methods, have potential to achieve automatic and high biomedical registration performance.

In this chapter, two hybrid registration methods for medical images are presented. In these approaches, firstly, intensity-based affine registration is performed to provide an initial estimation; and then the registration results are registered with high accuracy in the second step by using landmark based approach. Automatic landmark localization methods are introduced and thin-plate splines are used as elastic registration interpolation method.

5.1 Thin-Plate Splines

Spline is referred to as a long flexible strip of metal, which takes a least bent shape when some points along the spline. This bent spline can be used to model the surface of deformed objects. Because it can produce a smooth spline interpolation, has high computation speed, and can correct the local elastic deformations by mapping the study landmark points to the corresponding points in the reference image, Thin-plate splines (TPS) are used in our elastic registration process. The thin-plate spline interpolation was firstly introduced into medical image registration area by Bookstein [BOO 1989] and since then, it has been one of commonly used elastic registration methods. [ROH 2000] gave a good study about elastic registration based on TPS.

The landmarks of reference image and study image are $P = \{p_i = (x_i, y_i) | i = 1,2,......n\} \in I_R$ and $Q = \{q_i = (x_i', y_i') | i = 1,2,......n\} \in I_S$. To map the corresponding landmark points and to produce a smooth interpolation, a transformation function f: $f(p_i) = q_i, i = 1,2,..., n$ used to minimize the energy function which reflects the amount of variation, must be determined. Thin-plate splines (TPS) are member of a family of splines that are based on radial basis functions. For a TPS function *f(x,y)*, the least bending energy of the thin-plate spline function is:

$$E = \iint_{R^2} \left(\left(\frac{\partial^2 f}{\partial x^2} \right)^2 + 2\left(\frac{\partial^2 f}{\partial x \partial y} \right) + \left(\frac{\partial^2 f}{\partial y^2} \right)^2 \right) dxdy \qquad \text{Equation 5-1}$$

The TPS model transforms the coordinate of the original image *(x,y)* into the new coordinate *(x',y')* by

$$(x', y') = (f_x(x, y), f_y(x, y)) \qquad \text{Equation 5-2}$$

where: $f_x(x,y)$ and $f_y(x,y)$ are the functions of displacements in x- and y-direction:

$$f(x, y) = a_1 + a_x x + a_y y + \sum_{i=1}^{n} w_i U(\|(x, y) - p_i\|) \qquad \text{Equation 5-3}$$

Where: the coefficients a_1, a_x *and* a_y define the affine part of the transformation, whereas the coefficient w defines the elastic deformation; P_i is the i^{th} landmark; and $U(\|(x,y)-p_i\|) = \|(x,y)-p_i\|^2 \log(\|(x,y)-p_i\|^2)$ is the radial basis function:

$$U(r) = r^2 \log(r^2)$$

Equation 5-4

where $r = \sqrt{x^2+y^2}$ is the Euclidean distance; U is the fundamental solution of the biharmonic equation $\Delta^2 U = 0$ that satisfies the minimum bending energy:

$$\Delta^2 U = \left(\frac{\partial^2}{\partial x^2} + \frac{\partial^2}{\partial y^2} \right)^2 U = 0$$

Equation 5-5

In order to keep $f(x,y)$ having square integrable second derivatives, the following conditions must be satisfied: $\sum_{i=1}^{n} w_i = 0$ and $\sum_{i=1}^{n} w_i x_i = \sum_{i=1}^{n} w_i y_i = 0$.

The advantage of writing the displacement function in this form is that it can be expressed in matrix form as follows:

$$f(x,y) = \begin{bmatrix} a_1 & a_x & a_y \end{bmatrix} \begin{bmatrix} 1 \\ x \\ y \end{bmatrix} + \begin{bmatrix} w_1 & w_2 & \dots & w_n \end{bmatrix} \begin{bmatrix} U(r_1) \\ \vdots \\ U(r_2) \end{bmatrix}$$

Equation 5-6

The coefficient vector $a = (a_1, a_x, a_y)^T$ and $w = (w_1, w_2, \dots, w_n)^T$ can be computed through the following linear equations:

$$Kw + Pa = v$$

$$P^T w = 0$$

Equation 5-7

where: v represents column vectors of landmarks; $k_{ij} = U_i(p_j) = U(\|(x_i, y_i) - (x_j, y_j)\|)$; and $(1, x_i, y_i)$ is the ith row in the P. These two vector equations can be solved by:

$$w = K^{-1}(v - Pw)$$

$$a = (P^T K^{-1} P)^{-1} P^T K^{-1} v$$

Equation 5-8

5.2 A Hybrid Registration Method for Monomodal Medical Images

In order to achieve registration results with both high precision and efficiency, in this part, we divide our automatic registration approach into two steps. During the first step, based on image intensity, the two images are registered rigidly and an initial estimation is provided. However, because tissues usually deform in complicated ways, the rigid registration method cannot register images with adequate accuracy. To improve registration accuracy, during the second step, the images are registered iteratively (Figure 5-1) by using thin-plate spline method to solve non-rigid matching by minimizing the bending energy to force correspondence landmarks, which are selected automatically, to good match.

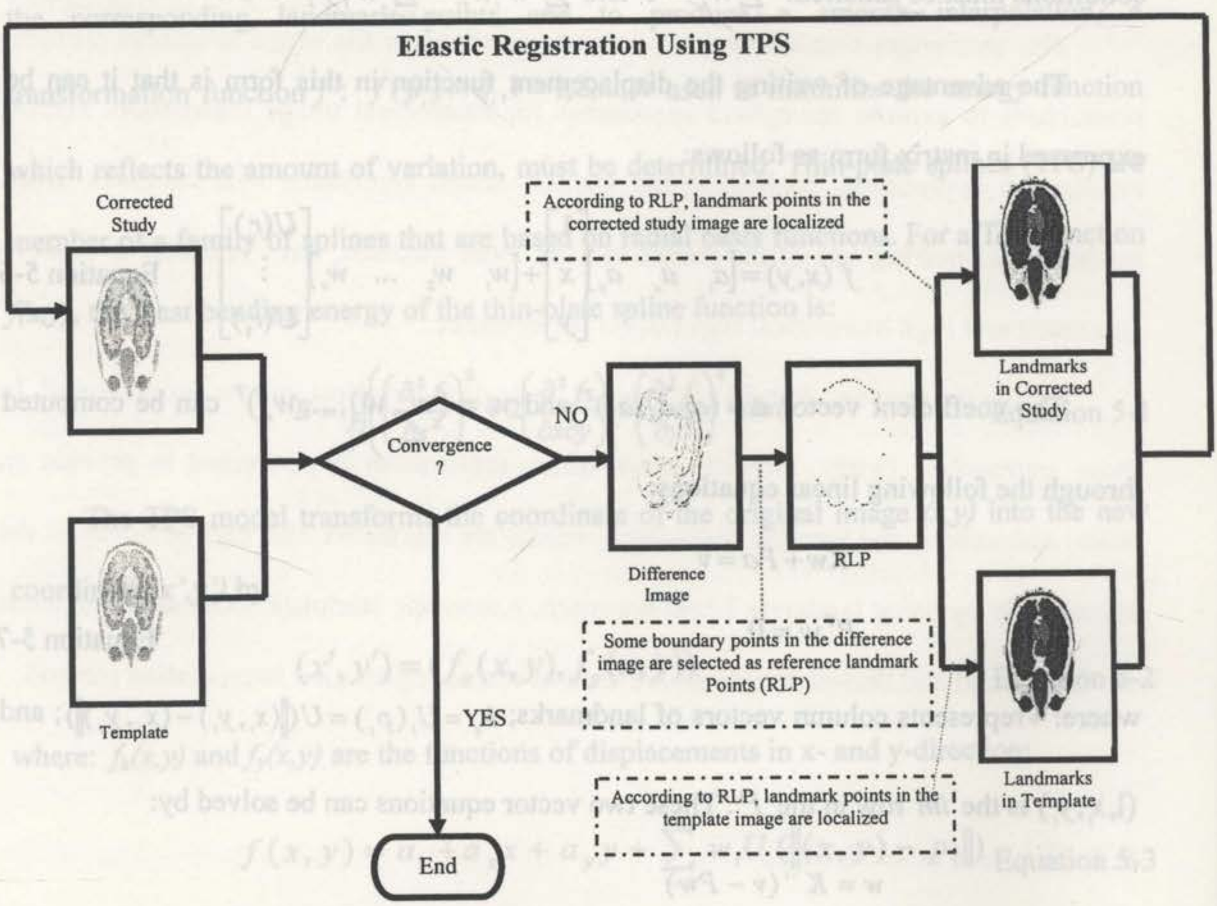

Figure 5-1 Illustration of the Automatic Optimal Registration Algorithm

5.2.1 Registration Method

5.2.1.1 **Step one: Intensity-based Affine Image Registration**

Correlation coefficient technique is used in intensity-based affine registration procedure to correct global differences of translation, rotation, and scaling. Correlation coefficient technique measures the quality of a least square fitting to the original data. The sum of squared values ss_{RR}, ss_{SS}, ss_{RS} of reference image and study image with size of $n = r * c$ can be defined as:

$$ss_{RR} = \sum(I_R(i) - \bar{I}_R)^2 = \sum I_R^{\ 2} - n\bar{I}_R^{\ 2}$$

$$ss_{SS} = \sum_i(I_S(i) - \bar{I}_S)^2 = \sum_i I_S^{\ 2} - n\bar{I}_S^{\ 2}$$

$$ss_{RS} = \sum_i(I_R(i) - \bar{I}_R)(I_S(i) - \bar{I}_S) = \sum_i I_R I_S - n\bar{I}_R\bar{I}_S$$

where $I_R(i)$ is the intensity value at position i of reference image R and $I_S(i)$ is the corresponding intensity value in study image S; $\bar{I}_R$ and $\bar{I}_S$ are the mean intensity value of reference and study image respectively.

The correlation coefficient r is defined as:

$$r = \frac{n\sum_i I_R I_S - \sum_i I_R \sum_i I_S}{\sqrt{[n\sum I_R^{\ 2} - (\sum_i I_R)^2][n\sum_i I_S^{\ 2} - (\sum I_S)^2]}} \qquad \text{Equation 5-9}$$

The sum of squared errors (SSE) is defined as:

$$SSE = ss_{SS}(1 - r^2) \qquad \text{Equation 5-10}$$

From Equation 5-9, we know that when $r^2 = 1$, $SSE = 0$ and good registration is achieved.

The optimization is achieved by Simplex optimization technique, and bilinear interpolation is used in registration transformations. After the global intensity-based registration, rigid displacements between the two images have been corrected.

5.2.1.2 Step two: Landmark-based Elastic Image Registration

The results of this first step rigid registration are used to initialize point correspondence based registration, which has high computation speed and can correct the local elastic deformations.

5.2.1.2.1 Automatic Landmark Points Localization and Elastic Registration Using Iterative Algorithm

Usually, landmark points are localized manually or semi-automatically and the procedure of extracting the corresponding landmarks from the two images is difficult. In our approach, iterative algorithm is used to localize the landmarks automatically and to refine the registration. The thin-plate spline is used as elastic registration method and also helps in landmark localization. Figure 5-2 explains the automatic method of selection landmarks from the images. The sum of squared differences (SSD) is used to measure the quality of the registration and serves as the stopping criterion of the iterations.

STEP 1: Intensity-Based Rigid Registration: Registration Initialization

STEP 2: Iterative Automatic Registration: Landmark-Based Elastic Registration Using TPS

To simplify the description, we assume the intensity of the image background is equal to zero.

1. The Reference Image Computation

   The difference image between the template (T) and the corrected study (CS) serves as the reference image in the following steps.

2. Region-of-Interest (ROI) Definition

   The zero regions imply that these regions in T and CS have been registered and can be ignored in the following registration iterations, so the non-zero regions of the reference image are defined as Region-of-Interest (ROI).

3. Reference Landmarks Definition

   In the reference image, some ROI boundary points are selected as reference landmarks:

   $$L_R = \{(x_i, y_i) \mid (x_i, y_i) \in ROI \;,\; i = 1, \cdots m + n\}$$

4. Corresponding Landmark Points Localization in the Template (T) and the Corrected Study (CS) images

   Landmarks are localized in the Template (T) and the Corrected Study image (CS) parallel. Once a point is selected as landmark in one of the images, the point with the same coordinates in the other image will not be selected as landmark anymore, i.e. $L_T \cap L_{CS} = \phi$ and $L_T \cap L_{CS} = L_R$.

   a. Landmark Localization in Template (T)

      Points in T, which have the same coordinates as the reference landmarks are selected as landmarks of T:

      $$L_T = \{(x_i, y_i) \mid (x_i, y_i) \in L_R \wedge (x_i, y_i) \notin L_{CS} \wedge (x_i, y_i) \in T \wedge I(x_i, y_i) \neq 0\},$$

      assumed to have m points in the set;

      Other n landmarks are searched in their corresponding 8-adjacent regions respectively and the closest to the reference landmarks are selected as

landmarks:

$$L_{TA} = \left\{ \begin{array}{l} (x_j, y_j) \mid (x_j, y_j) \in 8-adjacent \quad -region \quad of\ (x_p, y_p) \\ \quad \wedge \text{ closest to } \quad (x_p, y_p)\ ((x_p, y_p) \in L_R \wedge (x_p, y_p) \notin L_T) \\ \quad \wedge\ (x_j, y_j) \in T \wedge I(x_j, y_j) \neq 0 \end{array} \right\}$$

with m points.

Landmark points of template image are $L_{TP} = L_T \cup L_{TA}$.

b. Landmark Localization in Corrected Study (CS)

Points in CS, which have the same coordinates as the reference landmarks are selected as landmarks of CS:

$$L_{CS} = \{(x_i, y_i) \mid (x_i, y_i) \in L_R \wedge (x_i, y_i) \notin L_T \wedge (x_i, y_i) \in CS \wedge I(x_i, y_i) \neq 0\}$$

assumed to have m points;

Other m landmarks are searched in their corresponding 8-adjacent regions respectively and the closest to the reference landmarks are selected as landmarks:

$$L_{CSA} = \left\{ \begin{array}{l} (x_j, y_j) \mid (x_j, y_j) \in 8-adjacent \quad -region \quad of\ (x_q, y_q) \in L_R \\ \quad \wedge \text{ closest to } \quad (x_q, y_q)\ (x_q, y_q) \in L_R \wedge (x_q, y_q) \notin L_{CS}) \\ \quad \wedge\ (x_j, y_j) \in CS \wedge I(x_j, y_j) \neq 0 \end{array} \right\}$$

with n points.

Landmark points of corrected study image are $L_{CSP} = L_{CS} \cup L_{CSA}$.

5. Elastic Registration Using TPS
6. If the stopping criterion (SSD) is not met, then Goto 1.

Figure 5-2 Automatic Optimal Algorithm Description

5.2.1.2.2 Convergence Criterion

One of simple convergence criteria is the sum of squared differences (SSD) between the images, which exhibits a minimum in the case of good registration. We consider two concurrent criteria for deciding when to stop the iteration process. The first one is self-evident: we stop when a good match is met (Equation 5-11). The second relates to relative

SSD reducing ratio (Equation 5-12), (where i presents the ith iteration) at each successive iteration step: the convergence is obtained whenever this reducing ratio is less than a predetermined threshold.

$$E = \sum e^2 = \frac{1}{n} \sum_{(x,y)} (I_T(x,y) - I_s(x,y))^2 \qquad \text{Equation 5-11}$$

$$SSD\ \text{Re}\,ducing\ Ratio = {SSD_i}/{SSD_{i-1}} \qquad \text{Equation 5-12}$$

5.2.1.3 Convergence Speed and Continuity

In order to improve the convergence speed and keep the corrected study image continuous as well, we adopt two methods in the second registration step. Intuitively, in order to keep the corrected study image continuous, we interpolate the corrected study (CS) image in each iteration, Figure 5-3.

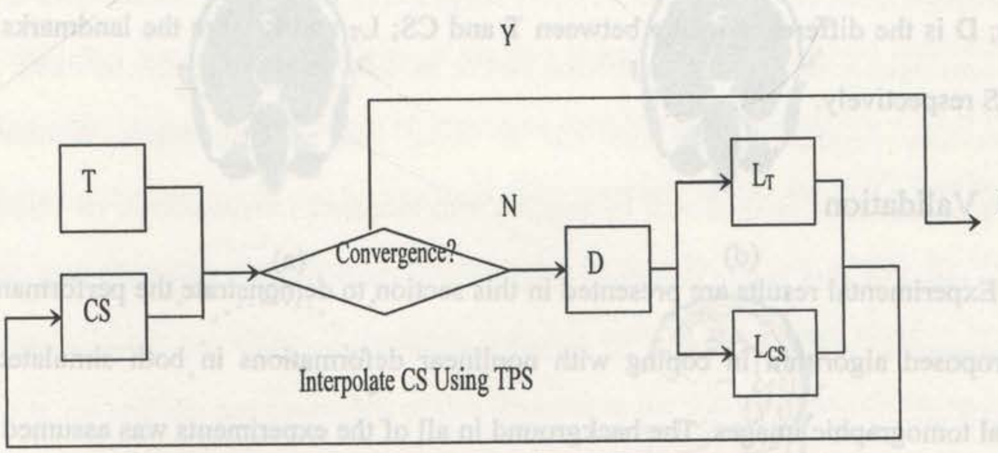

Figure 5-3 Method One for Keeping the Continuity of CS

Alternatively, we keep the registered parts of the CS image unmoved in the following iterations, i.e., we suppose we have found the accurate positions for these parts, Figure 5-4. By interpolating neighborhoods of the matched data and data to be refined in the following iteration, we can avoid the significant discontinuity. In order to keep local optima, we compare those overlapped parts with the registered data in the last iteration and keep the better ones. After we get an ideal registration results, we interpolate the CS image to guarantee its continuity. By using this method, we can keep the registered image continuous and can achieve a quick convergence as well.

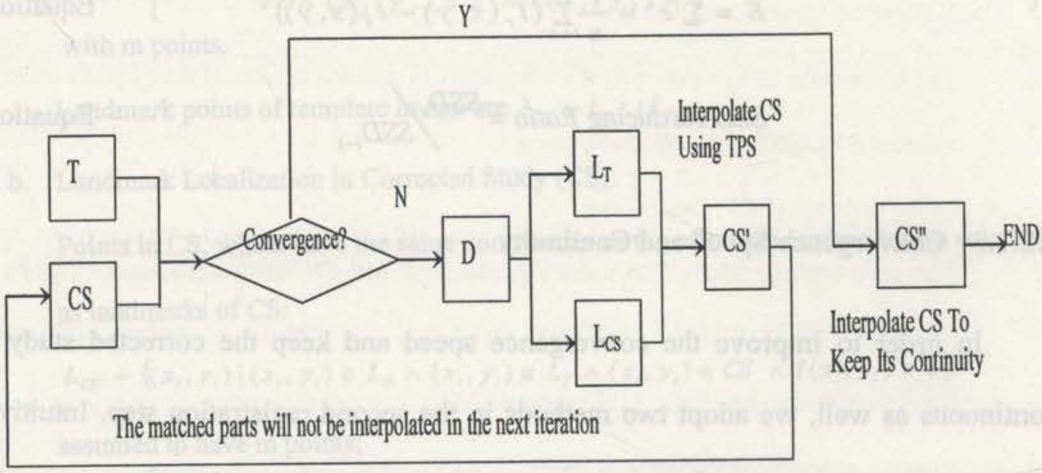

Figure 5-4 Method Two for Keeping the Continuity of CS

In Figure 5-3 and Figure 5-4, T is the template image; CS is the corrected study image; D is the difference image between T and CS; L_T and L_{CS} are the landmarks of T and CS respectively.

5.2.2 Validation

Experimental results are presented in this section to demonstrate the performance of the proposed algorithm in coping with nonlinear deformations in both simulated and clinical tomographic images. The background in all of the experiments was assumed to be black (intensity is equal to zero). Thus, we would not select landmark points from background.

We apply our method to 2D phantom images (Figure 5-5 and Figure 5-6) to test its validity. Figure 5-5 gives the global affine registration results that serve as initial guess for the automatic landmark localization and elastic registration. Figure 5-6 shows landmark points, displacements and elastic registration results.

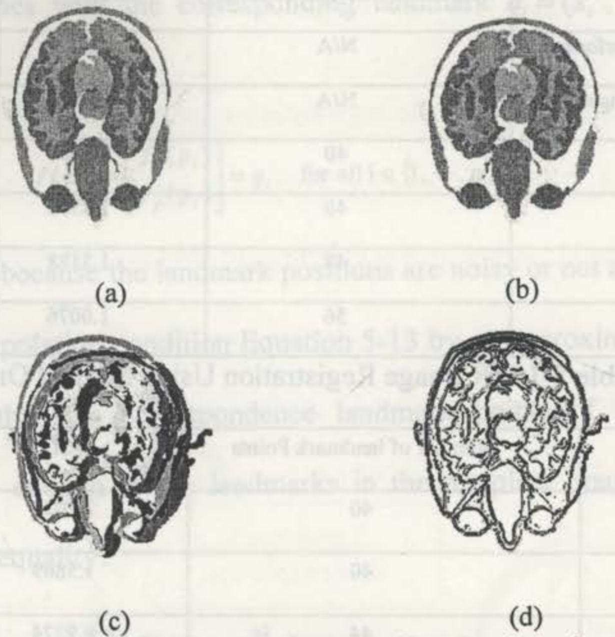

Figure 5-5 Intensity-based Affine Registration

(a) and (b) are the template and study images respectively; (c) is the difference between the two images; (d) is the result of the first-step registration.

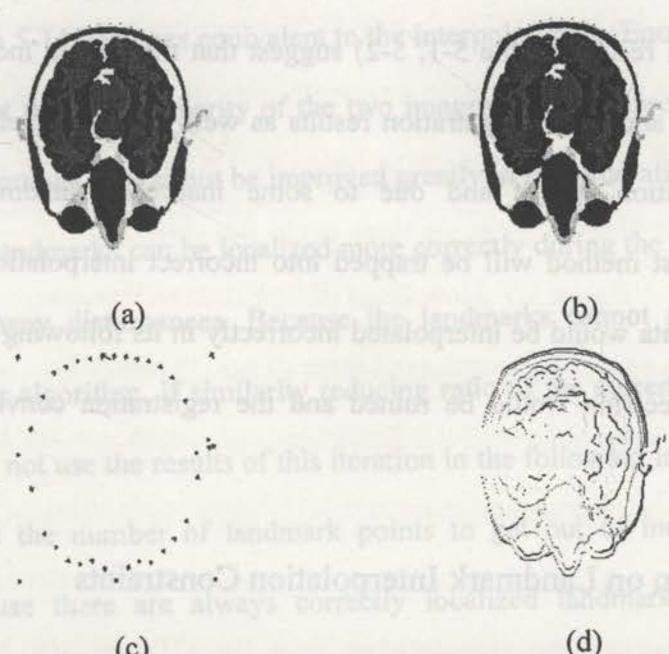

Figure 5-6 Registration Iteration with Automatic Landmark Localization

(a) and (b) are the ROI with landmark points shown by black dots of the registration; (c) the arrows show the displacements between the corresponding landmarks; (d) the differences between the template and the corrected study images after registration iterations using TPS

Iteration	Number of Landmark Points	SSD	SSD Ratio
No Registration Performed	N/A	6.6027	N/A
Global Affine Registration	N/A	3.9426	0.65416
3	40	2.8408	0.72048
7	40	1.7562	0.61820
12	48	1.3188	0.75093
19	56	1.0076	0.76400

Table 5-1 MR Image Registration Using Method One

Iteration No.	Number of landmark Points	SSD	SSD Ratio
3	40	2.7025	0.68197
7	40	1.5869	0.58725
11	44	0.9574	0.60326
15	50	0.5192	0.54231

Table 5-2 MR Image Registration Using Method Two

Experimental results (Table 5-1, 5-2) suggest that the second method give a more rapid convergence and better registration results as well. Comparatively, by using all of the previous iteration results and due to some inaccurate landmark localizations, sometimes, the first method will be trapped into incorrect interpolations, in which, the already matched data would be interpolated incorrectly in its following iterations. Hence, the registration precision would be ruined and the registration convergence would be slowed down.

5.2.3 Discussion on Landmark Interpolation Constraints

The constraints of landmark interpolation can be distinguished into two classes: hard constraints, which need exact interpolation, and soft constraints, which just need approximate interpolation. The obvious choice is to enforce the interpolating constraints so that the continuously interpolation function can interpolate landmark $p_i = (x_i, y_i)$ in the study image coincides with the corresponding landmark $q_i = (x_i', y_i')$ in the template image.

$$f(p_i) = \begin{bmatrix} f_x(p_i) \\ f_y(p_i) \end{bmatrix} = q_i \quad \text{for all } i \in \{1, \cdots, n\} \qquad \text{Equation 5-13}$$

Alternatively, because the landmark positions are noisy or not accurately known, we can replace the interpolation condition Equation 5-13 by an approximation inequality. We will only require that the correspondence landmark points of the study image be interpolated closely enough to the landmarks in the template image. For example, we might impose the inequality:

$$\sum_{i=1}^{n} \| f(p_i) - q_i \|^2 \le \varepsilon \qquad \text{Equation 5-14}$$

where: ε is a priori given threshold. Clearly, when ε tends to zero, the approximation problem Equation 5-14 becomes equivalent to the interpolation by Equation 5-13.

We find out that the similarity of the two images can be improved significantly in the first a few iterations but cannot be improved greatly in some iterations. This is because that most of the landmarks can be localized more correctly during the first a few iterations due to not so many disturbances. Because the landmarks cannot always be localized accurately, in our algorithm, if similarity reducing ratio of the current iteration is greater than 1.0, we will not use the results of this iteration in the following interpolation iteration and also change the number of landmark points to get out of incorrect interpolation iterations. Because there are always correctly localized landmarks and as iterations continue, we can get accurate registration result using both of methods described in Figure 5-3 and Figure 5-4.

5.3 Automated Elastic Image Registration Method for CT and MR Brain Images

In this part, an automated elastic registration approach for brain CT and MR images is presented (Figure 5-7). The registration process is carried out automatically and both geometrical features and image intensity information are used for similarity measure.

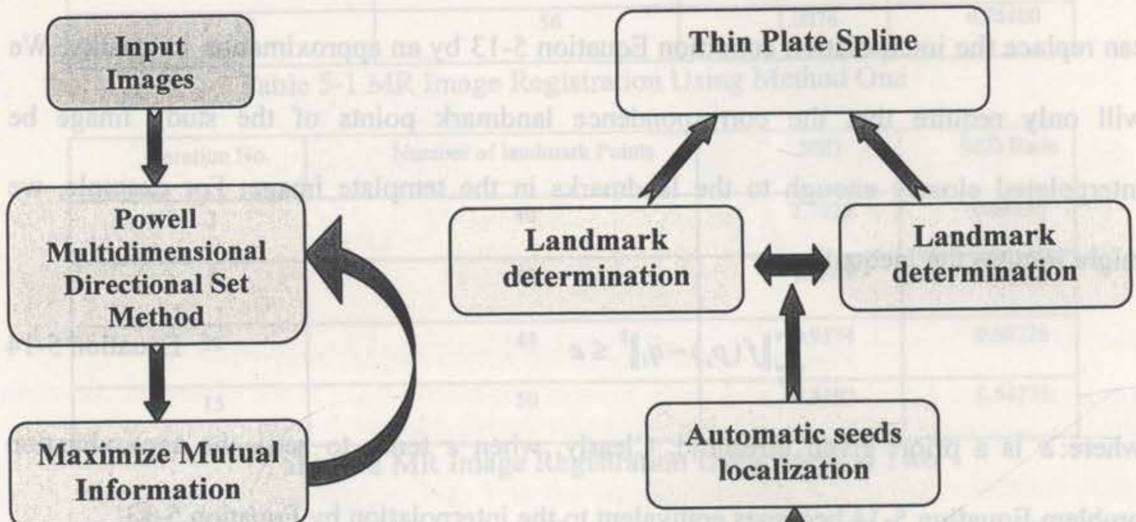

Figure 5-7 Flow Chart of Registration Process

The registration approach comprises of three stages (Figure 5-7):

(I) Maximization of mutual information: not dependent on assumptions about relation between image intensities in different modalities;

(II) Automatic landmark extraction: extracts landmarks automatically from the skull region upon segmentation from the CT and MR images and forms landmark point pairs;

(III) Thin-plate spline transformation: elastically registers the reference image using the extracted landmark point pairs.

5.3.1 Registration Method

5.3.1.1 Maximization of Mutual Information

As we mentioned previously, mutual information is the measure of difference in sum of entropies of the individual images at overlap and the joint entropy of the combined images. When two similar images are perfectly aligned, the amount of information that is shared by both images is maximized, whereas the amount of information shared is minimized when out of alignment between the images occurred. That means if the images are perfectly overlapped, the joint entropy is minimized and the MI is maximized.

5.3.1.2 Automatic Landmark Extraction

When register CT and MR images by landmark-based method, features that can be distinguished from both modalities are preferable. It is relatively easy to identify the skin surface in the MR and CT head images. However, because it will be easily deformed from scan to scan, skin is not a reliable feature for landmark extraction. Because skull is rigid structure, the inner rim and outer rim of the skull are more suitable features than the skin surface.

In CT images, the skull region has much higher intensity (a ridge), whereas the skull region in MR images has lower intensity (a trough) in MR image. Therefore, the skull region can be extracted by the ridge-seeking operator, and then the landmarks can be searched in the skull region. Differential operator is a good choice to detect ridge or trough region in an image. There are a number of geometrical operators that approximate ridges well. In this study, the *Ivv* operator, the second derivative of the image intensity function in direction of v is adopted [MAI 1996]. Define a local gradient based coordinate system spanned by a gradient $\boldsymbol{w}$ and its right-handed normal $\boldsymbol{v}$ as:

$$\mathbf{v} = \begin{bmatrix} I_y \\ -I_x \end{bmatrix} \quad \text{and} \quad \mathbf{w} = \begin{bmatrix} I_x \\ I_y \end{bmatrix} \qquad \text{Equation 5-15}$$

where I denotes the image intensity function and subscripts represent derivatives along specific directions. The second order derivative of the image intensity function in the v direction denoted by I_{vv} is a good ridge measure and it can be computed as follows:

$$I_{vv} = \frac{1}{\|v\|^2}(v \cdot \nabla)^2 I = (I_y^2 I_{xx} - 2I_x I_y I_{xy} + I_x^2 I_{yy})(I_x^2 + I_y^2)^{-1} \qquad \text{Equation 5-16}$$

where $\nabla = (\partial/\partial x, \partial/\partial y)$. Since Ivv operator uses a gradient-based local coordinate system (v,w) instead of the usual Cartesian coordinate system, it is invariant with respect to rotation and translation of the object. The Ivv feature image now depicts the ridge of the input image.

The skull can be segmented from the head image by average pixel intensity when the ridge operator locates the region of the skull. From the segmented skull images, the inner table and outer table of the skull can be extracted. When the skull table is delineated from the skull, edge detection is performed on the skull table. In a few cases, some of the irrelevant features may also be delineated as well, which will introduce weak edges on the edge image and result in incorrect landmark localization. To overcome this problem, the edge image needs to undergo the component labeling process where the image is scanned and its pixels are grouped into components based on pixel connectivity. After the component labeling process, landmarks are localized on the corners of the edge image. These landmarks are extracted and paired up with the corresponding landmarks in the other image.

5.3.1.3 Elastic Registration by Thin-Plate Splines (TPS)

After the landmark pairs are identified from the landmark extraction, the displacements necessary to map the location of the landmarks in the target (MR) image to the landmarks in the reference (CT) image can be approximated by analytical functions such as high-degree polynomials and splines. Thin-plate splines (TPS) is used in our registration refinement process.

5.3.2 Experiments and Discussion

Experiments are carried out to assess the performance of the proposed automated algorithm by registering some deformed Phantom images, and MR images to CT images.

5.3.2.1 Phantom Image Registration

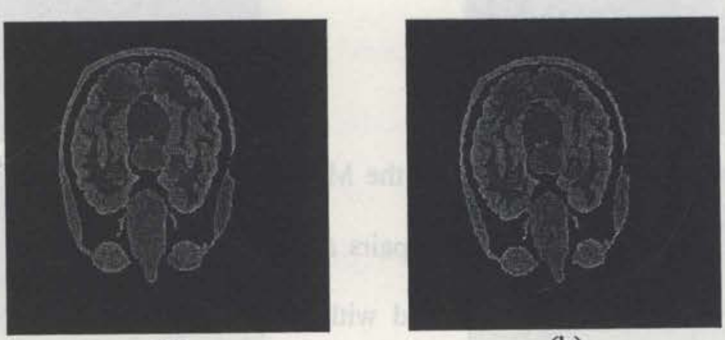

(a) (b)

Figure 5-8 Phantom Data for Registration

(a) Reference image; (b) Study image is deformed by 5 degrees rotation, 6 pixels displacement in x direction, and 2 pixels displacement in y direction

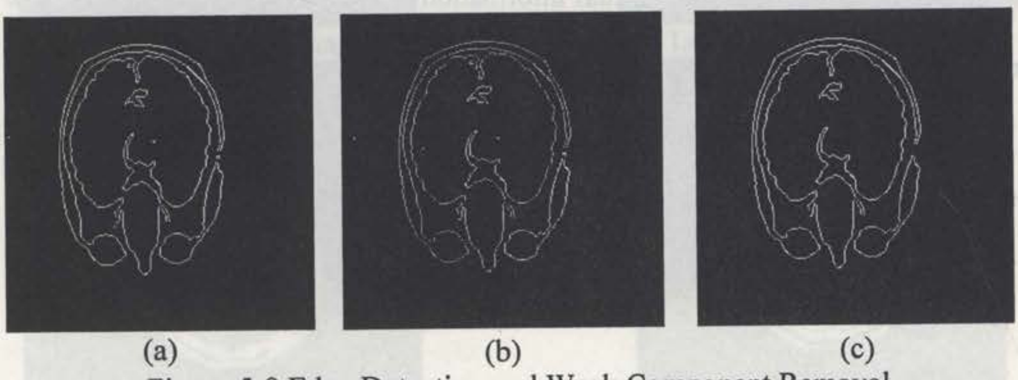

(a) (b) (c)

Figure 5-9 Edge Detection and Weak Component Removal

(a) Edge image detected using Sobel operator; (b) Connected component labeled by different colors (8-Neighbor); (c) Weak components removed

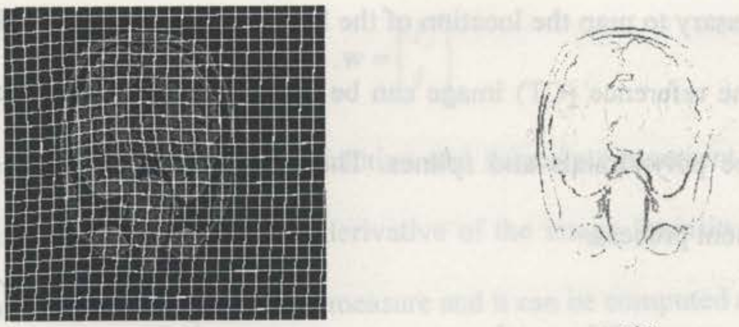

(a) (b)

Figure 5-10 Registration Result Using TPS

(a) Registration result with deformation grid overlaid; (b) Difference between reference and the corrected study image

5.3.2.2 MR-CT Image Registration

We present the results of two series of experiments:

(1) MR-T1 to CT;

(2) MR-T2 to CT.

In the first series of experiments, the MR-T1 images are rigidly registered to CT images in Stage I. The landmark point pairs are then extracted in Stage II. Finally, the MR-T1 images are elastically registered with the CT images in Stage III. The same approaches are used in the second series of experiment for MR-T2 to CT image registration. The maximization process is accomplished by Powell optimization method. Once the maximum value of the mutual information is found, the images should have been geometrically aligned.

Figure 5-11 and 5-12 show, the registration sequences of MR-T1 to CT and MR-T2 to CT respectively.

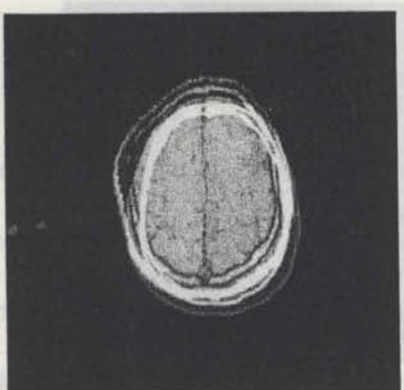

Combined image before registration

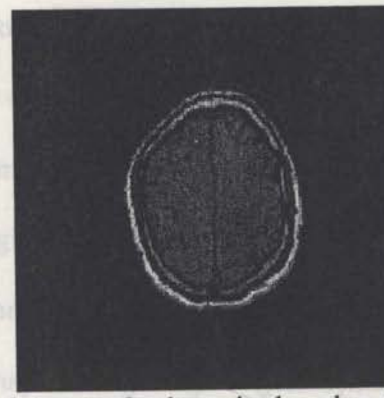

MR-T1 image after intensity-based registration

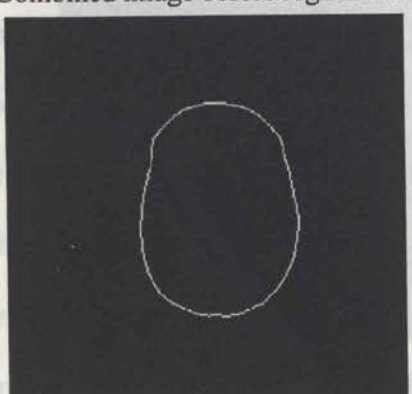

Contour of CT image

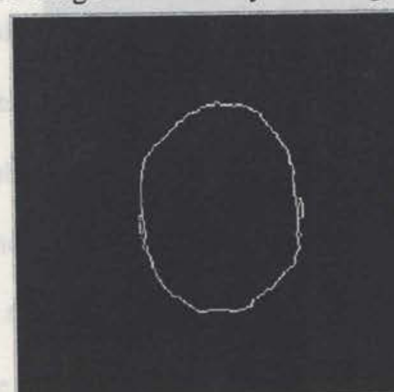

Contour on MR-T1 image

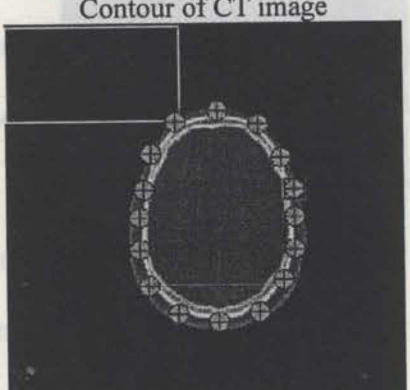

Landmarks on CT image

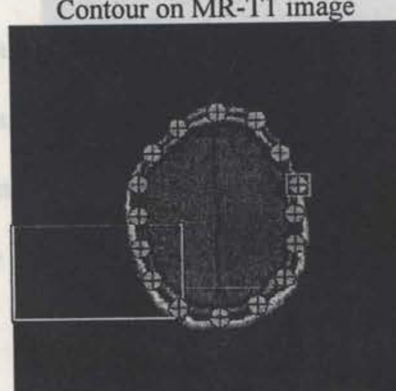

Landmarks on MR image

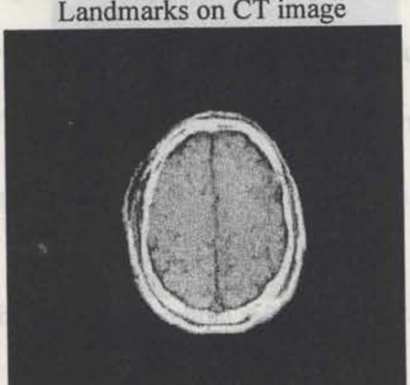

Combined image after intensity-based registration

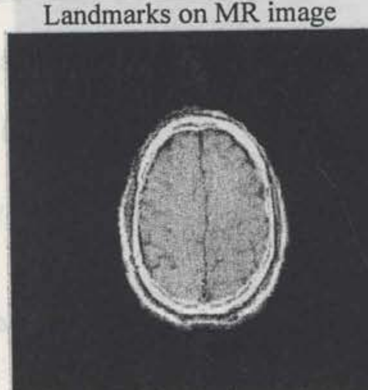

Combined image after landmark-based registration

Figure 5-11 Registration between MR-T1 and CT image

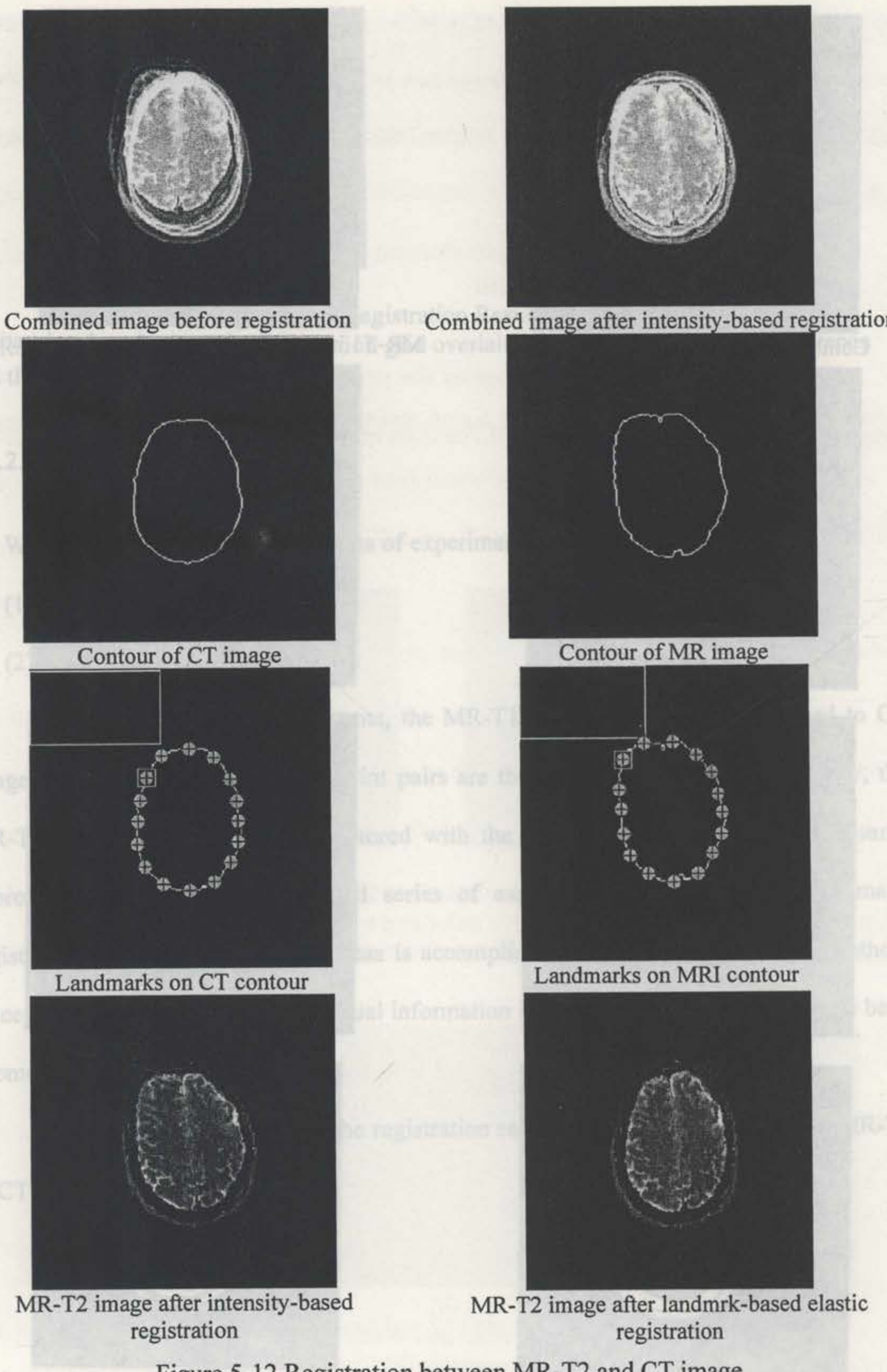

Figure 5-12 Registration between MR-T2 and CT image

As expected, the maximization of MI yields good results in correcting the translation and rotation difference between images for a coarse registration. However, from experiments, we can discover that the elastic deformation cannot be corrected. Therefore, the elastic registration is required to get better registration performance. The automatic landmark extraction process can extract landmarks from images with a clear and continuous definition of skull region. However, it may fail for image slices acquired at the top portion of the head. This is because the outer table and the inner table of the skull are connected in these images and it is very difficult to distinguish them with an automatic algorithm. The identification process of the skull table is generally easier in CT and MR-T2 than that in MR-T1. This may be due to the fact that CT head images have a larger contrast between the skull and the tissues, whereas the MR-T2 head images have a larger contrast between the skull and the CSF. While the skull region appears dark in MR-T1 images, the surrounding tissue appears rather dim as well. Therefore, incorrect landmark extraction may occur more frequently in MR-T1 images.

For the TPS transformation process, deformation near the landmarks is corrected. The registration result is enhanced as the number of landmark points increase and the landmarks distribute around deformed regions. When incorporating the landmarks point pairs generated from the automatic landmarks extraction process, images with deformation near the skull can be successfully registered. However, the results are not satisfactory for images with deformation in the inner brain and the scalps, as the landmarks for this region are difficult to be defined.

5.4 Summary

In this chapter, two hybrid automatic registration methods have been described. In these methods, firstly, intensity-based registration is carried out to correct rigid deformations and provide initial estimation for the landmark-based elastic registration procedure. Then, in the second registration step, two automatic landmark selection methods are introduced and elastic deformations are corrected based on the landmark points localized automatically. The whole registration processes can be carried out automatically, and able to register deformed images. The registration methods yield good results in correcting the difference in spatial alignment between the images when deformation occurs. It is shown that the combination of intensity-based and landmark-based registration increases the registration speed and enables a registration of finer details.

CHAPTER 6 ABDOMINAL IMAGE REGISTRATION BASED ON ACTIVE CONTOUR

Abdominal image registration is a complex and challenging task because of the non-rigid and involuntary motion caused by breath and heartbeat, and elastic deformation of organ structure and volume makes the undertaking even more difficult. Moreover, the improvement of iterative registration efficiency is required for clinical applications. This chapter aims to address these issues.

In this chapter, an efficient, automatic, abdominal image registration method is presented (Figure 6-1). Firstly, on the basis of automatically selected feature points, affine registration is carried out by minimizing the *mean squared error* (MSE) so that affine transformation parameters can be derived directly. Then, based on the contour of the image that has been transformed, the contour of images can be extracted automatically by using active contour model. Finally, the elastic transformation is then performed based on the displacement field obtained by the active contour model.

The proposed approach has been validated by the experiments with PET (Positron Emission Tomography) and CT (Computed Tomography) abdominal images of both intra-subject and inter-subject, monomodal and multimodal images. Experimental results demonstrate that our proposed algorithm has high effectiveness and accuracy, and is efficiently performed, and inexpensive in computation.

Besides, comparison of different active contour approaches, such as traditional snakes, balloon, and Gradient Vector Flow (GVF), are performed to test their influence on registration performance. The comparison results lead to the conclusion that GVF gives the most appropriate results among these approaches.

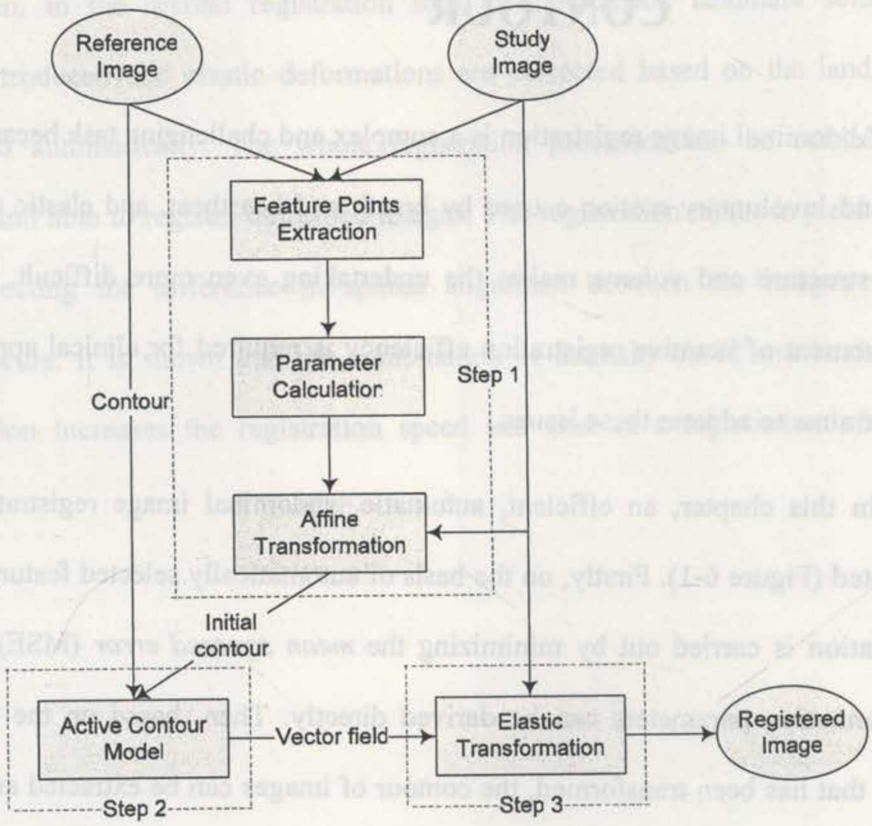

Figure 6-1 Non-iterative, automatic image registration

6.1 Affine Registration

Usually, an optimization algorithm is needed in the registration procedure to serve as a searching strategy; however, the iterative optimization procedure is time-consuming. In order to improve registration efficiency, a non-iterative and automatic affine registration method is proposed.

6.1.1 Automatic Feature Extraction

To get affine transformation parameters, some corresponding feature points between the two images need to be obtained from both statistical and geometrical properties. As the statistical properties, affine-invariant moment-based features are extracted from both images, including the centroids and the focuses of the ellipse that have the same second order moment as each image.

For a discrete function $I(x, y)$, moment of order p and q, m_{pq}, is defined as [NIX 2002]:

$$m_{pq} = \sum_x \sum_y x^p y^q I(x,y) \qquad \text{Equation 6-1}$$

The total mass of a function is represented by zero-order moment:

$$m_{00} = \sum_x \sum_y I(x,y) \qquad \text{Equation 6-2}$$

Thus, the centre of mass $(\bar{x}, \bar{y})$ can be obtained from the ratio of the first-order and the zero-order moment:

$$\bar{x} = \frac{m_{10}}{m_{00}} \text{ and } \bar{y} = \frac{m_{01}}{m_{00}} \qquad \text{Equation 6-3}$$

Some other feature points are obtained from the boundary of the images. First, the boundary of each image is tracked; then several evenly distributed points from each boundary are detected with respect to particular angles between the maximum axes of the images. This is to maintain both the consistency of the correspondence points from both images, and even distribution of the feature points.

Another approach to obtain the feature points is based on the intensity characteristic of the images. In some images, the salient objects might have significant changes in intensity compared to their neighborhood. This nature can be useful to acquire the corresponding points between two images. However, this intensity-based feature point extraction approach is not a good option in multimodal registration due to different intensity characteristics in multimodal images.

In our implementation, we provide a flexible choice for the user to determine how many points required and whether the feature points based on the intensity need to be extracted from the images.

6.1.2 Efficient Affine Transformation Parameter Calculation

In order to improve the registration efficiency, instead of using the traditional iterative optimization method, affine registration parameters are directly derived by minimizing Mean Squared Error (MSE). This approach not only can provide efficient computation but also can generate the smallest difference between the two images to be registered. Umeyama [UME1991] has presented a solution in theorem 1 below that has been proven to give the correct transformation parameters even when the data is corrupted. By using this theorem, the affine transformation parameters that are minimized the MSE can be obtained.

***Theorem* 1**: Let $X = \{x_1, x_2, \ldots, x_n\}$ and $Y = \{y_1, y_2, \ldots, y_n\}$ be corresponding point patterns in m-dimensional space. The minimum value ε^2 of the mean squared error:

$$\varepsilon^2(R,t,c) = \frac{1}{n}\sum_{i=1}^{n}\left\| y_i - (cRx_i + t)\right\|^2 \qquad \text{Equation 6-4}$$

of these two point patterns with respect to the similarity transformation parameters (R: rotation, t: translation, and c: scaling) is given as follows:

$$\varepsilon^2 = \sigma_y^2 - \frac{tr(DS)}{\sigma_x^2}$$ Equation 6-5

where: $$\mu_x = \frac{1}{n}\sum_{i=1}^{n} x_i$$ Equation 6-6

$$\mu_y = \frac{1}{n}\sum_{i=1}^{n} y_i$$ Equation 6-7

$$\sigma_x^2 = \frac{1}{n}\sum_{i=1}^{n}\|x_i - \mu_x\|^2$$ Equation 6-8

$$\sigma_y^2 = \frac{1}{n}\sum_{i=1}^{n}\|y_i - \mu_y\|^2$$ Equation 6-9

$$\Sigma_{xy} = \frac{1}{n}\sum_{i=1}^{n}(y_i - \mu_y)(x_i - \mu_x)^T$$ Equation 6-10

And let a singular value decomposition of Σ_{xy} be UDV^T ($D = \text{diag}(d_i)$, $d_1 \geq d_2 \geq \ldots \geq d_m \geq 0$ and

$$S = \begin{cases} I & if \det(\Sigma_{xy}) \geq 0 \\ diag(1,1,..,1,-1) & if \det(\Sigma_{xy}) < 0 \end{cases}$$ Equation 6-11

Σ_{xy} is a covariance matrix of X and Y, μ_x and μ_y are mean vectors of X and Y, and σ_x^2 and σ_y^2 are variances around the mean vectors of X and Y respectively.

When $\text{rank}(\Sigma_{xy}) > m - 1$, the optimum transformation parameters are determined uniquely as fellows:

$$R = USV^T$$ Equation 6-12

$$t = \mu_y - cR\mu_x$$ Equation 6-13

$$c = \frac{1}{\sigma_x^2} tr(DS) \qquad \text{Equation 6-14}$$

where S in Equ.6-11 must be chosen as:

$$S = \begin{cases} I & if \det(U)\det(V) = 1 \\ diag(1,1,..,1,-1) & if \det(U)\det(V) = -1 \end{cases} \qquad \text{Equation 6-15}$$

when rank(Σ_{xy})=m-1.

Let A and B be the set of the feature points taken from each image, and let the $n \times n$ normalization matrix $K = I - \left(\frac{1}{n}\right)hh^T$, where $h = (1,1,\ldots,1)^T$, then Equation 6-8-Equation 6-10 can be represented as:

$$\sigma_x^2 = \frac{1}{n}\|AK\|^2 \qquad \text{Equation 6-16}$$

$$\sigma_y^2 = \frac{1}{n}\|BK\|^2 \qquad \text{Equation 6-17}$$

$$\Sigma_{xy} = \frac{1}{n} YKX^T \qquad \text{Equation 6-18}$$

and the affine transformation parameters can be obtained from Equation 6-12 to Equation 6-14 where UDV^T is the singular value decomposition of Σ_{xy} and μ_x and μ_y are the mean of A and B respectively.

6.2 Active Contour

6.2.1 Definition

Active contour or Snake is an energy minimizing spline developed by Kass et al [KAS 1988]. The classic snake model attracts initial contour to some image features and minimizes the object energy function, Equation 6-19.

$$E^{*}_{snake} = \int_0^1 E_{snake}(v(s))ds$$

$$= \int_0^1 E_{\text{int}}(v(s)) + E_{image}(v(s)) + E_{con}(v(s))ds \quad \text{Equation 6-19}$$

An active contour can be represented by a curve $v(s) = [x(s), y(s)]$. The contour coordinates (x, y) can be expressed as the function of arc length s. The snakes are influenced by internal forces, image forces, and external constraint forces.

- The internal forces caused by stretching and bending, serve as a smoothness constraint to keep the contour from discontinuity or bending too much. The internal energy responsible for the smoothness and deformation of the contour can be expressed as:

$$E_{\text{int}} = \left(\alpha(s)\left|\frac{dv}{ds}\right|^2 + \beta(s)\left|\frac{d^2v}{ds^2}\right|^2 \right) \Big/ 2 \quad \text{Equation 6-20}$$

$\alpha(s)$ and $\beta(s)$ are the measure elasticity and stiffness of the snake. If $\alpha = 0$ discontinuity happened whereas if $\beta = 0$, the snake will develop a corner.

- The second term of Equation 6-19 is image forces responsible for attracting the snake to the true edge of the image. Kass et al presents three different energy functions, i.e. line, edge and termination, which can be expressed as:

$$E_{image} = w_{line}E_{line} + w_{edge}E_{edge} + w_{term}E_{term} \quad \text{Equation 6-21}$$

- The third term of Equation 6-19 comes from external constraints imposed either by a user or some other higher level process which may force the snake toward or away from particular features.

6.2.2 Active Contour Models

The classic active contour model above is flexible since it maintains the shape as a curve and the final form of the contour can be influenced by feedback from a higher level process. However, this classic snake is sensitive to the initial contour guess and cannot deal with concavity. Some approaches have been proposed to solve these problems, for example, balloon and gradient vector flow (GVF).

6.2.2.1 Balloon

Cohen [COH 1993] proposed an active contour known as "balloon". In balloon model, the initial contour does not need to be close to the target contour as in the original version of snake. The original snake is modified by using an inflation force so that the curve reacts like a balloon. The contour will be inflated and pass the weak edges but will be stopped if the edge is strong with respect to the inflation force.

6.2.2.2 Gradient Vector Flow

Another solution to solve the problem of initialization and convergence of the classic snake has been proposed by Xu et al. [XU 1998]. In this new solution, an external force field, which is called *gradient vector flow* (GVF) is defined to move boundary into concavities. GVF model is more insensitive to the initial contour than the traditional snake. The GVF is defined as a vector field $\mathbf{v}(x, y) = (u(x,y), v(x,y))$ that minimizes the energy function:

$$\varepsilon = \iint \mu\left(u_x^2 + u_y^2 + v_x^2 + v_y^2\right) + |\nabla f|^2 |\mathbf{v} - \nabla f|^2 \, dxdy \qquad \text{Equation 6-22}$$

where μ is a regularization parameter which should be set according to the amount of noise of the image and $f(x, y)$ is the edge map derived from the image.

6.2.3 Image Registration Using Active Contour

The application of active contours in image registration has been studied by many researchers. [DAV 1996] proposed brain image registration that utilizes active contour algorithms as the first stage of their approach. In the first stage, they identify *J* corresponding regions in the two images. Thus the active contour algorithm is used to extract the boundary of each of the *J* selected regions in each image. Then the mapping is used later in elastic deformation transformation to perform the registration. The method was tested by registering magnetic resonance images to atlas images.

Another current application of active contour in image registration was performed by [KIN 2004]. The active contour technique was adopted in the second stage of the image segmentation before the registration of Cervigram images. The initial contour was then derived from the first stage of the segmentation step that utilized clustering. After the active contour converges to the desired boundary, Fourier and correlation methods were used to make some corrections necessary for the registration.

6.2.4 The Implementation of Active Contour

The reason we adopt the active contour algorithm is that it can produce the motion field of the contour that will be used to perform the elastic transformation, by an efficient computation.

6.2.4.1 Numerical Implementation

Snake can be implemented numerically in the form of matrix equation:

$$\mathbf{x}_t = (\mathbf{A} + \gamma\mathbf{I})^{-1}(\mathbf{x}_{t-1} - f\!x(\mathbf{x}_{t-1}, \mathbf{y}_{t-1})) \qquad \text{Equation 6-23}$$

$$\mathbf{y}_t = (\mathbf{A} + \gamma\mathbf{I})^{-1}(\mathbf{y}_{t-1} - f\!y(\mathbf{x}_{t-1}, \mathbf{y}_{t-1})) \qquad \text{Equation 6-24}$$

where: $fx(\mathbf{x,y})$ and $fy(\mathbf{x,y})$ are the first-order differential of the edge magnitude along the x axis and y axis respectively, γ is a step size and **A** is a diagonal banded matrix. If a contour is discretized into S points equally spaced by an arc length h and $s \in [1, S)$ then **A** can be represented as [NIX 2002]:

$$\mathbf{A} = \begin{bmatrix} c_1 & d_1 & e_1 & 0 & \cdots & a_1 & b_1 \\ b_2 & c_2 & d_2 & e_2 & 0 & \cdots & a_2 \\ a_3 & b_3 & c_3 & d_3 & e_3 & 0 & \\ \vdots & \vdots & \vdots & \vdots & \vdots & & \\ e_{s-1} & 0 & \cdots & a_{s-1} & b_{s-1} & c_{s-1} & d_{s-1} \\ d_s & e_s & 0 & & a_s & b_s & c_s \end{bmatrix} \quad \text{Equation 6-25}$$

Where:

$$a_s = \frac{\beta_{s-1}}{h^4}; \quad b_s = -\frac{2(\beta_s + \beta_{s-1})}{h^4} - \frac{\alpha_s}{h^2}; \quad c_s = \frac{\beta_{s+1} + 4\beta_s + \beta_{s-1}}{h^4} + \frac{\alpha_{s+1} + \alpha_s}{h^2};$$

$$d_s = -\frac{2(\beta_{s+1} + \beta_s)}{h^4} - \frac{\alpha_{s+1}}{h^2}; \quad e_s = \frac{\beta_{s+1}}{h^4}.$$

6.2.4.2 Active Contour Implementation

Firstly, the contours from both the reference image and the study image that has been transformed using affine transformation are extracted. Let C_a be the contour of the reference image and C_b be the contour of the study image, then C_b is used for the first iteration in Equation 6-23 and Equation 6-24 as $\mathbf{x}_{t-1}$ and $\mathbf{y}_{t-1}$. The matrix **A** can be obtained by using Equation 6-25 where the length of $\alpha(s)$ and $\beta(s)$ equal to the length of C_b.

Then, the next step is calculating $fx(\mathbf{x,y})$ and $fy(\mathbf{x,y})$ to be used in Equation 6-23 and Equation 6-24. Let $[px, py]$ be the gradient of C_a, then $fx(\mathbf{x,y})$ and $fy(\mathbf{x,y})$ can be obtained by using an interpolation of C_b specify by the matrices px and py respectively.

6.3 Elastic Registration

The spatial differences between the initial contour and the deformed contour from the active contour algorithm specify the displacement vectors that can be used to warp the study image to fit into the reference image.

If (x,y) is a point in an image, elastic transformation can be done by using the equation proposed by [PIE 2000]:

$$T(x,y)=(x,y)+\frac{\sum_{k=1}^{m} w_k(x,y)[(u_k,v_k)-(x_k,y_k)]}{\sum_{k=1}^{m} w_k(x,y)} \qquad \text{Equation 6-26}$$

where: $\{(u_k,v_k)\,|\,1\le k\le m\}$ is the initial contour; $\{(x_k,y_k)\,|\,1\le k\le m\}$ is the deformed contour; and $w_k(x,y)$ is the distance weighting function of a single point (x,y), given by:

$$w_k(x,y)=e^{-\beta(|x-x_k|+|y-y_k|)} \qquad \text{Equation 6-27}$$

where: β is the weighting factor.

6.4 Experiments and Discussion

The image registration algorithm proposed in this chapter has been validated with the experiments on CT and PET abdominal images from single subject or multiple subjects.

First, different abdominal images taken from the same patient are registered (*intra-subject registration*). This intra-subject registration includes monomodal registration which is performed by registering CT images, and multimodal registration, by registering CT images with PET images.

Then the registration over abdominal images taken from different patients (*inter-subject registration*) is carried out, followed by the experiment results on different active contour approaches.

In the last section, an experiment on three dimensional abdominal images series is presented, including the comparison between with and without applying affine registration before active contour algorithm. Before these experimental results are presented, some implementation issues are addressed.

6.4.1 Preprocessing Step

Before the image registration algorithm is applied to the images, sometimes the preprocessing step is needed to clean up the background noise and unnecessary part for registration procedure. For example, the images may contain elements that are not part of the abdominal information (e.g., imaging cushion). Besides, the backgrounds of the images are interfered with some noises that might disturb the image registration process. Since the focus of the image registration is only on the abdominal information, the rest of the image, including the background, need to be set to zero to ease the image registration process.

There are many methods to get rid of this unnecessary information, for example, morphological operation. However, the morphological operation will also alter some small details of the main part of the images. The method used in our experiments is first obtaining the information of pixel values and locations of the main part of the images; then restoring the information to new images with the background that has been set to zero. By this method, both the noisy background and the unwanted elements can be eliminated.

6.4.2 Intra-subject Registration

To facilitate the diagnosis, usually, the same subject needs to undergo different medical check either over time or by using different imaging sensors.

6.4.2.1 CT to CT Registration

Because monomodality registration of the same subject is very useful for treatment assessment and disease monitoring, in our first series of experiments, abdominal CT images (512*512) taken from the same patient have been registered. Some corresponding feature points were automatically extracted from both images, using the first and second moments, intensity-based and some edge points that have evenly distributed angle from the centroids of the images.

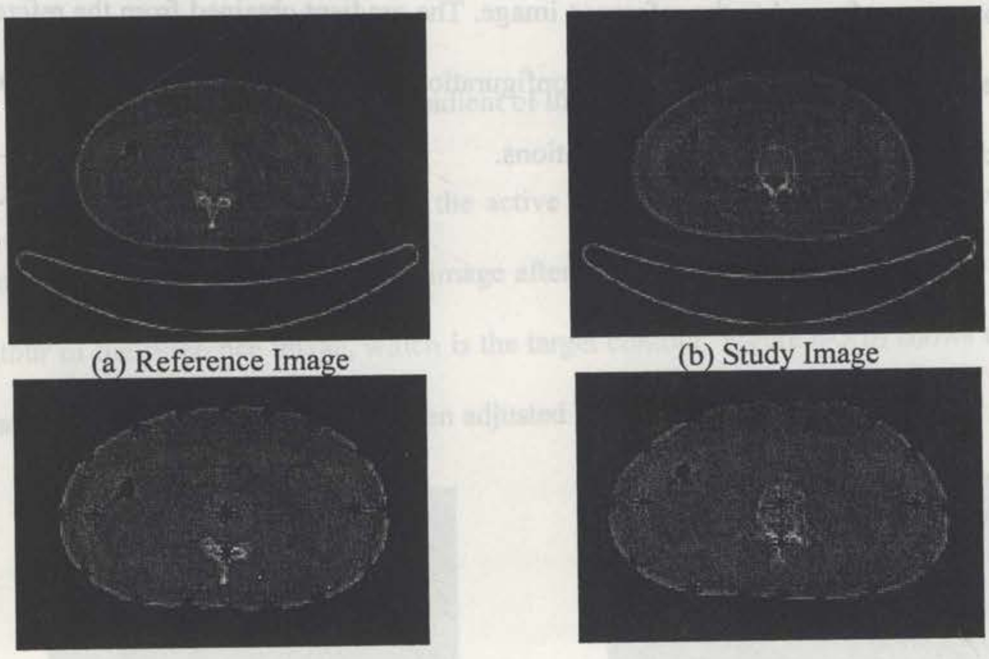

(a) Reference Image (b) Study Image

(c) Reference with Feature Points (d) Study with Feature Points

Figure 6-2 Abdominal CT images with corresponding feature points

After the affine transformation parameters are calculated, affine transformation is then performed on the study image. Figure 6-3 shows the difference between reference image and study image (Figure 6-3 (a)) and the difference between reference image and the study image after affine transformation (Figure 6-3 (b)).

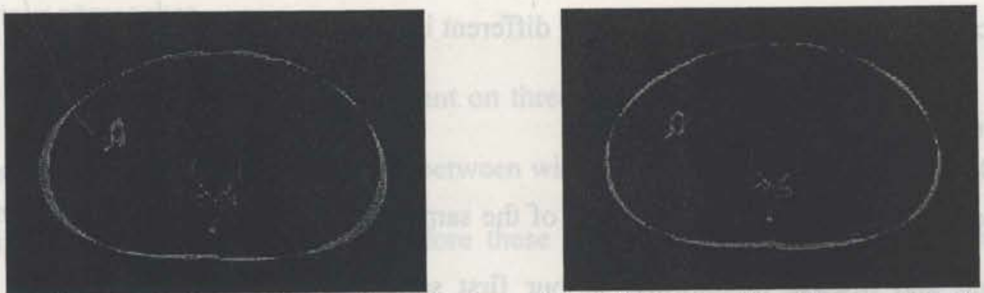

(a) Difference before affine registration (b) Difference after affine registration

Figure 6-3 Difference between reference image and study image

For the active contour model, based on our experiments, the parameters are set as $\alpha = 0.1$, $\beta = 0.1$, and $\gamma = 0.5$, and this combination has been proven to be able to give good performance to the active contour. To make the capture of the active contour bigger, blur operation was performed to the reference image. The gradient obtained from the reference image is shown in Figure 6-4. With the configuration mentioned above, the active contour can reach the convergence within 78 iterations.

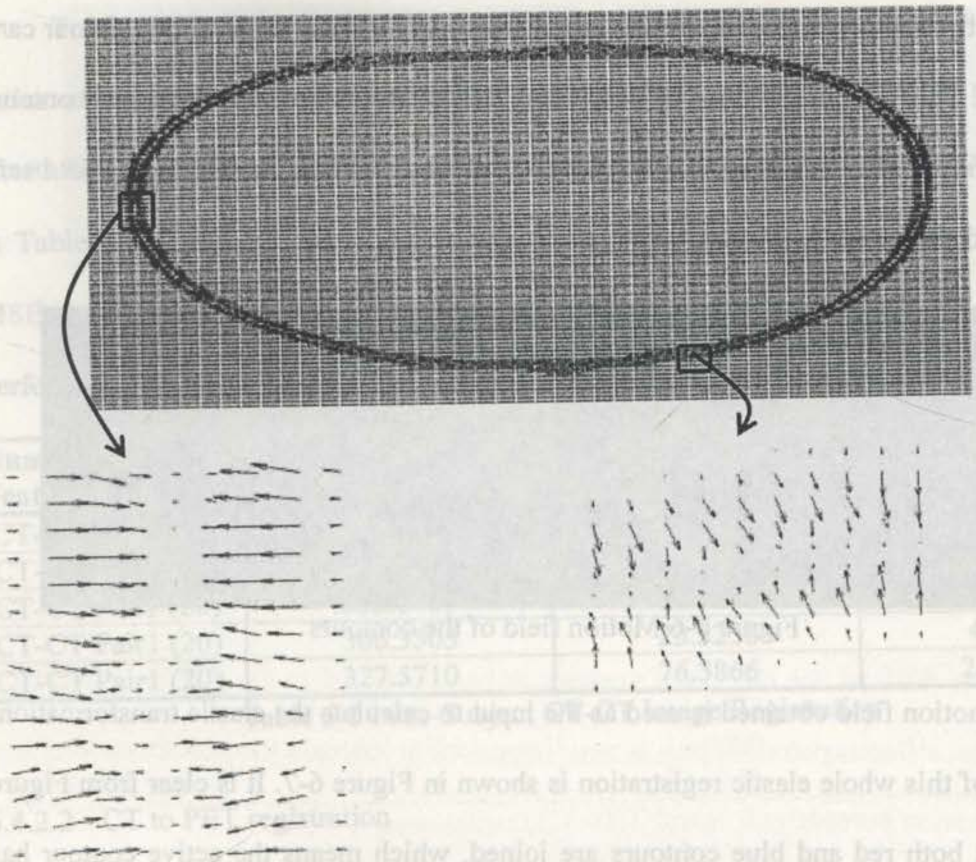

Figure 6-4 Gradient of the reference image

Figure 6-5 shows the result of the active contour procedure. The green contour in Figure 6-5(a) is the contour in study image after affine transformation. The red one is the contour of the reference image, which is the target contour. Figure 6-5(b) shows that after iteration 78, the green contour has been adjusted to fit the target contour.

(a) (b)

Figure 6-5 Study image overlapped with active contours (a) iteration 0 (b) iteration 78

After the active contour procedure is performed, the motion fields of the contour can be obtained. This is basically done by examining the difference between the initial contour and the contour after reaching convergence. Some part of this motion field has been enlarged and shown in Figure 6-6.

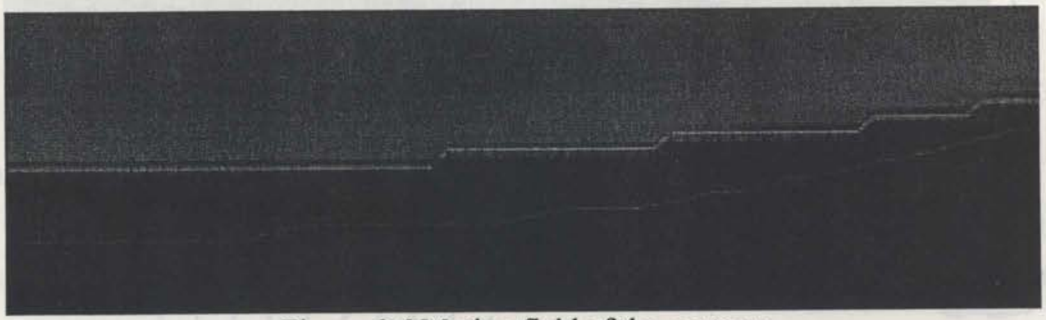

Figure 6-6 Motion field of the contours

The motion field obtained is used as the input to calculate the elastic transformation. The result of this whole elastic registration is shown in Figure 6-7. It is clear from Figure 6-7 (d) that both red and blue contours are joined, which means the active contour has been converged, and the study image has been deformed to fit to the reference image.

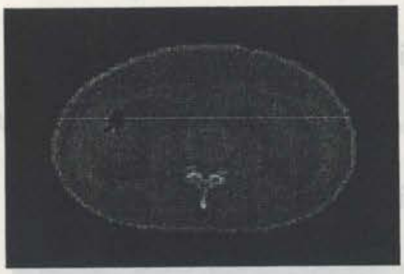

(a) Reference image

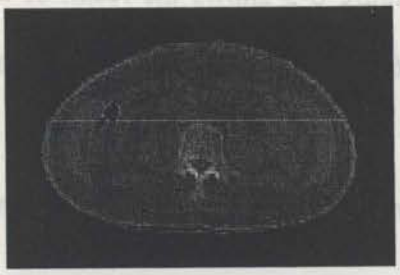

(b) Study image

(c) Study image after affine registration

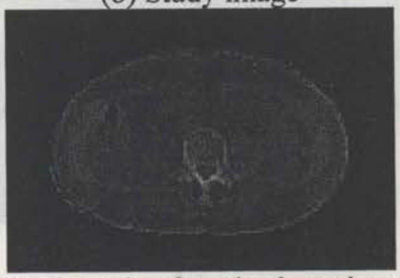

(d) Final result, after elastic registration

Figure 6-7 CT to CT Intra-subject Abdominal Image Registration

To further test the performance of the proposed elastic registration algorithm, a series of experiments have been carried out and MSE is calculated before registration, after affine registration, and after elastic registration. The experimental results are shown in Table 6-1. From this table, we can discover that the affine registration can decrease MSE greatly while elastic registration can be used to further improve the registration performance.

Number of Feature Points	Before registration	Affine Registration	Elastic Registration
CT-CT Pair1 (20)	32.6791	15.0086	6.4303
CT-CT Pair1 (19)	347.5675	74.1383	33.2040
CT-CT Pair1 (20)	332.0487	68.6348	45.9530
CT-CT Pair1 (20)	306.3503	23.3256	4.4214
CT-CT Pair1 (20)	327.5710	76.3866	26.2266

Table 6-1 Intra-Subject CT-CT Image Registration

6.4.2.2 CT to PET registration

CT images provide high quality anatomical details while PET images provide functional information. Proper registration of these functional-to-anatomical data is very helpful for diagnosis and surgical operation, especially for tele-surgery.

This sequence of experiments has performed on the images taken from the same patient by different sensors, CT and PET. Figure 6-8 shows two images with some corresponding feature points selected automatically. However, in this series of experiments, the intensity-based feature points are not used, because CT and PET sensors produce significantly different intensity characteristics.

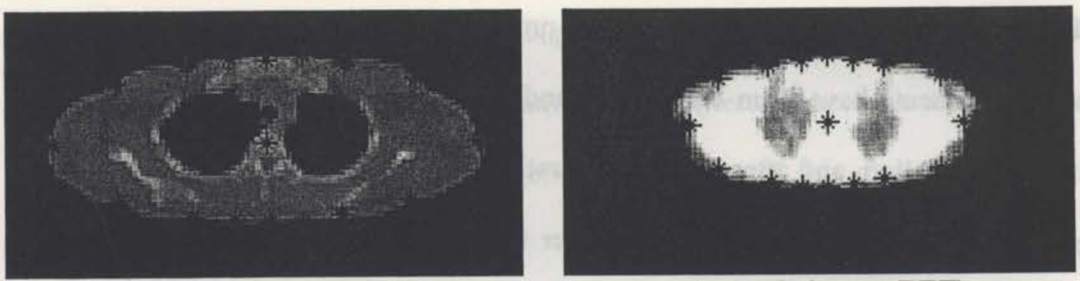

(a) Reference image (CT) (b) Study image (PET)

Figure 6-8 Abdominal images with corresponding feature points

Since the image size in this experiment are relatively small, 128×128 pixels, the active contour can be converged within 18 iterations. Figure 6-9 shows the results of this experiment. Because the two images differ significantly both in size and in image intensity, it is difficult for the initial contour to be converged to the reference contour. Therefore, the affine registration step is very important to increase the performance of the whole registration process.

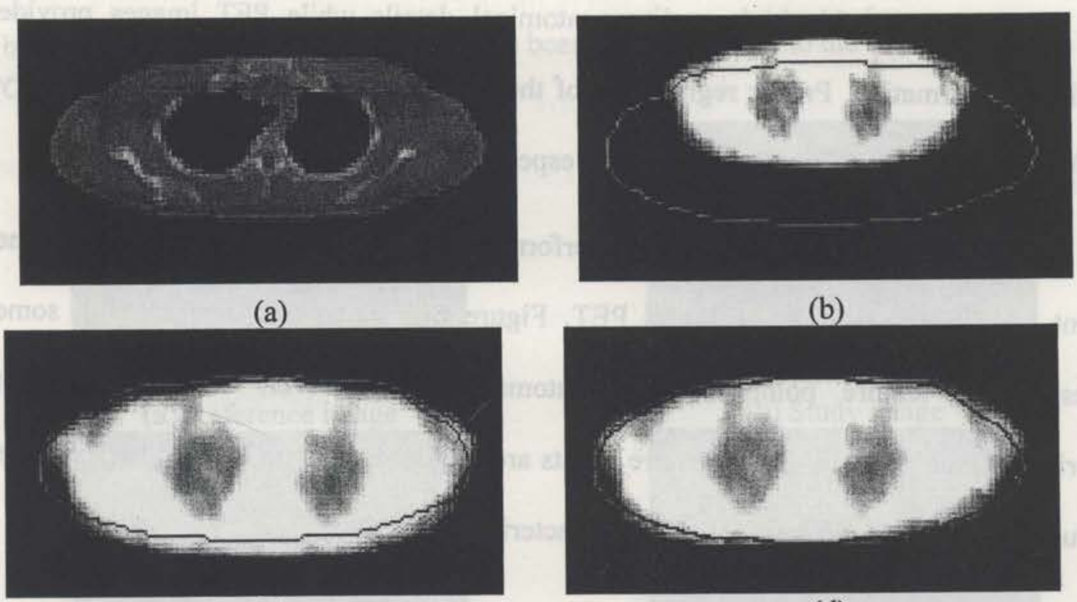

(a) (b) (c) (d)

Figure 6-9 CT to PET intra-subject thorax image registration process

(a) is reference image with contour overlapped; (b) is Study image with reference contour overlapped; (c) is study image after affine registration; and (d) is final result after elastic registration

MSE of 19 automatically selected feature point pairs is calculated before registration, after affine registration, and after elastic registration. From the experimental results listed in Table 6-2, we can find out that MSE is comparatively less than that of CT-CT experiments. This is mainly because that the image size in this sequence of experiments is smaller that that of CT-CT experiments. However, these experiments come to the same conclusion that our proposed method is stable and reliable to register both monomodal images and multimodal images.

Number of Feature Points	Before registration	Affine Registration	Elastic Registration
CT31-PET31(19)	162.0094	14.9679	4.9769
CT32-PET32(19)	164.0058	12.8577	4.3821
CT33-PET33(19)	162.4365	14.3552	5.1078
CT34-PET34(19)	159.7266	13.3452	5.5559
CT35-PET35(19)	160.2521	16.6090	6.8262
CT36-PET36(19)	164.4082	13.7143	5.4592

Table 6-2 Intra-subject CT-PET Image Registration

6.4.3 Inter-subject Registration

6.4.3.1 CT to CT Registration

Inter-subject registration experiments involve images from different subjects, e.g., as shown in Figure 6-10(a) and Figure 6-10(b). It can be seen that the two images here have a relatively big difference.

(a) Reference image

(b) Study image

Figure 6-10 Abdominal inter-subject CT images

Figure 6-11 shows the original difference image and the difference image after affine registration between reference and study. The experiment result shows that the affine registration has reduced the difference between the two images significantly but there are still local elastic differences which cannot be corrected by using this affine transformation.

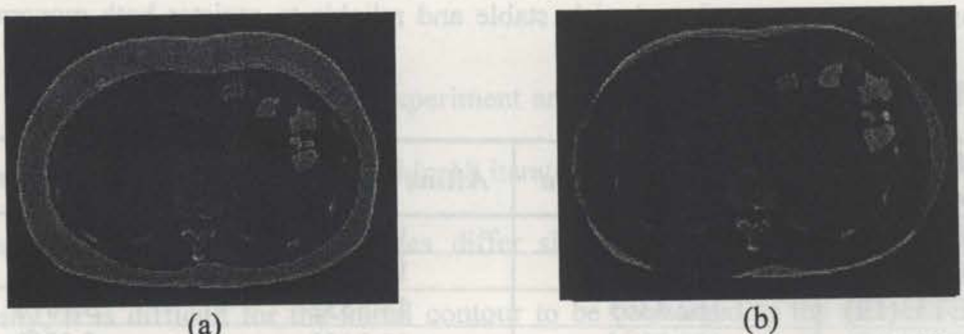

Figure 6-11 Difference between reference image and study image (a) before affine transformation (b) after affine transformation

Compared with the previous experiments, during the active contour convergence procedure, this experiment needs more iterations (378 iterations), it is mainly because the two images used in this experiment have much more difference.

The motion field that was obtained from the active contour step was then used in the elastic transformation step to produce the final result of registration. The result of this experiment is shown in Figure 6-12.

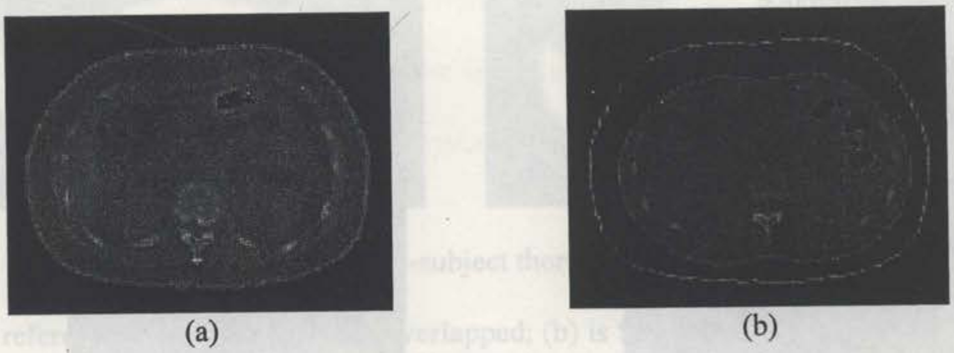

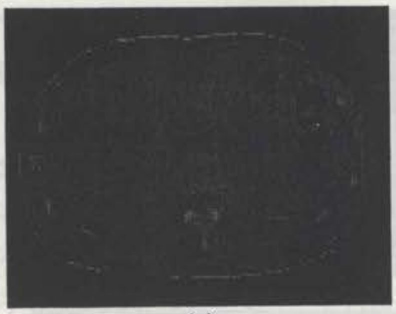

(c)

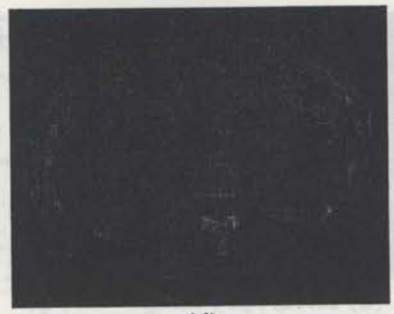

(d)

Figure 6-12 CT to CT, intra-subject, abdominal image registration proces

(a) is reference image; (b) is study image with reference contour (in red color) overlapped; (c) is study image after affine registration with reference contour (red) and study contour (blue) overlapped; and (d) is final result, after elastic registration

6.4.3.2 CT to PET registration

Inter-subject registration experiments have also been performed on images from different imaging modalities, CT and PET images in Figure 6-13. Since the two images are significantly different, the affine transformation plays an important role in reducing the difference.

(a) Reference image with feature points

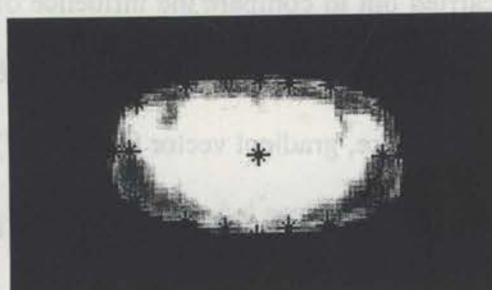

(b) Study image with feature points

Figure 6-13 Abdominal CT and PET images with corresponding feature points

The active contour algorithm was performed very effectively in this experiment since the initial contour converged to the target contour very rapidly, within 5 iterations. The images' size used in this experiment is 128×128 pixels. The process and result of this experiment is shown in Figure 6-14.

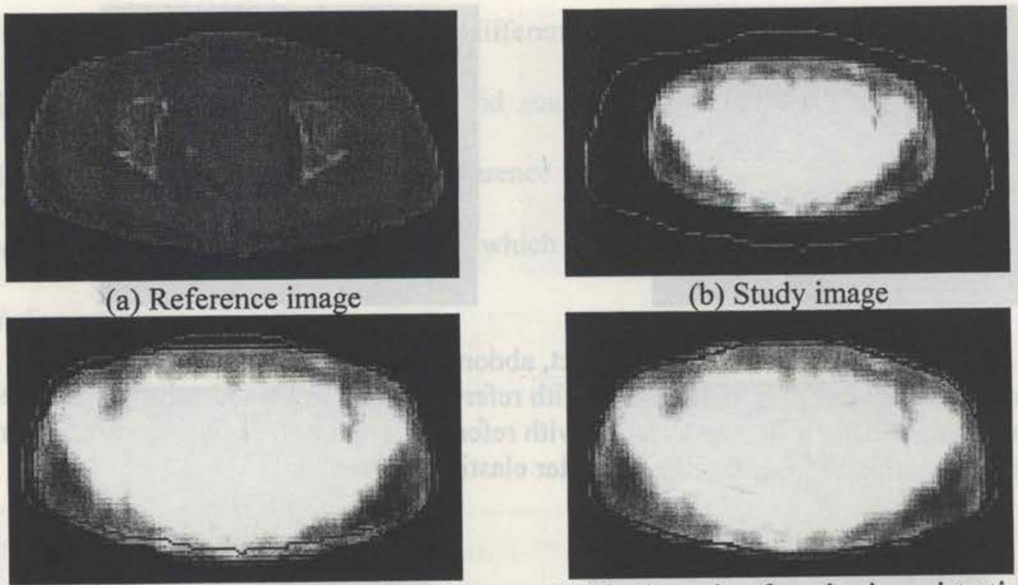

(a) Reference image (b) Study image

(c) Study image after affine registration (d) Final result, after elastic registration

Figure 6-14 CT to PET, intra-subject, abdominal image registration process

6.4.4 Performance Comparison on Active Contour Methods

In this section, comparison experiments on different active contour approaches have been carried out to compare the influence of the different approaches on the performance and results of registration. In these experiments, three different approaches are examined: traditional snake, gradient vector flow (GVF), and balloon.

Firstly, experiments were performed on CT to CT registration with 5 pairs of CT images, and another series of experiments were carried out on CT-PET registration also with 5 pairs of CT-PET images. Table 6-1 represents the results of these series of experiments by showing the number of iteration needed for the initial contour to be converged to the reference contour for each approach: traditional snake, GVF, and balloon with force weight parameter 0.05 and 0.01. The image size used in the first five experiments (CT to CT) are 512 × 512 pixels, whereas the image size used in the other five experiments (CT to PET) are 128 × 128 pixels, which made them converge faster than the previous experiments.

Images to be registered	Number of iteration			
	Traditional snake	GVF	Balloon (w = 0.05)	Balloon (w = 0.01)
CT-CT pair 1	78	60	22	54
CT-CT pair 2	168	130	29	99
CT-CT pair 3	230	218	-	269
CT-CT pair 4	109	78	32	75
CT-CT pair 5	246	232	-	275
CT-PET pair 1	18	11	13	17
CT-PET pair 2	10	9	10	10
CT-PET pair 3	16	11	25	18
CT-PET pair 4	18	12	22	17
CT-PET pair 5	15	9	25	18

Table 6-3 Comparison of convergence speed of different active contour models

From Table 6-1, it can be observed that the GVF approach always reaches the convergence faster than the traditional snake, whereas the results of balloon approach vary. Some experiments also have been done in modifying the parameter of balloon's force weight. Greater parameter made the contour faster to converge, but in some cases it made the contour fail to converge.

Besides convergence speed, the results between traditional snake, GVF, and balloon approach are comparable. That is because the images used in those experiments are relatively smooth and do not contain a concave shape. The results of the deformed contour for CT-CT pair 3 in Table 6-1 are presented in Figure 6-15. In these images, the yellow contours represent the reference contours, whereas the red contours represent the deformed contour after they converged. It can be seen that the deformed contour fits perfectly in the reference contour.

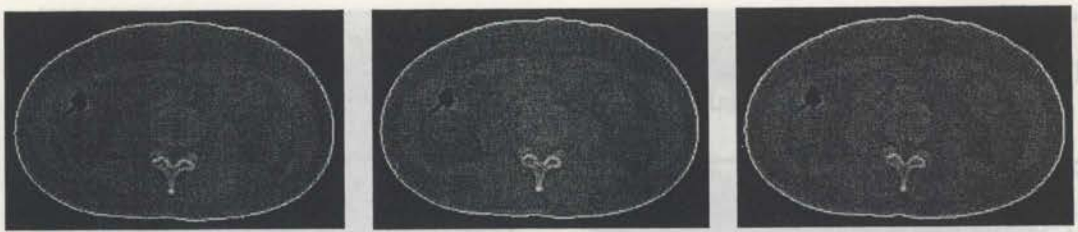

(a) Traditional Snake (b) GVF (c) Balloon

Figure 6-15 Result of the active contour algorithm after convergence.

Experiments on brain images have been carried out to further test the performance of GVF and experimental results (Figure 6-16) show that the results of the GVF approach are slightly better than the other approaches concerning the convergence to boundary concavities. Especially the three areas (signed with the red stars) show where the deformed curves fail to fit perfectly to the reference contour. These areas are and the enlarged images are shown in Figure 6-17.

(a) Traditional Snake

(b) GVF

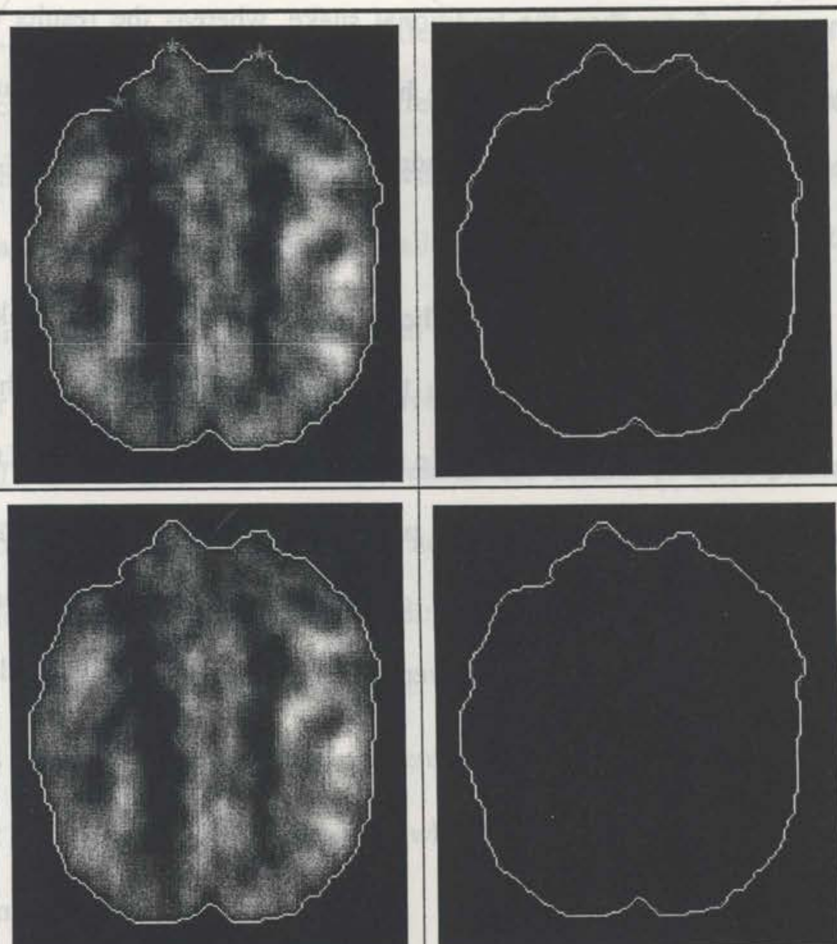

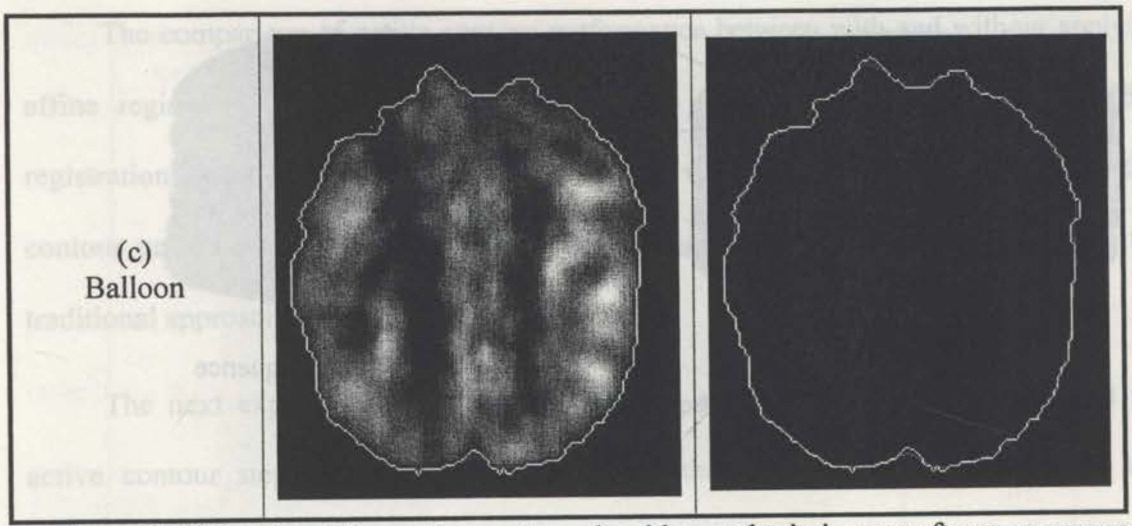

Figure 6-16 Results of the active contour algorithm on brain images after convergence

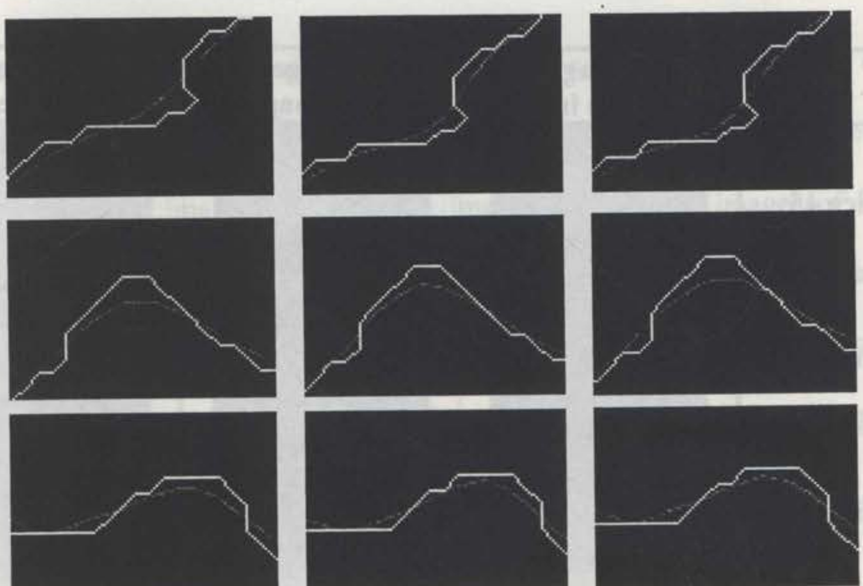

Figure 6-17 Enlarged results of the active contour algorithms after convergence

6.5 Three-Dimensional Abdominal Image Registration

Three-dimensional image registration can be obtained by registering each corresponding slice as performed in the previous experiments. Figure 6-18 illustrates this process.

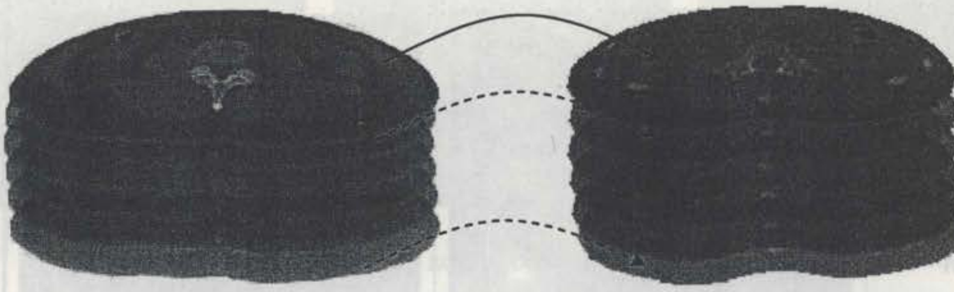

(a) Reference image sequence (b) Study image squence

Figure 6-18 Three-dimensional image registration

In this experimental example, five slices in a series of three-dimensional images taken from different patients are shown in Figure 6-19.

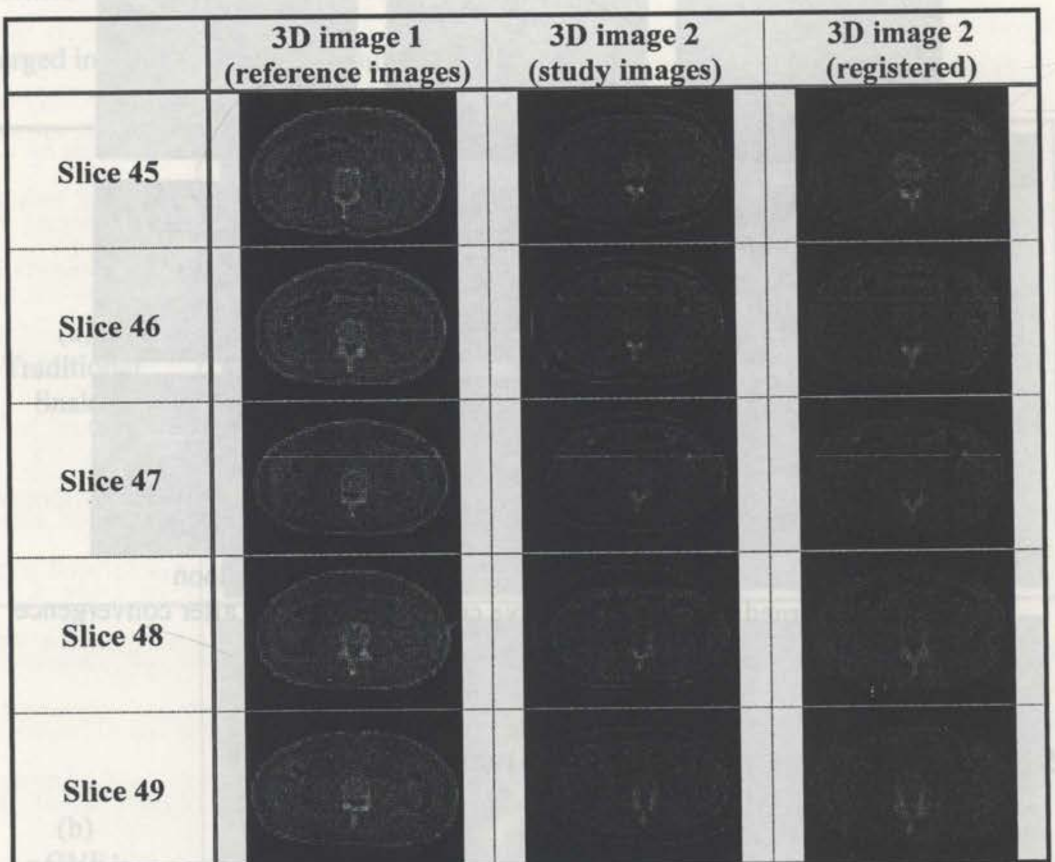

Figure 6-19 Image registration result for five slices

The comparison of active contour performance between with and without applying affine registration has also been carried out in this experiment. Firstly, the affine registration is performed before starting the active contour procedure and then the active contour procedure is carried out by using the GVF approach which is faster than the traditional approach.

The next experiment is carried out without applying affine registration, and the active contour step is performed straightly on the images to be registered. In this experiment, two active contour approaches, GVF and balloon, are used to further analyze the performance of the balloon approach.

Figure 6-20 illustrates the distance of the initial contour and the target contour for each experiment. The images of right column in Figure 6-20 represent the difference between the reference image and the study image, whereas the images of left column represent the difference between the reference image and the study image after the affine registration. It is clear that the affine transformation contributes significantly to reduce the distance between the reference image and the study image, and hence will speed up the elastic registration process.

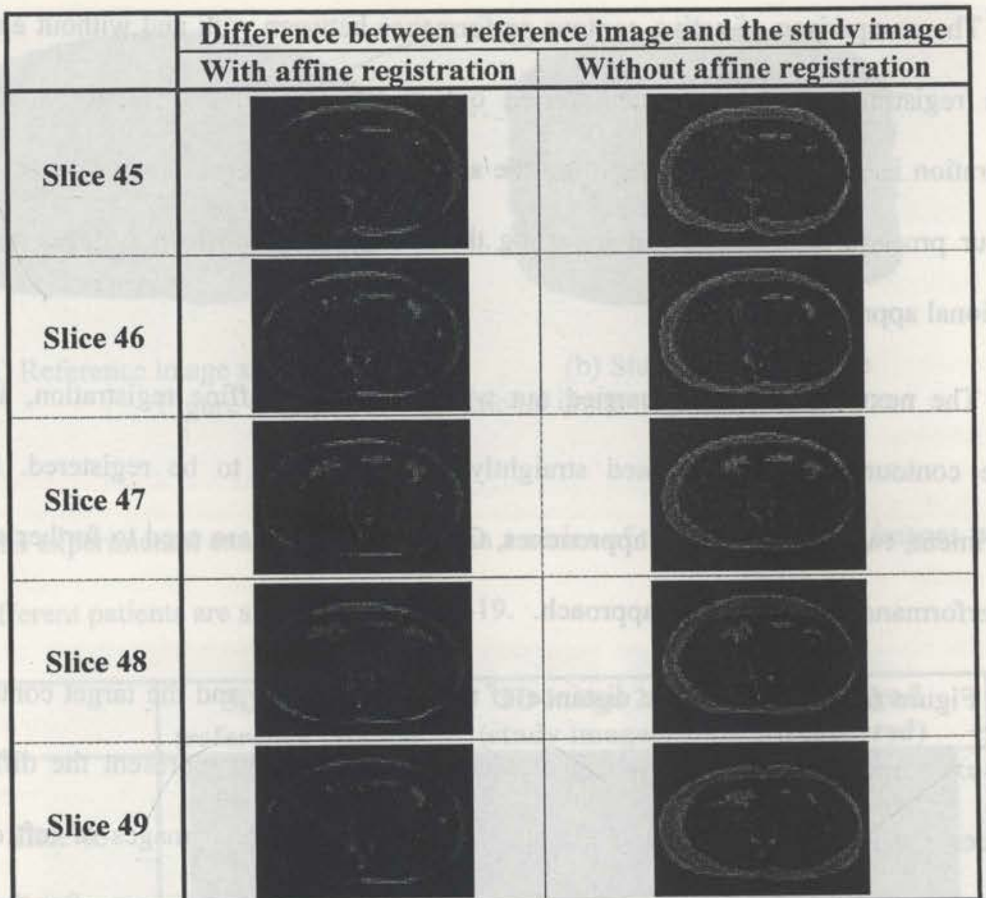

Figure 6-20 The difference between reference and study image

The matrix used in this comparison is the number of iteration needed for the initial contour to be converged to the reference contour, and the result of the comparison is shown in Table 6-4.

	The number of iteration needed		
	With affine (GVF)	**Without affine (GVF)**	**Without affine (balloon)**
Pair 45	87	942	85
Pair 46	77	550	80
Pair 47	10	514	98
Pair 48	80	783	118
Pair 49	31	950	157

Table 6-4 Comparison of iterations required

Figure 6-21 emphasizes the difference between the two approaches and the performance of the balloon method for the second approach. It can be seen that the affine transformation step reduced the number of iteration needed to the initial contour to be converged to the reference contour significantly, by using GVF. The figure also shows that the performance of balloon method in this experiment is much better than that in the previous experiment. This is because the initial contours in all pairs of images are positioned inside the reference contours, which is an ideal condition for balloon method. In balloon method, the expanding pressure force contributes more than the shrinking force.

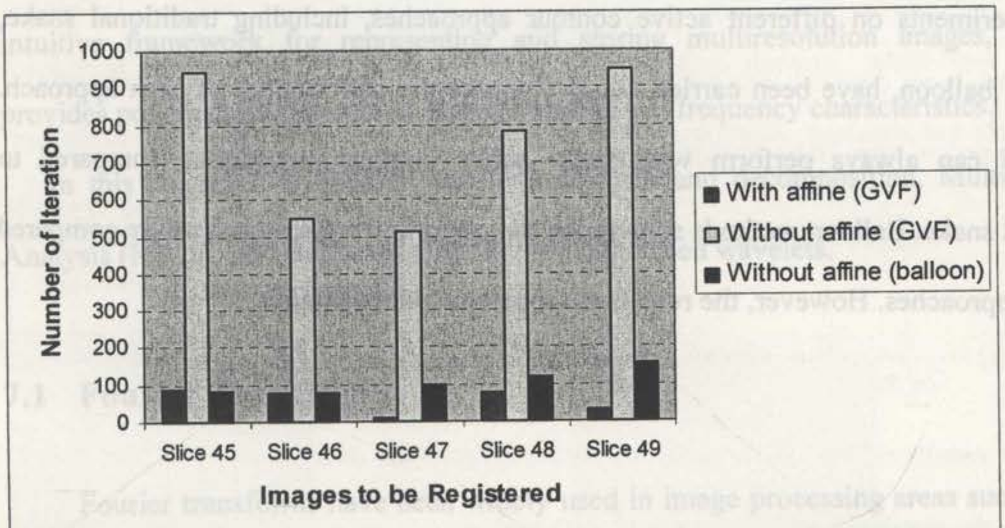

Figure 6-21 Performance comparison of the active contour models with and without affine registration

6.6 Summary

To improve the efficiency and effectiveness of abdominal image registration, in this chapter, an elastic registration method is proposed. The proposed method is divided into three main steps: non-iterative and automatic affine registration, active contour generation procedure, and elastic registration procedure. Experiments using CT and PET images have validated the performance of the method proposed. The experimental results show that the method proposed is reliable to produce good registration. Besides, the proposed registration process is efficient. It is because firstly during the affine registration procedure, the transformation parameters can be derived directly from MSE and the time-consuming iterative optimization procedure can be avoided; secondly the initial contour for the active contour algorithm is close to the reference contour after affine transformation has been applied to the study image, which can dramatically accelerate vector field extraction. This method can be applied to 2D and 3D monomodal and multimodal registration, intra-subject and inter-subject registration as well.

Experiments on different active contour approaches, including traditional snake, GVF, and balloon, have been carried out to compare the performance of each approach. The GVF can always perform with faster active contour procedures, compared to traditional snake. Balloon methods sometimes can perform the fastest procedure compared to other approaches. However, the results are somehow unpredictable.

CHAPTER 7 WAVELET TRANSFORM AND DECOMPOSITION

The Fourier transforms have been widely used in image processing and analysis; however, they only reveal the frequency characteristics of an image. When digital images are to be viewed or processed at multiple resolutions, the discrete wavelet transform (DWT) is the mathematical tool of choice. In addition to being an efficient, highly intuitive framework for representing and storing multiresolution images, the DWT provides powerful insight into an image's spatial and frequency characteristics.

In this chapter, we explore wavelet transform and decomposition, MultiResolution Analysis (MRA), and characteristics of some often used wavelets.

7.1 Fourier Transforms

Fourier transforms have been widely used in image processing areas such as image enhancement, image restoration, and image compression. The Fourier transform of an absolutely integrable function $f(x) \in L^{1}(R)$ can be defined by:

$$F(\omega) = \int_{-\infty}^{+\infty} e^{-i\omega t} f(t)dt \qquad \text{Equation 7-1}$$

The inverse Fourier transform of $F(\omega)$ is defined by:

$$f(t) = \frac{1}{2\pi}\int_{-\infty}^{\infty} e^{i\omega t} F(\omega)d\omega \qquad \text{Equation 7-2}$$

Fourier transformations can separate signal characteristics into time domain and frequency domain. However, it cannot give a proper connection of these two domains. From Equation 7-1 and 7-2, we know that Fourier transforms are obtained by integrating in the whole time domain and lack the ability of local information analysis. Fourier transforms work well when $f(x)$ is only consisted of harmonic components. However, small changes in such transforms will lead to changes spreading over the whole time domain.

7.2 Short-Time Fourier Transform

To facilitate non-stationary signal analysis, the Short-Time Fourier Transform (STFT) had been devised. For example, in STFT, when Gaussian function is used as window function, then Gabor transform is produced by:

$$S(\omega,\tau) = < g_{\tau,\omega}(t), f(t) > = \int_{-\infty}^{+\infty} e^{-i\omega t} f(t) g_a(t-\tau) dt \quad \text{Equation 7-3}$$

where $g_a(t) = \frac{1}{2\sqrt{\pi a}} e^{-\frac{t^2}{4a}}$ is Gaussian function; and $g_{\tau,\omega} = g_a(t-\tau)e^{i\omega t}$ is the shifted and modulated results of the basic window function. From the definition, STFT can also be thought as the similarity measurement of $f(t)$ and $g_{\tau,\omega}$.

With fixed size windows, STFT lacks the flexible division of time-frequency domain and only provides uniform resolution over the entire time-frequency domain. Because most images have the properties of high-frequency contents with small range spatial distribution and low-frequency contents with larger range of spatial distribution, STFT is not the most optimal solution to image processing and analysis.

Wavelets were firstly introduced by Haar in 1910, while the two breakthrough concepts of the first orthogonal wavelet bases [DAU 1988] and multiresolution analysis [MAL 1989] have inspired great enthusiasms in image processing community [UNS 2003].

7.3 Wavelet Transform and Wavelet Decomposition

7.3.1 Continuous Wavelet Transform

Instead of shifting and modulating the basic window function, the wavelet transforms are produced by translating and dilating the kernel function, known as "mother wavelet". With variable size windows along time-frequency (time-scale) domain, wavelets are able to analyze data at different resolutions (Figure 7-1). With high frequency resolution and low time resolution in low-frequency domain, while low frequency resolution and high time resolution in low-frequency domain, wavelets are ideal solution of image processing and analysis.

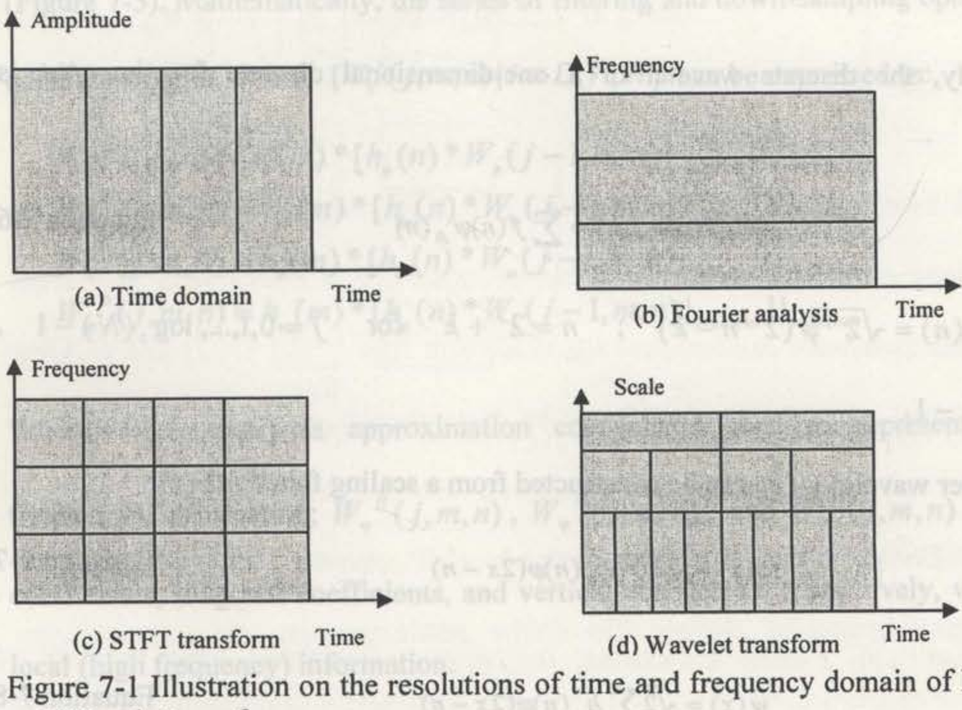

Figure 7-1 Illustration on the resolutions of time and frequency domain of Fourier, STFT, and Wavelet transform

The continuous wavelet transform of a function $f(x) \in L^2(\Re)$ can be defined as ([MAL[1] 1992]):

$$(W_\psi f(x))(a,b) = \langle f(x), \psi_{ab}(x) \rangle = \frac{1}{\sqrt{|a|}} \int_{\Re} f(x)\psi\left(\frac{x-b}{a}\right)dx$$

Equation 7-4

where the function $\psi_{ab}(x)$ defines the family of the wavelet functions with $a,b \in \Re$ and $a \neq 0$ is the dilation parameter and b is the translation parameter. The definition also provides the similarity measurement of $f(x)$ and wavelets $\psi_{ab}(x)$ obtained from mother wavelet $\psi(x)$ by dilation and translation:

$$\psi_{ab}(x) = \frac{1}{\sqrt{|a|}}\psi\left(\frac{x-b}{a}\right)$$

Equation 7-5

7.3.2 Discrete Wavelet

Similarly, the discrete wavelet of a one-dimensional discrete function $f(n)$ is defined as:

$$(W_\psi f(n))(j,k) = \sum_n f(n)\psi_{jk}(n)$$

Equation 7-6

where: $\psi_{jk}(n) = \sqrt{2^{-j}}\psi(2^{-j}n - k)$; $n = 2^j + k$ for $j = 0,1,..., \log_2(N) - 1$, $k = 0,1,...,2^j - 1$.

The mother wavelet $\psi(x)$ can be constructed from a scaling function $\varphi(x)$:

$$\varphi(x) = \sqrt{2}\sum_n h_\varphi(n)\varphi(2x-n)$$

Equation 7-7

and

$$\psi(x) = \sqrt{2}\sum_n h_\psi(n)\varphi(2x-n)$$

Equation 7-8

where: $h_\varphi(n)$ is the impulse response of a discrete filter which needs to meet some requirements to ensure the set of basis wavelet functions to be orthonormal and unique; while $h_\psi(n)$ can be extracted from $h_\varphi(n)$:

$$h_\psi(n) = (-1)^n h_\varphi(1-n)$$ Equation 7-9

where: $h_\varphi(n)$ and $h_\psi(n)$ are lowpass and highpass filters.

7.3.3 Multiresolution Analysis

The concept of multiresolution analysis (MRA) ([MAL[1] 1998]) is important to construct fast two-dimensional discrete wavelet from one-dimensional one. For a given 2-dimensional image of size $2^m * 2^n$, the wavelet-based image decomposition (Figure 7-2) can be achieved by convolving the wavelet low-pass filter $h_\varphi(n)$ and the wavelet high-pass filter $h_\psi(n)$ and down-sampling by a factor of 2 along rows and columns independently (Figure 7-3). Mathematically, the series of filtering and down-sampling operations used to compute $W_\Psi(j,m,n)$ and $\{W_\Psi^{\,i}(j,m,n) \mid i = D,V,H\}$ can be expressed as:

$$\begin{aligned}
W_\Psi(j,m,n) &= h_\varphi(m) * [h_\varphi(n) * W_\varphi(j-1,m,n)|_{n=2k,k\ge0}]|_{m=2k,k\ge0} \\
W_\Psi^{\,H}(j,m,n) &= h_\psi(m) * [h_\varphi(n) * W_\varphi(j-1,m,n)|_{n=2k,k\ge0}]|_{m=2k,k\ge0} \\
W_\Psi^{\,V}(j,m,n) &= h_\varphi(m) * [h_\psi(n) * W_\varphi(j-1,m,n)|_{n=2k,k\ge0}]|_{m=2k,k\ge0} \\
W_\Psi^{\,D}(j,m,n) &= h_\psi(m) * [h_\psi(n) * W_\varphi(j-1,m,n)|_{n=2k,k\ge0}]|_{m=2k,k\ge0}
\end{aligned}$$

Equation 7-10

Where: $W_\Psi(j,m,n)$ is approximation coefficients used to represent global (low frequency) information; $W_\Psi^{\,H}(j,m,n)$, $W_\Psi^{\,D}(j,m,n)$, and $W_\Psi^{\,V}(j,m,n)$ are horizontal coefficients, diagonal coefficients, and vertical coefficients respectively, which represent local (high frequency) information.

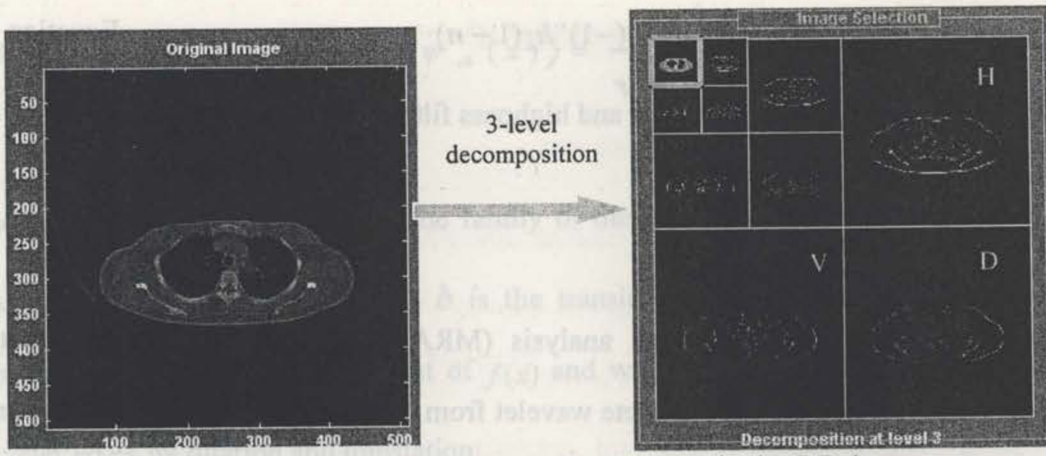

Figure 7-2 Image Decomposition at Level 3 by DB 4

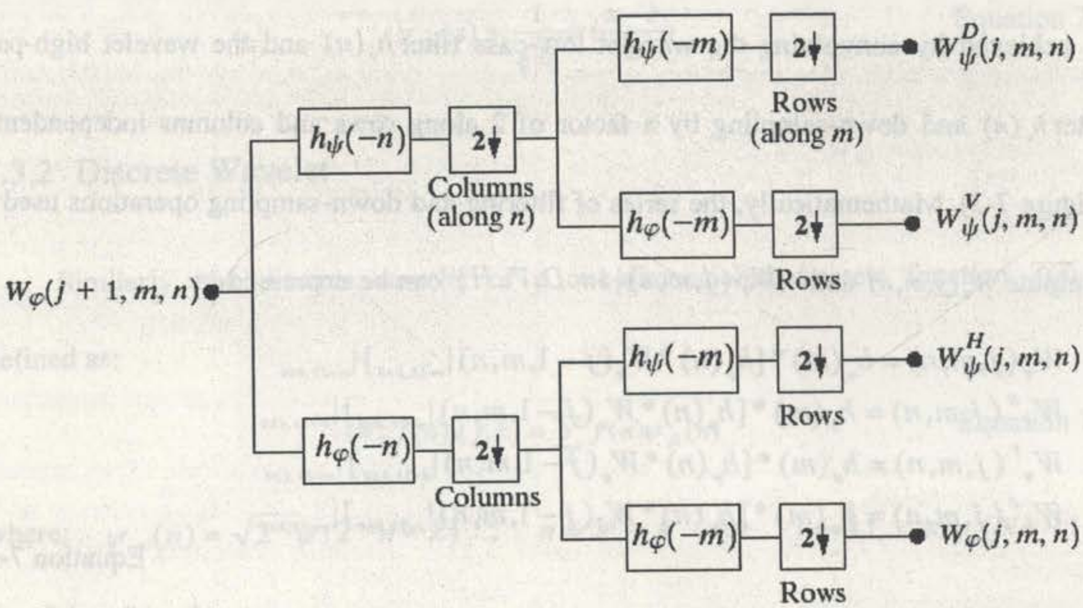

Figure 7-3 Wavelet Decomposition of $W_\varphi(j+1, m, n)$ into Quarter-size Subimages

7.3.4 Wavelet Filters

Compared with Fourier transforms, the wavelet transforms have property of variability due to different mother wavelets. Different wavelets would have strong impact on the results of image processing and analysis and selecting proper wavelets for the concrete image processing subject is a challenging issue. According to different characteristics, wavelets can be classified into different categories. The properties of the often used wavelets ([DAU 1994]) are listed in Table 7-1.

Wavelet	Haar	Daubechies	Biorthogonal	Coiflets	Symlets	Meyer
Orthogonal	Yes	Yes	No	Yes	Yes	Yes
Biorthogonal	Yes	Yes	Yes	Yes	Yes	Yes
Compact support	Yes	Yes	Yes	Yes	Yes	No
DWT	Possible	Possible	Possible	Possible	Possible	Possible
CWT	Possible	Possible	Possible	Possible	Possible	possible
Support width	1	2N-1	2Nr+1 for reconstruction; 2Nd+1 for decomposition	6N-1	2N-1	Infinite
Filters length	2	2N	max(2Nr,2Nd)+2	6N	2N	[-8 8]
Symmetry	Yes	Far	Yes	Near	Near	Yes
Number of vanishing moments for ψ	1	N	Nr	2N	N	-
Number of vanishing moments for φ	-	-		2N-1	-	

Table 7-1 General characteristics of often used Wavelets

7.4 Summary

Due to their capability of distinguishing image data into different frequencies and preserving information at different resolutions, wavelets have been applied in medical imaging area [UNS 2003], e.g., medical image compression, denoising, enhancement, and reconstruction. Because this property of wavelets is suitable for building registration pyramid as well, research of wavelet-based hierarchical registration has attracted an increasing research interest. This chapter focuses on basic technology of wavelet transformation and decomposition, which will provide theoretical foundation for our research exploration of hierarchical registration in the following chapters. In this chapter, some important image processing techniques, such as Fourier transforms, Short –Time Fourier transform, and wavelet, have been introduced briefly. Especially, Multiresolution analysis (MRA) technique used to construct fast 2-D discrete wavelet has been emphasized.

CHAPTER 8 HIERARCHICAL BIOMEDICAL IMAGE REGISTRATION BASED ON WAVELETS

8.1 Introduction of Hierarchical Medical Image Registration

Although an enormous number of biomedical image registration methods have been proposed, researchers are still facing challenges of producing registration approaches with both high precision and computation efficiency. Hierarchical biomedical image registration has been proposed to meet this requirement, which has advantages of both increased computation efficiency and the ability to find better solutions ([KOV 1998]).

In hierarchical registration strategy, the image data sets to be registered are divided into multiple resolution levels to compose registration pyramids, and then registration procedure is carried out from low resolution levels to high resolution levels. This "coarse-to-fine" registration scheme has several superior merits. Firstly, the main global information of images provided by the low resolution levels helps the avoidance of being trapped in the local minima. Furthermore, the initial registration estimation provided by low registration levels not only contributes to the improvement of registration performance, but also accelerates computational efficiency. Based on this estimation, the registration precision of high resolution levels can be further improved by adding more registration information. Because usually most of registration iterations are spent on low resolution levels while fewer are required in high resolution levels, efficient registration can be achieved in hierarchical registration methods.

One of the key issues in hierarchical registration schemes is how to build registration pyramids. Several categories of hierarchical registration methods have been proposed

[LES 1999], for example, Gaussian pyramids, Spline pyramids [THÉ 2000], mathematical morphology based methods, and wavelet-based registration. In these multiresolution registration approaches, the registration pyramids are usually created by successively filtering and then downsampling the datasets. However, in morphological hierarchical approaches, unsatisfactory registration may result from false structure, while spline pyramids mainly limit to affine registration [LES 1999].

Because of its superior performance of representing image information at multiple resolution and different frequency, wavelet provides a good option to hierarchical registration. In this chapter, wavelet-based automatic and elastic registration methods are presented to register brain images and abdominal images.

8.2 Steerable Wavelet Based Brain Image Registration

In this part, a new hierarchical elastic medical image registration is described to improve the registration efficiency and performance.

8.2.1 Algorithm Description

Intensity based registration, especially for the mutual information based registration, has the property of high precision, but it is also time consuming. To improve the computational efficiency, a hierarchical method is proposed, in which the images are registered from low resolution (high level) of the registration pyramids to high resolution (low level) of the registration pyramids (Fig. 8-1).

- **Step one**: Based on wavelets, the images are decomposed into subbands. Because the low-frequency subbands provide the compact and smooth information of their original images, we use the low-frequency subbands as searching spaces in each hierarchy of the registration pyramids.

- **Step two**: In each hierarchy, based on mutual information criterion, the registration is performed to correct rotation and translation displacements between the images. The results of the current registration hierarchy are used as the initial estimation for the next hierarchy.
- **Step three**: To further improve the registration performance, the block matching technique is adopted on the lowest level (corresponding to the original resolution level) of the pyramids.

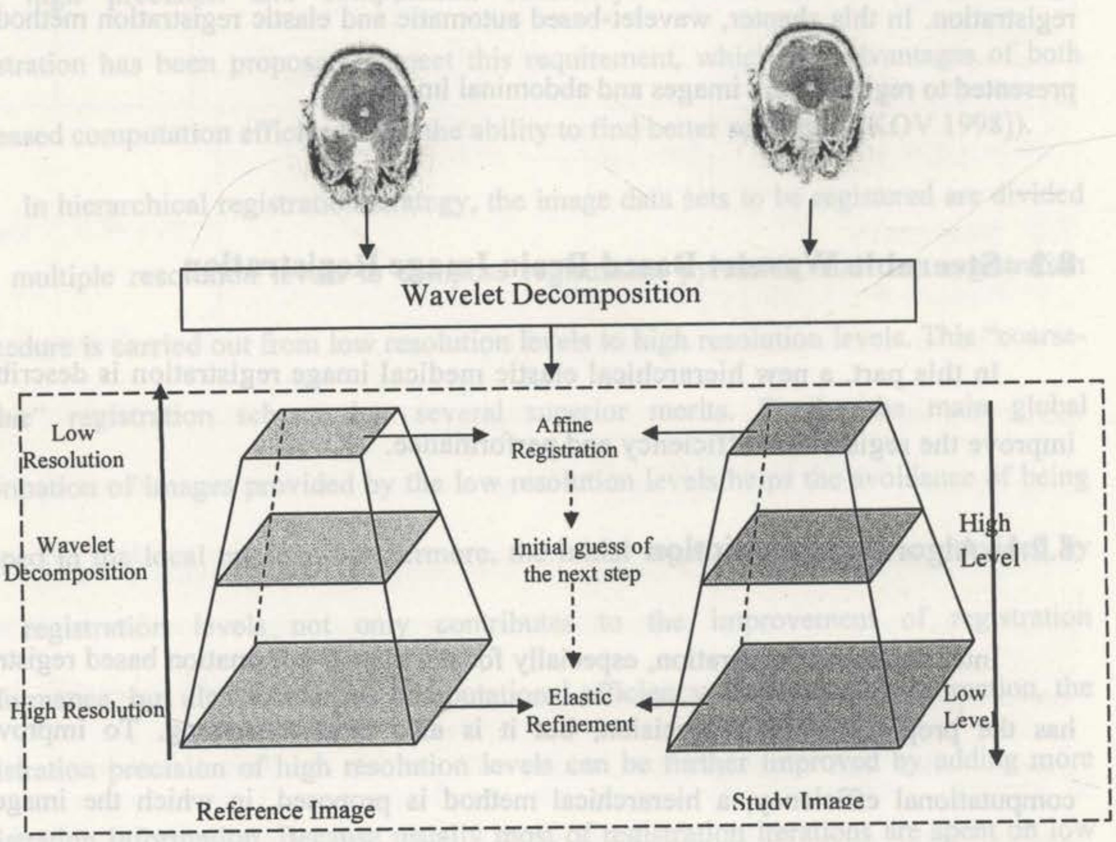

Figure 8-1 Hierarchical Registration Pyramids Based on Wavelet Decomposition

8.2.2 Local Elastic Registration

This wavelet-based hierarchical registration procedure is suitable to correct global rigid displacements. To correct complex differences, a further elastic refinement procedure is needed. The hierarchical registration results are used as inputs to initialize the elastic registration. In our brain image registration, the study image is divided into equal sized, unoverlapped blocks. By iteratively moving the study block on the reference image within a searching range, the local similarity can be optimized and the best position for each study window can be found (Figure 8-2). Then, a local transformation can be obtained for each individual block, and the global elastic transformation is achieved by assimilating all of the local transformations into a continuous transformation.

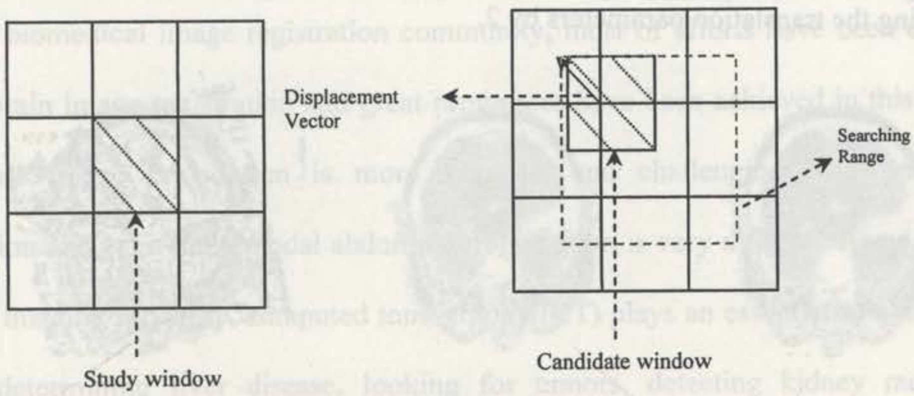

Figure 8-2 Block Matching

8.2.3 Experiments

Experiments are presented in this section to demonstrate the performance of the proposed algorithm in coping with nonlinear deformations in clinical tomographic images. Transverse slices of 3-D MR volume of 256*256*46 are registered and the quality of the registration is assessed by comparing the transformed slices with the original ones.

Figure 8-3 The 3rd Hierarchy of Registration Pyramids

The 1st and 2nd columns are the low-frequency subbands of reference and study images with size of 32*32; the 3rd and 4th columns are the difference images before and after MI registration. The results of this registration hierarchy are used as the initial guess for the following hierarchy by keeping the rotation and scaling parameters unchanged and multiplying the translation parameters by 2.

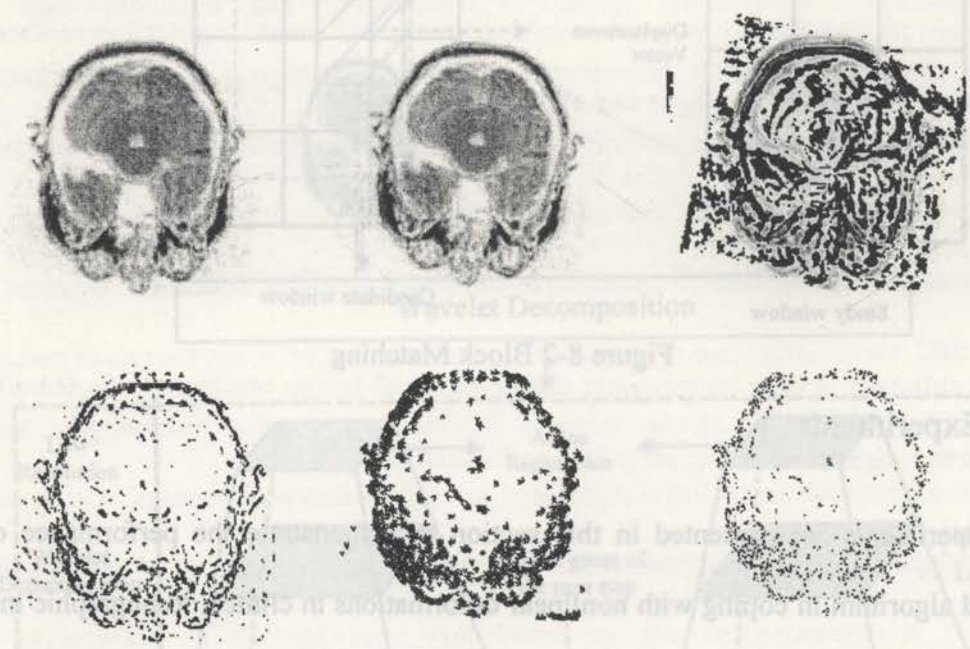

Figure 8-4 The Lowest Hierarchy of Registration Pyramids of Size 256*256

The 1st row is the reference image, study image, and the difference image before registration; the 2nd row is the difference image after the registration based on MI, the displacement fields, and final difference image after the elastic registration refinement.

In this algorithm, the raw image information or coefficients has (have) been used as registration feature space and the pre-processing step is unnecessary. By using the new hierarchical medical registration method, high computational efficiency can be achieved, and both rigid and elastic deformations can be corrected.

Because we limit the transformation to translation in our block-based elastic registration procedure, the registration cost is not high. However, this also limits the ability of our registration method to correct only simple local elastic displacements. By allowing more complex transformations for each block, the algorithm can be used to correct more complicated distortions; however, the registration complexity may be increased dramatically as well.

8.3 Automatic Registration for 2-Dimensional CT Abdominal Images

In biomedical image registration community, most of efforts have been devoted to human brain image registration and great progresses have been achieved in this area. The abdominal image registration is more complex and challenging than brain image registration and even monomodal abdominal registration is very difficult. As an important medical imaging modality, computed tomography (CT) plays an essential role in checking injury, determining liver disease, looking for tumors, detecting kidney masses, and evaluating the response to a therapy, therefore, the registration of CT abdominal images is required in clinical applications.

In this section, an automatic hybrid registration approach is proposed to register CT abdominal images over time intervals (Figure 8-5). In intensity-based registration procedure, in order to speed up registration convergence and to improve registration computation efficiency, the wavelet-based hierarchical method is used, in which the global displacements are corrected using mutual information algorithm. Then, in landmark-based registration procedure, firstly, the landmark points are selected automatically; and then, the local non-linear deformations are corrected using thin-plate splines elastically.

8.3.1 Automatic Hybrid Medical Image Registration Approach

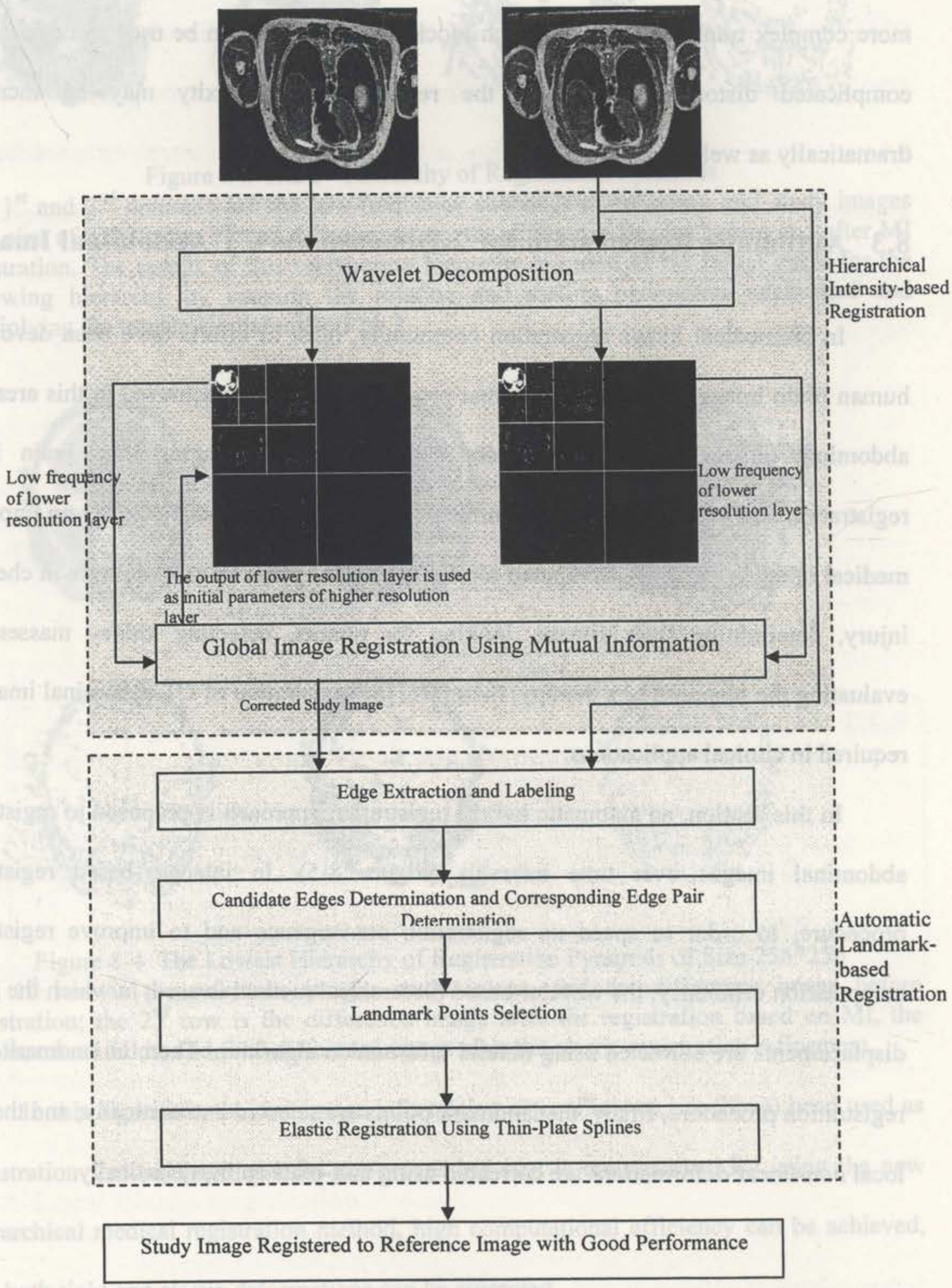

Figure 8-5 Hybrid Registration of CT Abdominal Images Illustration

The block-based registration is an option to correct nonrigid distortions, however, it mainly focuses on very simple transformation and more complex transformations would lead to computation efficiency declination. Therefore, block-based elastic registration is not suitable for more complex abdominal image registration.

Landmark points based registration has advantage of high computation efficiency. Landmark points can be either intrinsic (anatomical features) or extrinsic (markers attached to the subject). Abdominal registration based on extrinsic landmarks maybe invasive or less accurate because of non-rigid movement of abdomen. While intrinsic landmark based registration usually involves frequent user intervention. Automatic medical registration is still a challenging and ongoing research topic. In this section, an automatic landmark point based method is proposed and the detailed explanation of automatic landmark selection is described as follows:

1. Edge extraction: Due to its optimal property of noise suppression, Canny edge detection algorithm ([CAN 1986]) is selected to extract the edges from the output images of the first global intensity-based registration. In Canny method, the image is convolved with a Gussian filter; then the local maxima of the image gradient is achieved; using two thresholds, the edge candidates are examined and the connectivity is maximized.
2. Edge labeling: The region-growing technique is used to label the 8-connected objects in the binary edge images and then the edges are ranked according to their perimeters.
3. Candidate edge determination: The edges which perimeters are greater than a predetermined threshold are chosen as candidate edges for the following automatic landmark point selection procedure. Through this step, those edges with small perimeter are eliminated and the influence of noise is avoided.

4. Corresponding edge pair searching: For each labeled edge of study image, in order to find its corresponding edge in reference image, we iteratively move the edge of study image on the reference image within a searching range and select the one with the most similar perimeter and least distance from it as its corresponding edge.
5. Landmark point selection: For each pair of corresponding edge, the centroid points, the points with maximum and minimum distances to their centroid points are selected as landmark points for the elastic registration.

After the corresponding landmark points selected automatically, the Thin-Plate Splines are used to register the images elastically.

8.3.2 Experimental Validation and Discussion

To validate the proposed approach, CT abdominal images came from the same subject who underwent different medical examinations over time intervals are used as registration experiment data.

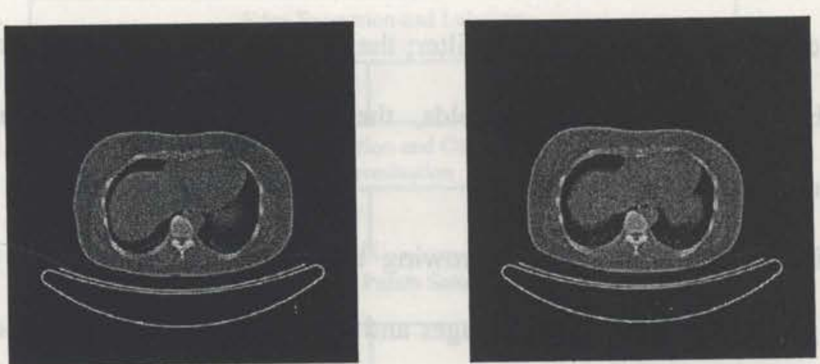

(a) Reference Image (b) Study Image

Figure 8-6 Registration Data

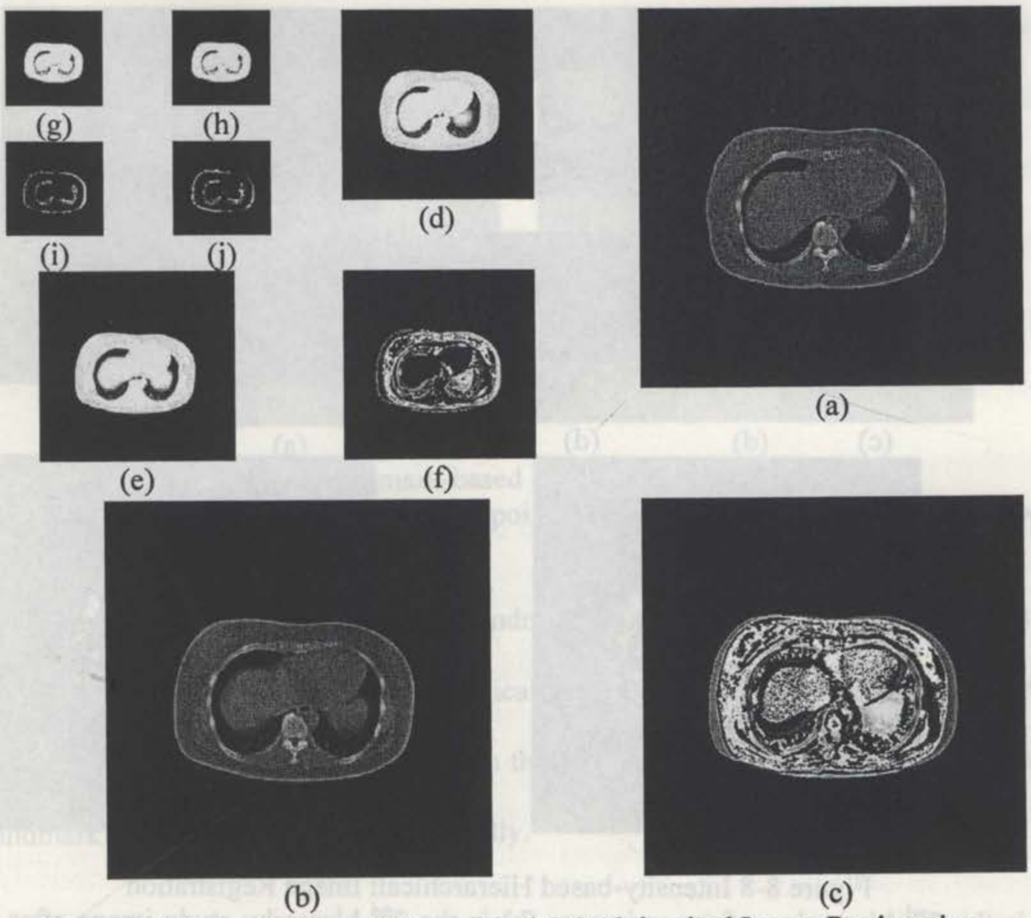

Figure 8-7 Intensity-based Hierarchical CT Abdominal Image Registration

(a), (b), and (c) are the 1st hierarchy reference image, study image, and difference image before registration; (d), (e), and (f) are the 2nd hierarchy reference image, study image, and difference image before registration; (g), (h), and (i) are the 3rd hierarchy reference image, study image, and difference image before registration; (j) is the difference image after affine registration of (g) and (h).

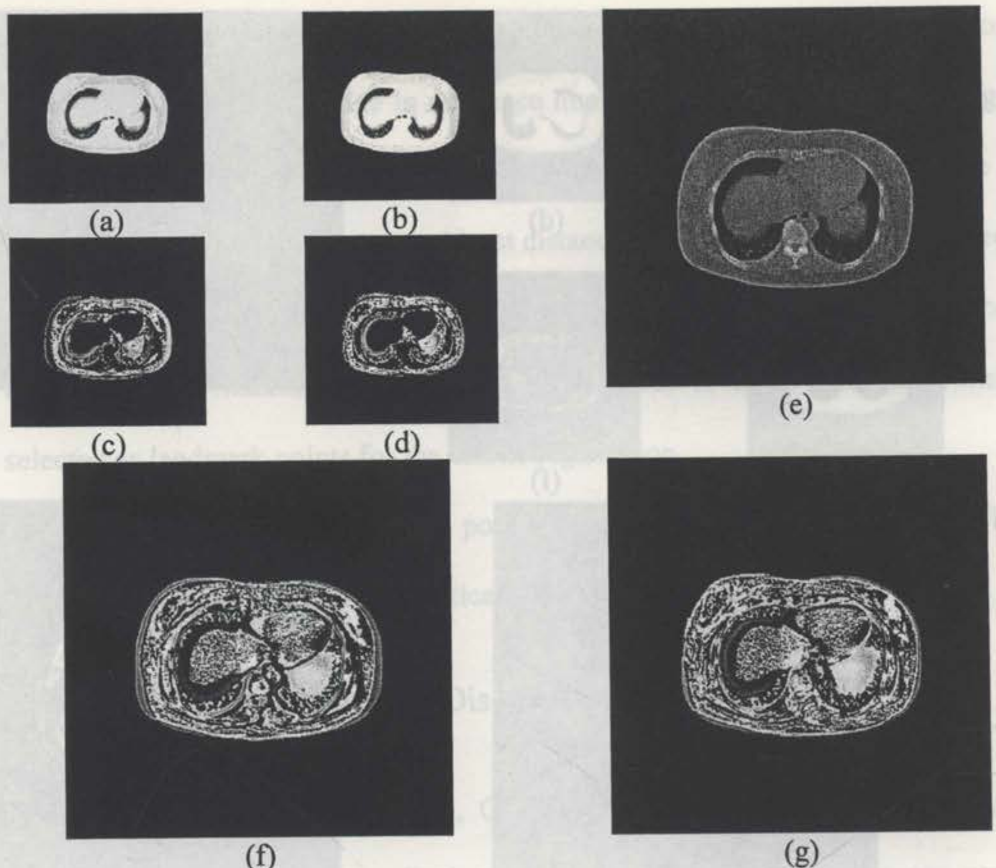

Figure 8-8 Intensity-based Hierarchicall Image Registration

(a) is the 2nd hierarchy reference image; (b) is the 2nd hierarchy study image after being initialized using the results of the 3rd hierarchy registration results (Figure 3 (j)); (c) is the difference image before registration being carried out in the 2nd hierarchy; (d) is the difference image after the registration in the same hierarchy; (e) is the final study image after the registration being carried out in the 1st hierarchy; (f) is the difference image after the study image being initialized by the result of 2nd hierarchy; and (g) is the difference image after the intensity-based registration.

The experimental results show that the lower resolution hierarchy, the less intensity information, and therefore, the worse registration precision. Even though low resolution hierarchy cannot provide very good registration accuracy, it can provide rough initial guess for high resolution hierarchies. Hence, the registration efficiency and precision can be improved. Because the extremely low resolution cannot contribute a lot to the final registration result, in our experiments, we divide the images into three hierarchies.

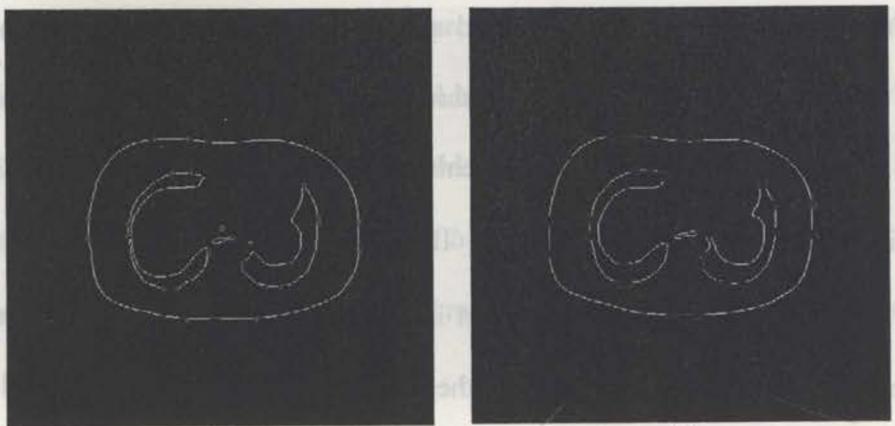

(a) (b)
Figure 8-9 Landmark-based Elastic Image Registration
(a) and (b) are the corresponding landmark points selected automatically in the reference edge image and the study edge image.

In our experiments of automatic landmark selection, to eliminate redundant and small-sized edges, we carry out morphological operations, closing and opening, before the edge extraction procedure is carried out. In the experimental results shown in Figure 8-9, 25 landmark points are selected automatically.

8.4 Application of Medical Image Registration Algorithm in Bioinformatics

8.4.1 Introduction of 2-D Gel Protein Image Registration

Proteomics is the study and analysis of the nature and function of DNA and protein sequence data. In the post-genome era, the analysis and study of proteomics are playing a more and more important role in the areas such as life science, therapeutics, and disease prevention and inhibition. Two-dimensional gel protein eletrophoresis is one of the main technologies in the analysis and separation of complex protein mixtures. This technology provides sufficient information about a variety of proteins simultaneously and hence can enhance and facilitate the quantitative and qualitative research of patterns of protein expression.

Image registration techniques are an important tool for the comparison and analysis of two-dimensional protein expression and structure. The paradigm of protein profiles matching methods is usually divided into three steps (Figure 9-1): pre-processing; spot detection and pattern matching. These matching algorithms often have drawbacks of high computational expense and low precision. There has a growing amount of interest in applying medical image registration in gel image processing, refer to papers of [DUN 2001] and [VEE 2001]. Because of the current technology of 2D gel protein eletrophoresis, the obtained images may be deformed randomly. Therefore, rigid registration which only corrects the rotation and translation deformations is not effective and the more complicated registration approaches are needed to solve these non-linear deformations. Principally, elastic registration approaches can be distinguished into intensity-based and feature-based methods. Feature-based registration approaches are widely used in registering 2D gel protein images because of high computational efficiency. In these approaches, the features can be extracted manually or interactively.

Fully and directly exploiting the image intensities, the intensity-based gel image registration algorithms have the advantages of no segmentation required. However, this registration category neglects the structural or morphological information of the images and the computational complexity is very high because of the large registration feature involved.

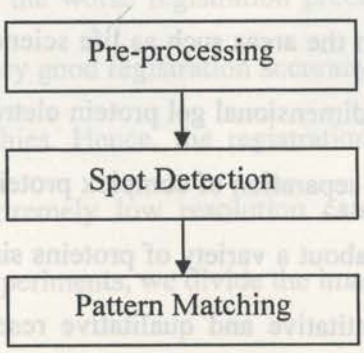

Figure 8-10 Paradigm of Some Existing Protein Profiles Matching Methods

Because of the important role of gel protein image registration in application and research, in our work, we extend our medical image registration algorithms to gel protein image registration area. Because hybrid and hierarchical registration approaches have the potential to achieve more efficient and more optimal registration results, in this part, the application of the proposed automatic hybrid method in bioinformatics is explored.

8.4.2 Experimental Validation

To access the performance of our proposed hybrid algorithm in the registration of biological images, experiments are carried out using 2D gel images of human blood plasma, human hela cell, and cerebrospinal fluid downloaded from Swiss-2DPAGE. Firstly, we deform the reference images with predetermined polynomial warping, translations, and rotations to create the study images. Then the proposed registration procedure is carried out to transform the study images to their corresponding reference images.

8.4.2.1 Intensity (Coefficient) Based Hierarchical Registration of Human Blood Plasma Gel Images

In our experiments, the global displacements are corrected by using hierarchical intensity-based method (Figure 8-11, Figure 8-12). The results of low-resolution layers are used as initial estimation for the high-resolution layers.

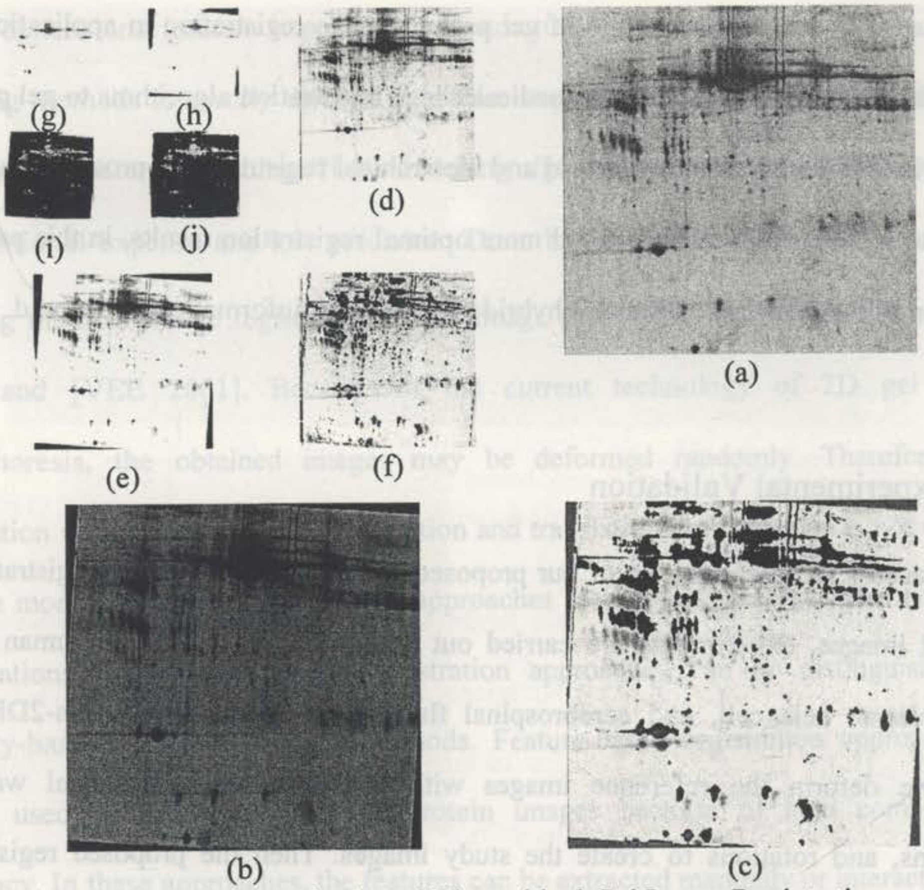

Figure 8-11 Intensity-based Hierarchical Gel Image Registration
(a), (b), and (c) are the 1st hierarchy reference image, study image, and difference image before registration; (d), (e), and (f) are the 2nd hierarchy reference image, study image, and difference image before registration; (g), (h), and (i) are the 3rd hierarchy reference image, study image, and difference image before registration; (j) is the difference image after affine registration of (g) and (h).

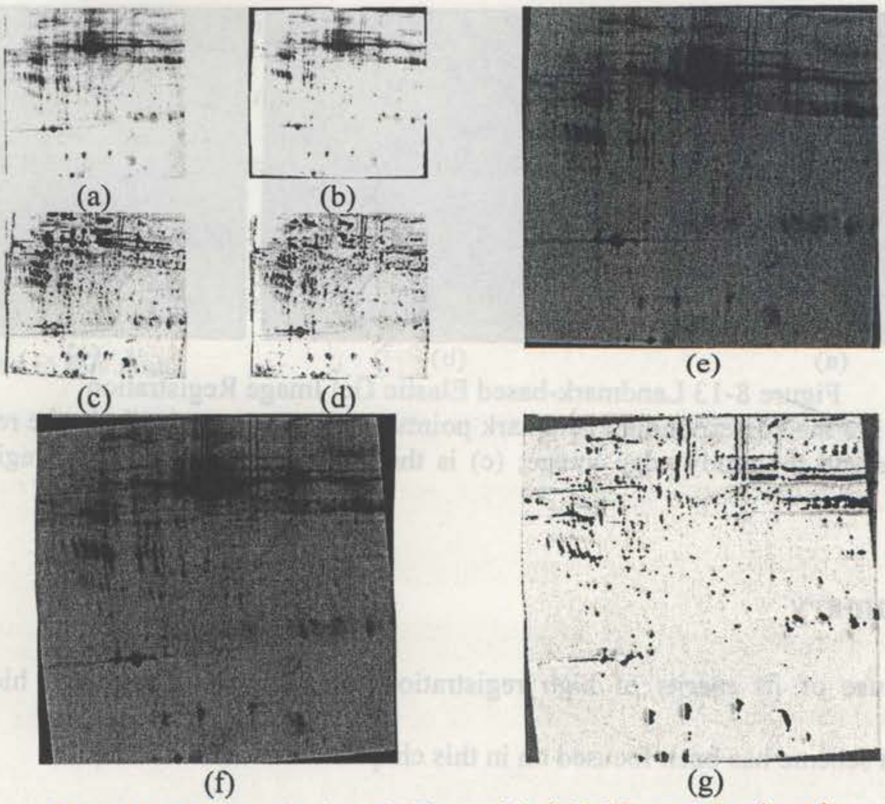

Figure 8-12 Intensity-based Hierarchical Gel Image Registration

(a) is the 2nd hierarchy reference image; (b) is the 2nd hierarchy study image after being initialized using the results of the 3rd hierarchy registration results (Figure 3 (j)); (c) is the difference image before registration being carried out in the 2nd hierarchy; (d) is the difference image after the registration in the same hierarchy; (e) is the study image of the 1st hierarchy after being initialized using the results of hierarchy 2; (f) is the final study image after the registration being carried out in the 1st hierarchy and (g) is the difference image after the intensity-based registration.

Similarly in experimental results on abdominal image registration, from the first stage registration experiments, we find out that the registration of very low resolution hierarchy images is not very helpful for the final registration results. It is mainly because we carry out our registration procedure in the low frequency domains, and excessive decomposition will lead to the loss of too much information.

8.4.2.2 Landmark-based Elastic Registration of Human Blood Plasma Gel Images

To further improve the registration accuracy, the elastic registration is carried out by using the automatically selected landmarks points (Figure 8-13).

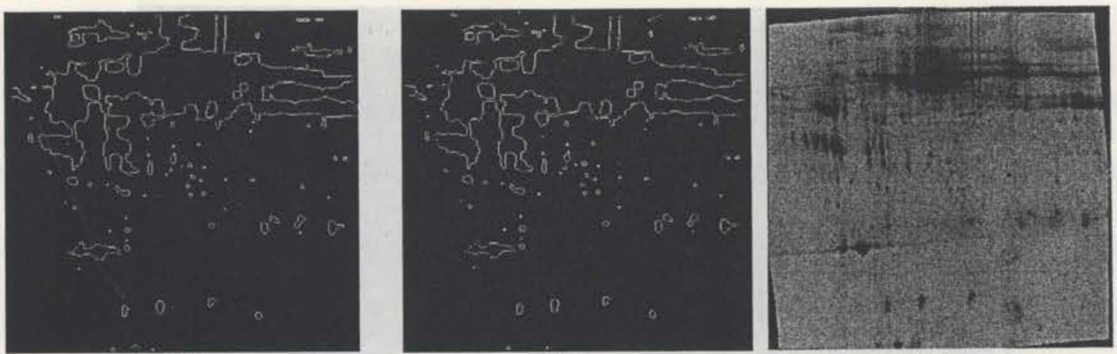

(a) (b) (c)

Figure 8-13 Landmark-based Elastic Gel Image Registration

(a) and (b) are the corresponding landmark points selected automatically in the reference edge image and the study edge image; (c) is the study image after elastic registration using TPS.

8.5 Summary

Because of its merits of high registration efficiency and accuracy, hierarchical registration scheme has been focused on in this chapter.

The registration approaches have been presented based on steerable wavelet transforms. However, these steerable wavelet based registrations can only deal with rigid displacements, and to register nonrigid distortions, further refinement is required. In the proposed brain image registration, the image intensity is used as registration feature space to avoid preprocessing; while in CT abdominal image registration, hybrid method is used to correct complex displacements between the images over time intervals.

Image registration technique is fundamental to the accurate and efficient analysis and comparison of protein sequence data. The hybrid medical image registration algorithm also has been extended to 2D gel protein image registration to facilitate the investigation of protein expression. By introducing the wavelet-based hierarchical algorithm to the 2D gel protein image registration area, the algorithm uses the low-frequency subbands as searching spaces in each registration pyramid hierarchy and provides high registration efficiency. In the second registration stage, the landmark points are selected automatically and then thin-plate splines are used to further improve the registration accuracy and performance by elastic registration. By making use of the merits of the intensity-based techniques and the feature-based registration methods, the algorithm can achieve registration results automatically. Further research efforts need to be devoted in this area.

CHAPTER 9 NON-ITERATIVE AND AUTOMATIC HIERARCHICAL REGISTRATION BASED ON IMAGE FEATURES

The fast wavelet transform can be obtained by MRA. However, coefficients of the shifted and rotated versions of the same dataset may be distributed differently. The lack of translation invariance and rotation invariance, which are the basic requirement for image registration procedure, makes the discrete wavelet based registration, especially the intensity or coefficient based registration, difficult.

Research efforts have been devoted to break the barrier of translation- and rotation-invariance, and innovative techniques such as steerable pyramid ([SIM 1992]) and translation invariant wavelets ([LIA 1996]), have been proposed. Accordingly, on the basis of the steerable filter, multiresolution registration method ([COL 2003]) was proposed. To cope with rotation displacements in wavelet-based matching, a rotation-invariant pattern matching method was introduced ([TSA 2002]), and adopted by [XUE 2004]. However, because the translation-invariance is neglected by this rotation-invariant pattern matching method, it would not be robust in dealing with more significant and complex displacements. Our pervious research exploration in Chapter 7 demonstrates that the intensity-based registration based on steerable wavelet cannot produce very ideal results especially for the complex abdominal images.

Alternatively, feature-based method is a potential solution to the problem of rotation- and translation-invariance in wavelet-based multiresolution registration. A wavelet-based coarse-to-fine matching method using interesting points as feature space was proposed ([YOU 2000]), and surface alignment approach using multiresolution wavelet representation was introduced ([GEF 2004]).

In this section, we focus on the investigation of efficient and accurate registration and a non-iterative hierarchical medical image registration method based on wavelet decomposition is presented.

Instead of estimating the registration parameters by traditional iterative optimization algorithms, the affine parameters are derived by minimizing the mean squared error (MSE). Firstly, based on wavelets, the images are decomposed into subbands which compose the registration pyramids; then, in each registration hierarchy, affine registration based on automatically selected features is performed and points of interest (POI) are selected in low-frequency subimages, and results of the current registration are used as the initial guess for the next hierarchy; finally, to further improve the registration performance, the local elastic registration is carried out in the highest resolution level. The proposed algorithm has been validated by experiments on Phantom data and clinical tomographic data.

The proposed hierarchical registration is carried out from the lowest resolution level, $Level\_L$, to the highest resolution level (the original image resolution level), $Level\_0$. For a certain registration level, $Level\_j$, two successive procedures need to be carried out: global affine registration process and points of interest (POI) extraction process. Then, the resulting affine parameters together with POI are passed to and serve as initial estimations of higher resolution level: $Level\_j-1$. The overview of the proposed algorithm is illustrated in figure 9-1.

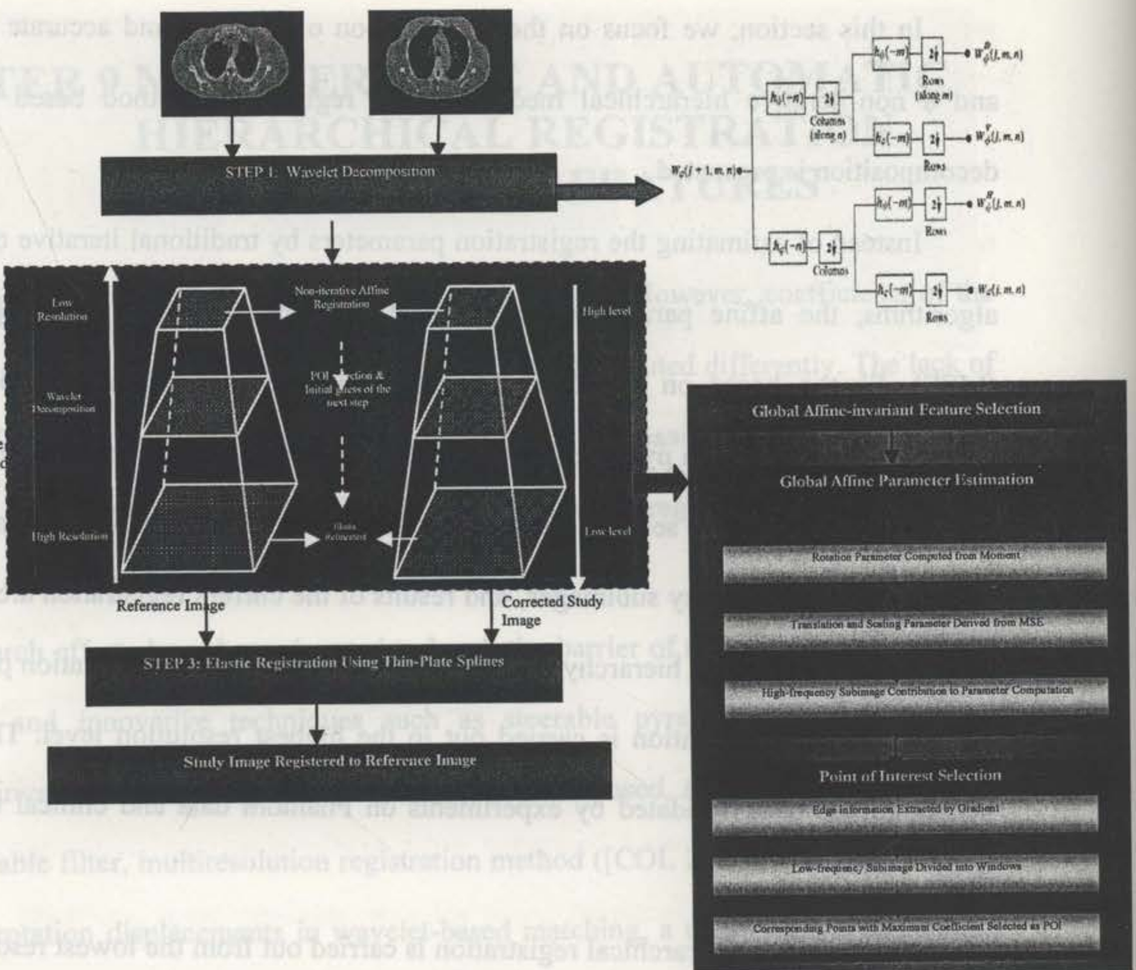

Figure 9-1 Non-iterative Wavelet-based Registration

9.1 Wavelet-Based Hierarchical Medical Image Registration

The main task of image registration is to determine a mapping to relate the pixels of one image to the corresponding pixels of a second image. For $p_i = (x, y) \in I_R$ and $q_i = (x', y') \in I_S$, where: I_R and I_S are 2-D reference image and study image, indexed by (x, y); affine transformation can be expressed in matrix form:

$$p_i = SRq_i + T = \begin{bmatrix} s_x & 0 \\ 0 & s_y \end{bmatrix} \begin{bmatrix} \cos\theta & -\sin\theta \\ \sin\theta & \cos\theta \end{bmatrix} \begin{bmatrix} x' \\ y' \end{bmatrix} + \begin{bmatrix} t_x \\ t_y \end{bmatrix}$$

Equation 9-1

9.1.1 Global Affine Registration Feature Extraction from Low-frequency Subimages

As mentioned previously, the feature-based registration has the advantage of high computation efficiency. However, how to automatically extract the corresponding features from the images to be registered is one of the significant challenges in this category of registration.

In our global affine registration, the features with property of affine transformation invariance are selected as basis for affine registration. The corresponding centroids, the points with maximum and minimum distance to the centroids, the first and second order moment invariants, the maximum axes, and the minimum axes are used as registration features. The reason for using these image features is because of the simple computation and the "physical" representation of image region. The corresponding points of these registration features are used to compose the global affine registration landmark pairs: $P_A = \{p_{Ai} | i = 1,2,.....n\} \in I_R$ and $Q_A = \{q_{Ai} | i = 1,2,.....n\} \in I_S$.

9.1.2 Non-iterative Affine Registration Parameter Determination

Once the corresponding affine registration pairs P_A and Q_A are extracted, another main concern is how to get the accurate transformation parameters. In global affine registration, the rotation parameters, scaling parameters and translation parameters need to be determined to minimize the mean squared error (MSE) of the corresponding landmark points.

$$E(S, R, T) = \frac{1}{n}\sum_{i=1}^{n} \|(SRq_{Ai} + T) - p_{Ai}\|^2$$

Equation 9-2

Iterative closest point (ICP) algorithm [BES 1992] is a good solution to image registration. However, the registration computational complexity of ICP is high [KAP

1999]. Instead of using iterative registration method, a non-iterative parameter estimation method is used in our approach to achieve efficient registration.

Step 1: Rotation Parameter Determination in Low-frequency Subimages

Usually, the calculation of optimal rotation parameter is difficult ([FIT 1998]). In this paper, we propose a simple method to determine the rotation parameter by using image features of major axes. Because of their insensitivity to the image intensity degradation, the major axes are used to estimate the rotation parameter in each registration pyramid layer. α_R and α_S, the angles between the x-axis and major axes of the images, are computed; then, the difference between α_s and α_R is used as the rotation parameter:

$$\theta_j = \alpha_S - \alpha_R \qquad \text{Equation 9-3}$$

Step 2: Translation and Scaling Parameter Calculation

Umeyama (1991) proposed a solution of deriving the affine transformation parameters by minimizing the mean squared error (Equation 9-2). We use this method to determine translation and scaling parameters. Umeyama proved that in order to minimize $E(S,R,T)$, $\frac{\partial E}{\partial T}$ must be equal to 0. From $\frac{\partial E}{\partial T} = 0$, we can get

$$T = \overline{p} - SR\overline{q} \qquad \text{Equation 9-4}$$

where: $\overline{q} = \frac{1}{n}\sum_{i=1}^{n} q_i$ and $\overline{p} = \frac{1}{n}\sum_{i=1}^{n} p_i$.

From $\frac{\partial E}{\partial S} = 0$, we can deduce

$$S = \frac{\sum_{i=1}^{n} \tilde{p}_i^{\,t} R \tilde{q}_i}{\sum_{i=1}^{n} \tilde{q}_i^{\,t} \tilde{q}_i} \qquad \text{Equation 9-5}$$

where $\tilde{q}_i = q_i - \overline{q}$ and $\tilde{p}_i = p_i - \overline{p}$.

Equation 9-4 and Equation 9-5 show that translation parameters and scaling parameters can be deduced from rotation parameter. By substituting θ in Equation 9-3 into Equation 9-4 and Equation 9-5, the translation parameters $T^c_j = \begin{bmatrix} t^c_{jx} \\ t^c_{jy} \end{bmatrix}$ and scaling parameters $S_j = \begin{bmatrix} s_{jx} \\ s_{jy} \end{bmatrix}$ can be calculated.

Step 3: High-frequency Subimage Contributions in Translation Parameter Estimation

So far, only the global information of low-frequency domain $W_\Psi(j)$ has been used in the global registration parameter determination. However, because the high-frequency subbands of $W_\Psi^{\,V}(j)$ and $W_\Psi^{\,H}(j)$ are important to represent local information in vertical and horizontal direction, this information is helpful in getting the accurate translation parameters.

After correcting the rotation and scaling displacements in the subimages, the vertical and horizontal displacements, $D_\Psi^{\,V}(j)$ and $D_\Psi^{\,H}(j)$, in subbands of $W_\Psi^{\,V}(j)$ and $W_\Psi^{\,H}(j)$, are calculated respectively. Then the final translation parameters of $Level\_j$ are determined by:

$$T_j = \begin{bmatrix} t_{jx} \\ t_{jy} \end{bmatrix} = \left(\begin{bmatrix} t^c{}_{jx} \\ t^c{}_{jy} \end{bmatrix} + \begin{bmatrix} D_\Psi^{\,H}(j) \\ D_\Psi^{\,V}(j) \end{bmatrix} \right) * \frac{1}{2} \qquad \text{Equation 9-6}$$

The transformation parameters obtained at current resolution level ($Level\_j$) are used as the initial estimation for the registration at a higher-resolution level ($Level\_j-1$) by keeping the rotation and scaling parameters unchanged and doubling the transformation parameters.

9.1.3 Points of Interest (POI) Extraction from Low-frequency Subimages

Even though the individual subband is not rotation-, translation-, and scale-invariant, the extreme coefficients of the subbands will keep as minimum and maximum coefficients after affine transformation. After the affine registration parameters are obtained, the global affine displacements between the subimages of $Level\_j$ can be corrected and there are only local elastic differences between the low-frequency subimages. Because wavelet transform not only can suppress the noise and small signal fluctuations ([MAL 1992]) but also provide compacted energy and local information in low-frequency domain, in this paper, we propose a method to extract Point of Interest (POI) from low-frequency subimages of each registration pyramid layer.

In low-frequency domain of layer j of registration pyramid:

Step 1: Firstly, the gradient magnitudes $g_{jR}(x,y)$ and $g_{jS}(x,y)$ of the low-frequency subimages of reference image and study image ($W_{\psi R}(j)$ and $W_{\psi S}(j)$) are calculated to extract edge information:

$$g_{jR}(x,y) = \left[G_{jRx}^{\ 2} + G_{jRy}^{\ 2}\right]^{1/2} = \left[(\partial I_{jR}/\partial x)^2 + (\partial I_{jR}/\partial y)^2\right]^{1/2}$$

and

$$g_{jS}(x,y) = \left[G_{jSx}^{\ 2} + G_{jSy}^{\ 2}\right]^{1/2} = \left[(\partial I_{jS}/\partial x)^2 + (\partial I_{jS}/\partial y)^2\right]^{1/2}$$

Step 2: Then, the low-frequency subimages, $W_{\Psi R}(j)$ and $W_{\Psi S}(j)$, are divided into n_{Rj} and n_{Sj} same-sized blocks and $n = \min(n_{Rj}, n_{Sj})$;

Step 3: POI pairs of $Level\_j$ selection: (To avoid POIs concentrate on a certain region of the image, at most one POI will be selected from each block)

For block_i=block_1 to block_n

1) find the points with maximum coefficient and maximum gradient (edge point) in block_i of $W_{\Psi R}(j)$ and $W_{\Psi S}(j)$ respectively:

$$P_{jRi} = \left\{ p_{jRim}(x_m, y_m) \middle| \begin{array}{l} m = 1..sizeof\ (block\_i); \\ (x_m, y_m) \in block\_i \text{ of } W_{\Psi R}(j) \wedge \\ W_{\Psi R}(j, x_m, y_m) = \max(W_{\Psi R}(j, block\_i)) \wedge \\ g_{jRi}(x_m, y_m) = \max(g_{jR}(block\_i)) \end{array} \right\}$$

and

$$Q_{jSi} = \left\{ q_{jSin}(x_n, y_n) \middle| \begin{array}{l} n = 1..sizeof\ (block\_i); \\ (x_n, y_n) \in block\_i \text{ of } W_{\Psi S}(j) \wedge \\ W_{\Psi S}(j, x_n, y_n) = \max(W_{\Psi S}(j, block\_i)) \wedge \\ g_{jSi}(x_n, y_n) = \max(g_{jS}(block\_i)) \end{array} \right\}.$$

2) POI correspondence:

if (there are more points in P_{jRi}), i.e., if ($m > 1$)

then {select the point with the smallest distance to the center point of block_i as the POI candidate: p_{jRi} };

If (there are more corresponding points POI in Q_{jSi}), i.e., if ($n > 1$)

then {select point q_{jSi} with the smallest distance with p_{jRi} as the corresponding POI candidate};

The results of (2) and (3) compose the $R-S$ POI candidate pair (p_{jRi}, q_{jSi});

3) Consistent POI pair determination:

check the POI candidate in $W_{rn}(j)$;

select the corresponding POI in $W_{sn}(j)$ to compose the $S-R$ POI candidate pair;

if ($S-R$ POI candidate pair== $R-S$ POI candidate pair)

then {it is selected as POI pair};

else {ignore both $S-R$ POI candidate pair and $R-S$ POI candidate pair}.

Step 4: Tune landmark points using cross correlation

For each point pair:

1) Extract an 11-by-11 template around the POI in study image and a 21-by-21 region around the POI in reference image
2) Calculate the normalized cross-correlation of the template with the region.
3) Find the absolute peak of the cross-correlation matrix.
4) Use the position of the peak to adjust the coordinates of the POI in study image.

Adjusted coordinates are accurate to one tenth of a pixel and subpixel accuracy can be achieved from the image content and POI pair selection.

9.2 Local Elastic Registration by Thin-Plate Spline

The results of the hierarchical registration are used to initialize the point-based elastic registration in the highest (original) resolution level of the registration pyramids. The automatically selected POI pairs are used as landmark points in the elastic registration process.

Thin-plate splines (TPS) is used in our registration refinement process. The POI of reference image and study image are $P = \{p_i = (x_i, y_i) | i = 1,2,......n\} \in I_R$ and

$Q = \{q_i = (x_i', y_i') | i = 1,2,......n\} \in I_S$, which compose n landmarks of reference image and study image respectively. After TPS interpolation, the POIs of study image can be wrapped to POIs of reference image as close as required. Therefore, the elastic deformations can be corrected.

9.3 Experiments

9.3.1 Experiments on Phantom Data

Phantom data (Figure 9-2) of 256*256 is used as reference image in this series of experiments. Study images are created by applying randomly generated affine transformations with parameters in the ranges of: $\theta \in [-\frac{\pi}{9}, \frac{\pi}{9}]$; $t_x \in [-20.0, 20.0]$; $t_y \in [-20.0, 20.0]$; $s_x \in [-0.8, 1.2]$; $s_y \in [-0.8, 1.2]$.

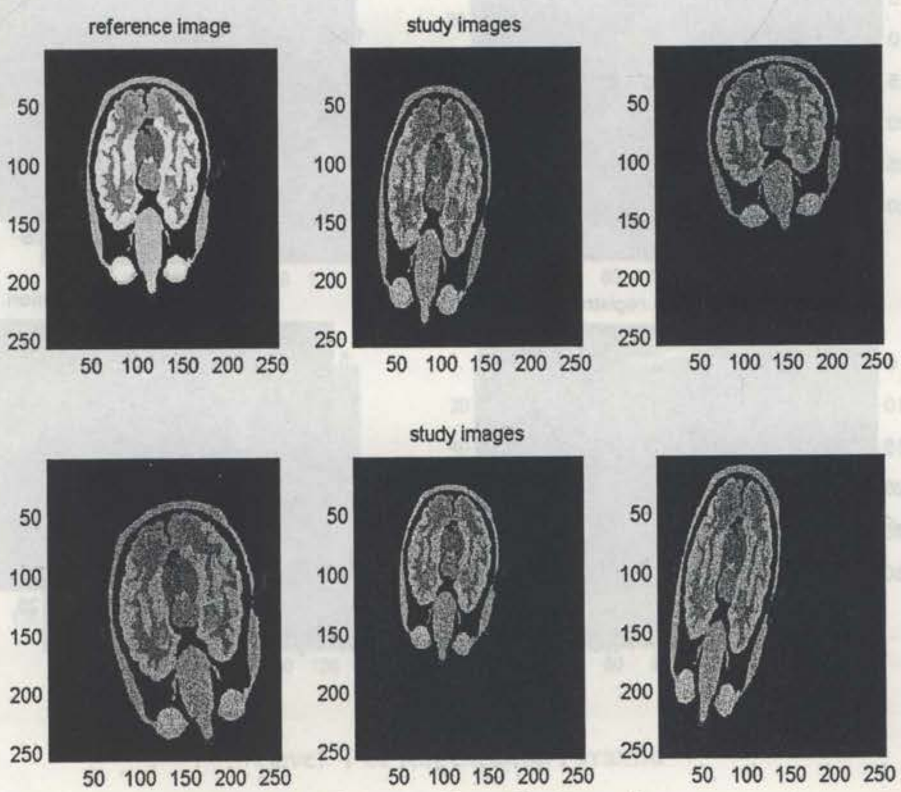

Figure 9-2 Phantom Data for Experiments

The images are decomposed into 4 levels to compose registration pyramids in this series of experiments. After the non-iterative affine registration in the lowest resolution level (level 3) with resolution of 32*32, Figure 9-3 (a), the low-frequency subimages are divided into blocks with size of 2*2, and POI pairs are selected. In the higher resolution levels (level 2 to level 0), the low-frequency subimages are initialized by the results of the previous level and further refined in the current level, and then are divided into blocks with size of 4 times of the corresponding blocks in the previous level. For each POI pair e.g., $(p_{jRi}(x_{jRi}, y_{jRi}), q_{jSi}(x_{jSi}, y_{jSi}))$ of the previous level, we search the blocks where $(2*x_{jRi}, 2*y_{jRi})$ and $(2*x_{jSi}, 2*y_{jSi})$ are located to find the POI pair in the current level. If coefficients of $(2*x_{jRi}, 2*y_{jRi})$ and $(2*x_{jSi}, 2*y_{jSi})$ also reach the maximum value, then this pair will be selected; otherwise, it will be discarded and the new pair will be selected.

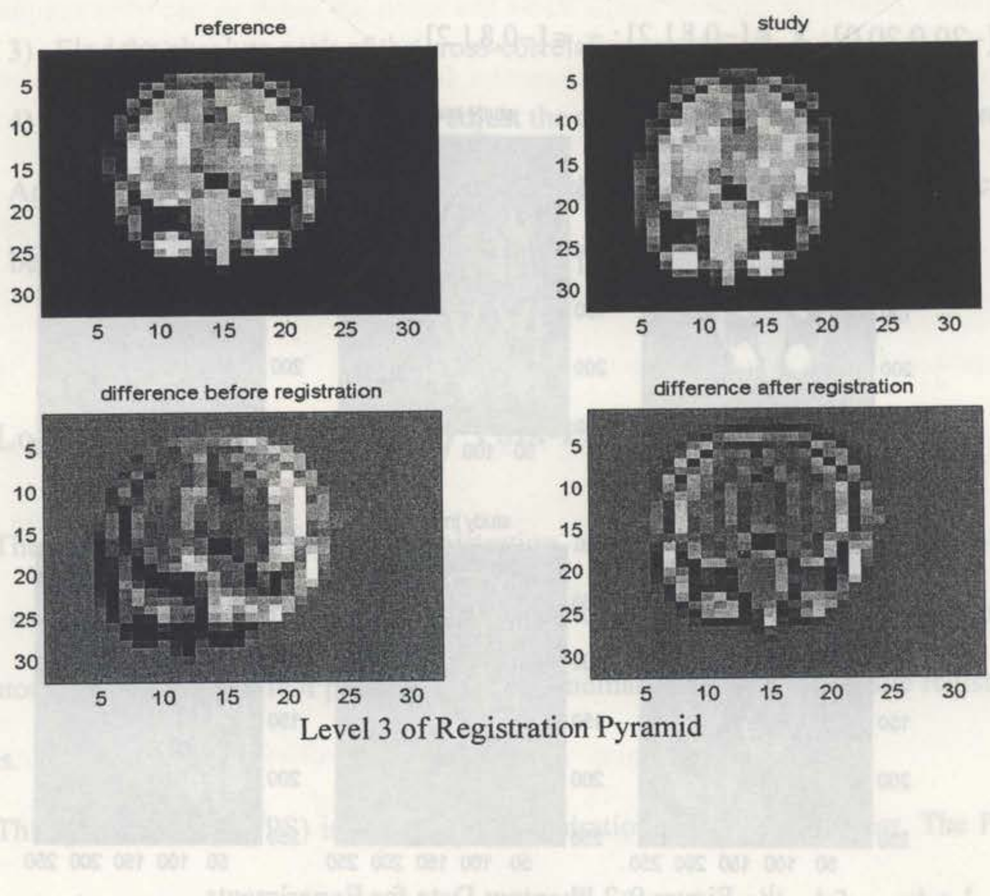

Level 3 of Registration Pyramid

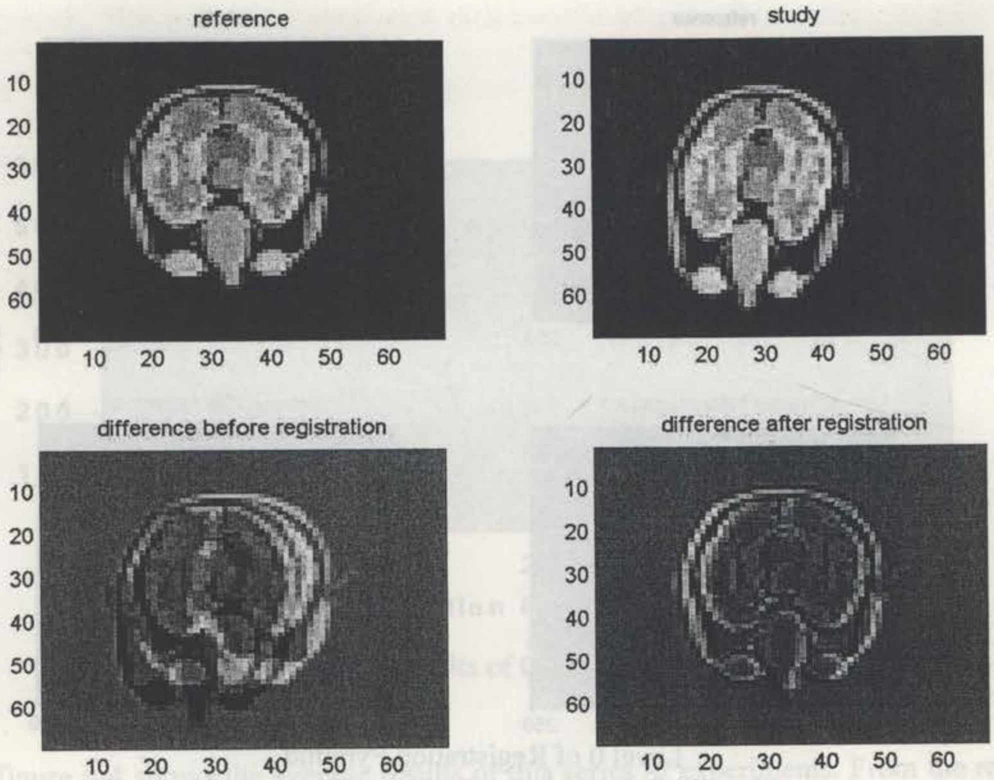

Level 2 of Registration Pyramid

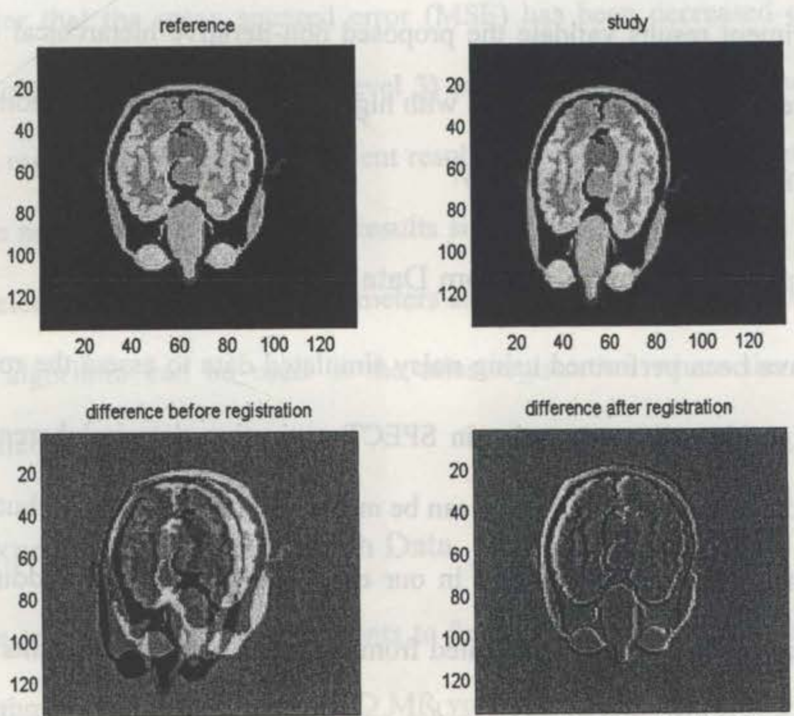

Level 1 of Registration Pyramid

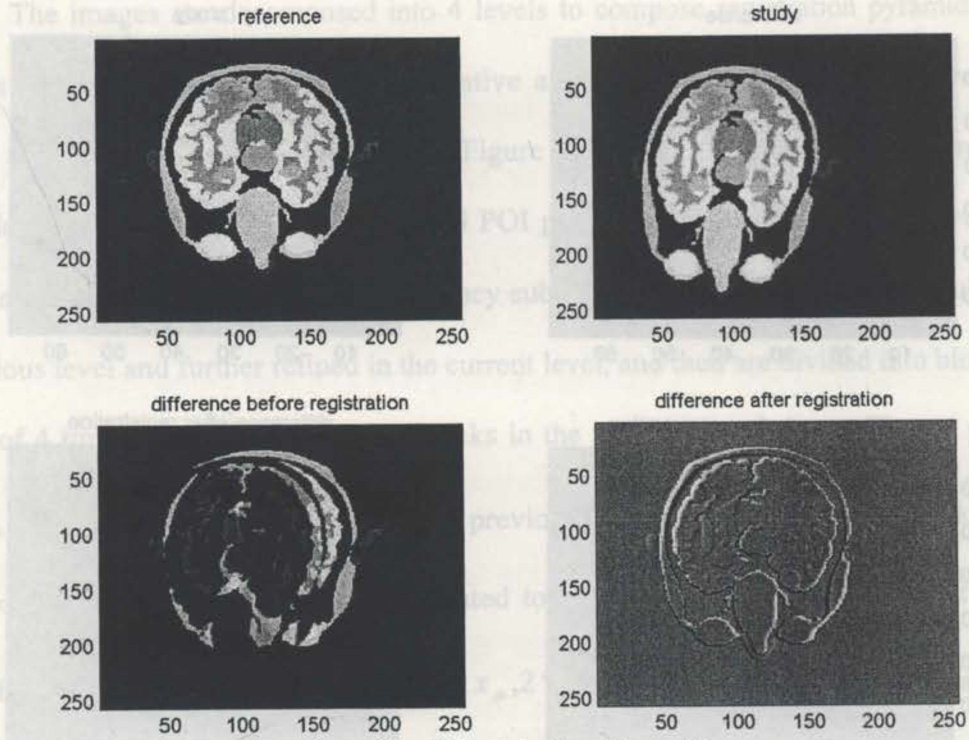

Level 0 of Registration Pyramid

Figure 9-3 Registration Results of Phantom Data

The experiment results validate the proposed non-iterative hierarchical registration method can correct the affine deformation with high precision and computation efficiency, and no elastic registration step is necessary.

9.3.2 Experiments on Noisy Phantom Data

Studies have been performed using noisy simulated data to assess the robustness of the proposed algorithm. Because noise in SPECT projection data is inherently Poisson distributed and the noise on the PET data can be modeled by a Poisson distribution as well, the images with Poisson noise are used in our experiments. Instead of adding artificial noise to the data, Poisson noise is generated from the data in our experiments to simulate noisy medical images. We superimpose noise onto the study images while the reference images are kept clean.

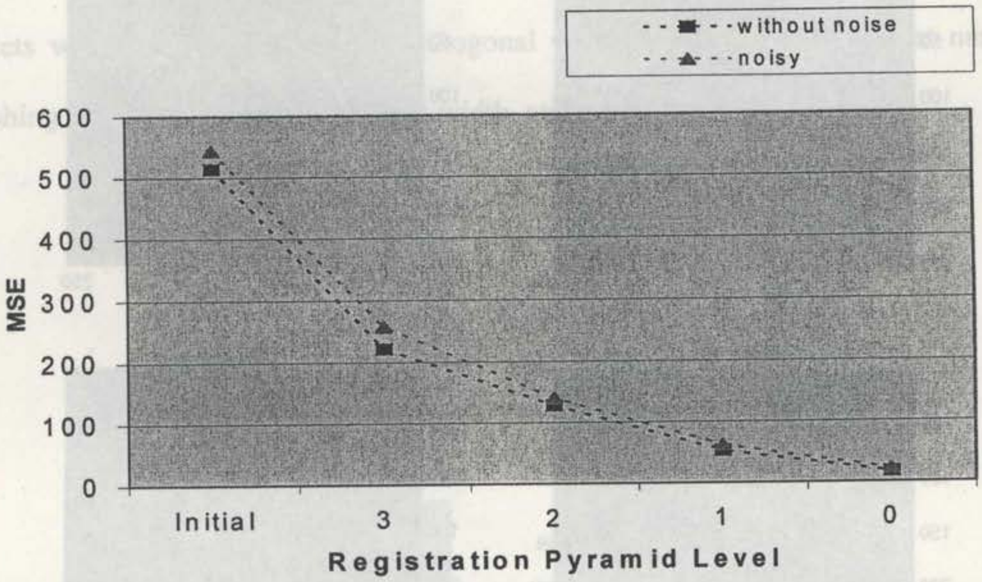

Figure 9-4 Experimental Results of Clean and Noisy Phantom Data

Figure 9-4 shows the average results of this series of experiments. From the results, we discover that the mean squared error (MSE) has been decreased greatly during the lowest resolution registration level (level 3) and the registration has been refined in high resolution registration levels. Experiment results in Table 9-4 demonstrate that the Poisson noise does not affect the registration results significantly, because both affine registration features selected and registration parameters are not changed when the noise is added. The proposed algorithm can be used in the atlas registration where the study images are contaminated by Poisson noise.

9.3.3 Experiments on MRI Brain Data

This section describes experiments to further evaluate accuracy and performance of the algorithm. Transverse slices of 3-D MR volume of same subject are registered. Before registration is conducted, automatic segmentation is carried out to extract cerebral tissue (Figure 9-5).

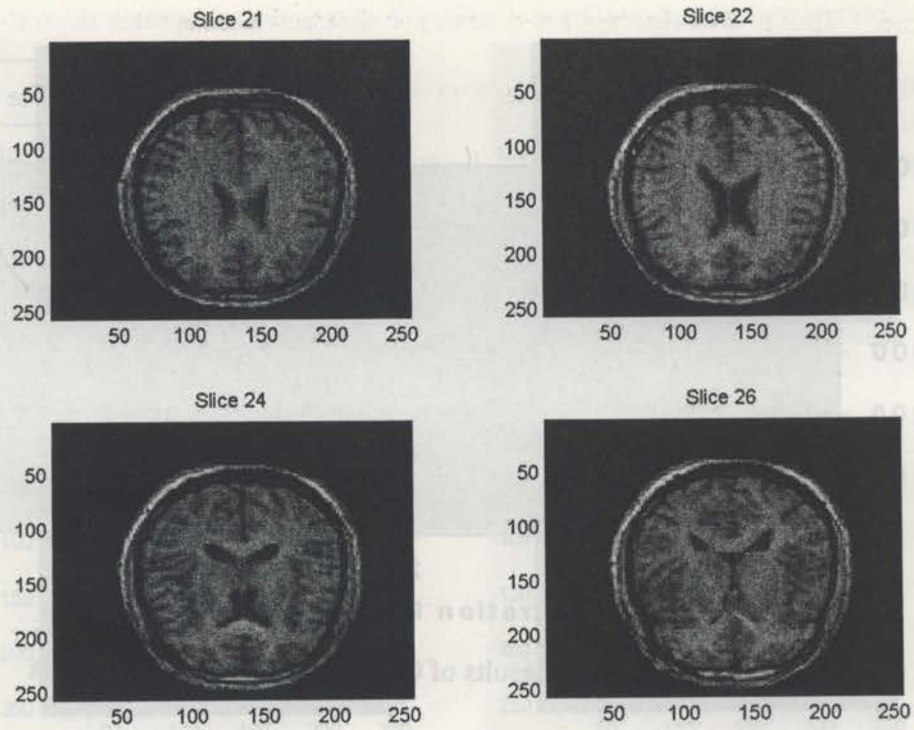

(a) MRI Brain Data

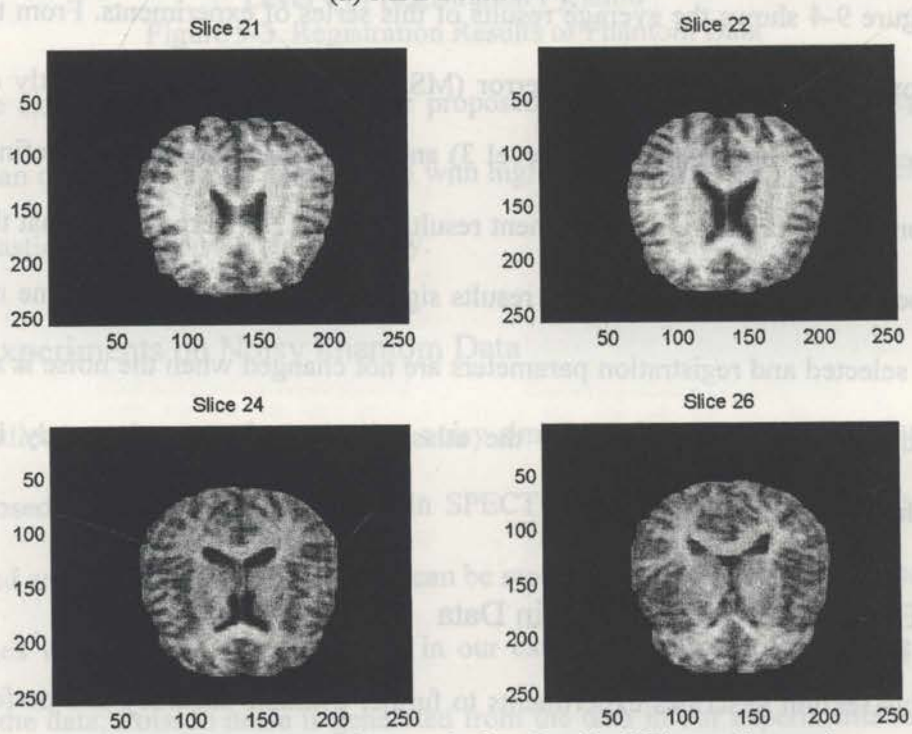

(b) MRI Brain Data before and after Cerebral Tissue Extraction

Figure 9-5 MRI Brain Data before and after Cerebral Tissue Extraction

Different wavelet filters are used to investigate their influence on the performance of the approach. The compactly supported orthogonal wavelets, Daubechies, Symlets, and Coiflets wavelets, and B-splines biorthogonal wavelets, which have highest number of vanishing moments for a given support width, are used in our experiments.

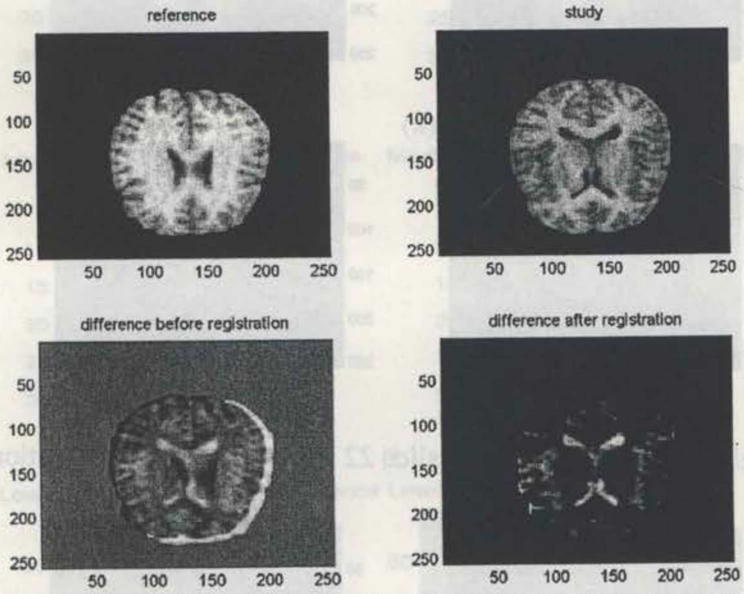

Registration of slice 21 and slice 25 by Symlet 8 Decomposition

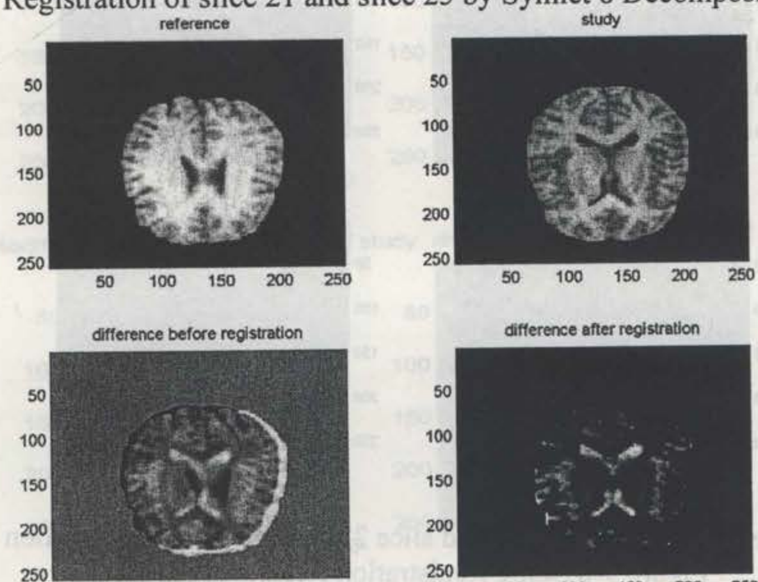

Registration of slice 21 and slice 25 by HAAR Decomposition

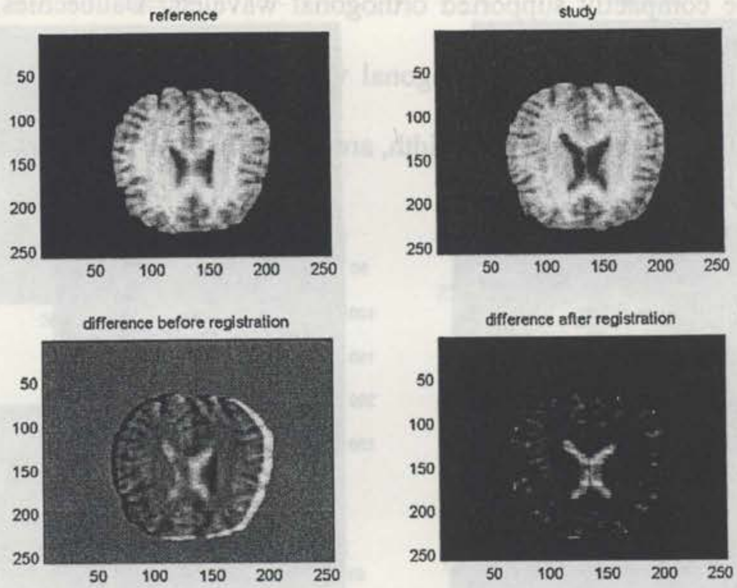

Registration of slice 21 and slice 22 by Symlet 8 Decomposition

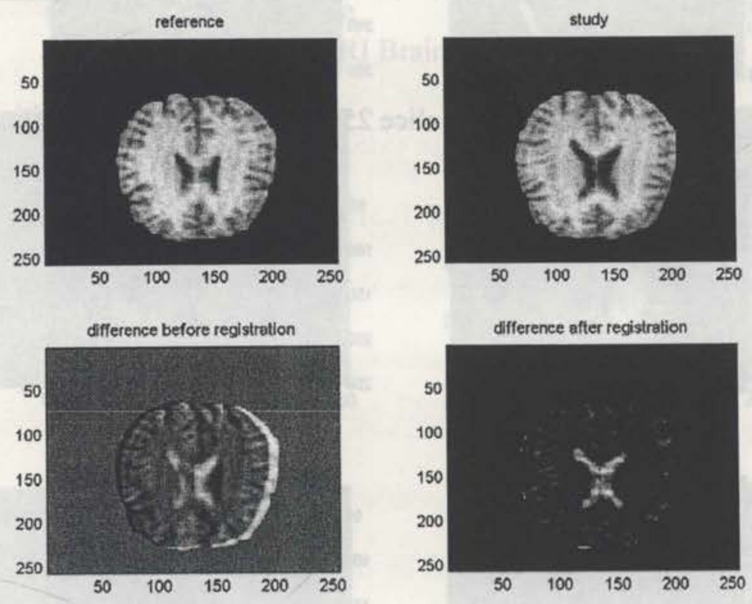

Registration of slice 21 and slice 22 by HAAR Decomposition

Figure 9-6 Some Registration Results of MRI Data

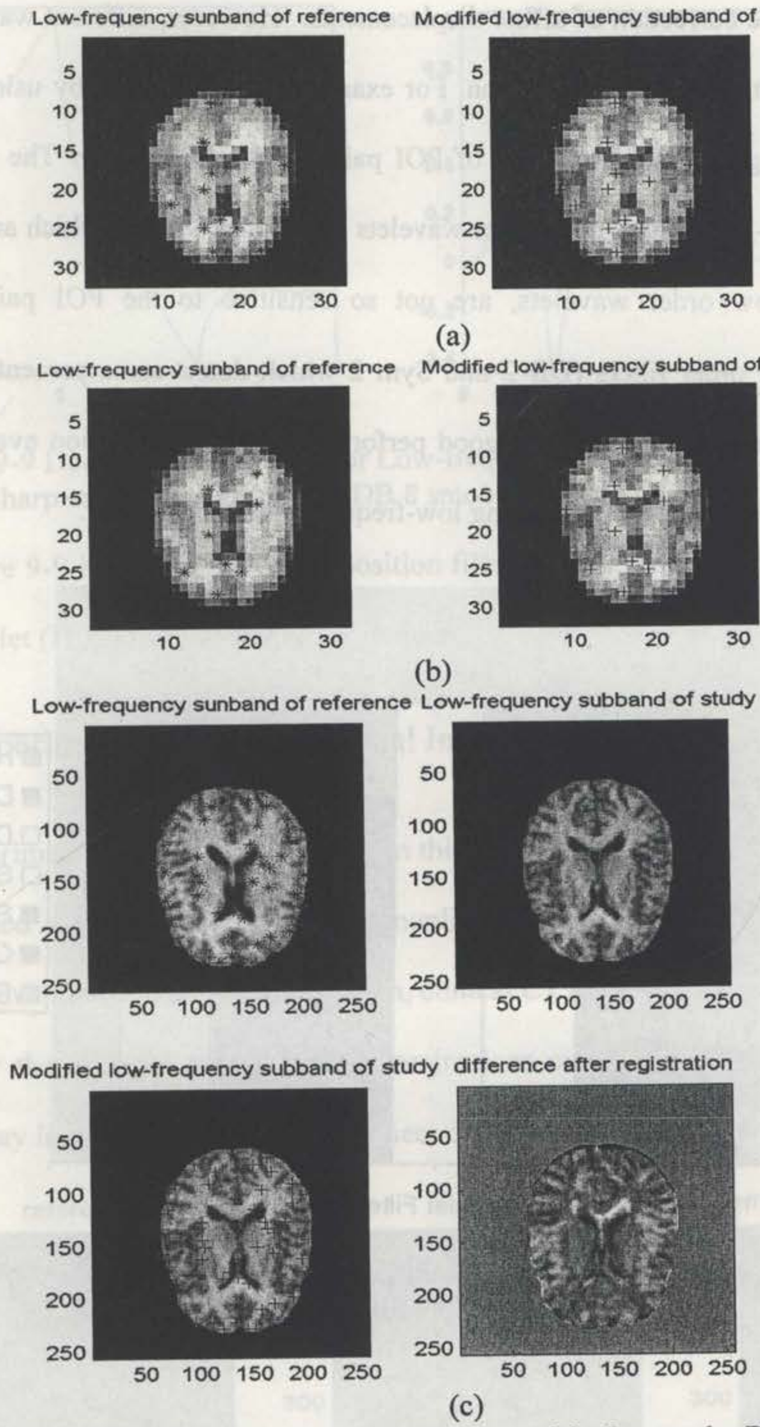

Figure 9-7 POI Pairs Selection in Low-frequency of the Images by Different Wavelets (a) by B-splines biorthogonal wavelet1.1; (b) by Haar wavelet; (c) POI pairs in the highest resolution level

In the affine registration procedure, selecting different wavelets does not affect the registration results significantly (Figure 9-6) because both the low-frequency domain and high-frequency domains in vertical and horizontal directions have been taken into consideration in the correction of affine displacements. However, different wavelet filters have strong impact on POI pair selection. For example, in Figure 9-7, by using different wavelets, we can get different number of POI pairs located differently. The experiment results in Figure 9-8 show that high order wavelets (DB 8 and Sym 8), which are smoother compared with low order wavelets, are not so sensitive to the POI pairs as their corresponding low order filters (DB 2 and Sym 2 which detect same percentage of POI pairs), B-splines biorthogonal 5.5 has good performance in POI detection even though it provides smoother wavelets for analyzing low-frequency domain as well.

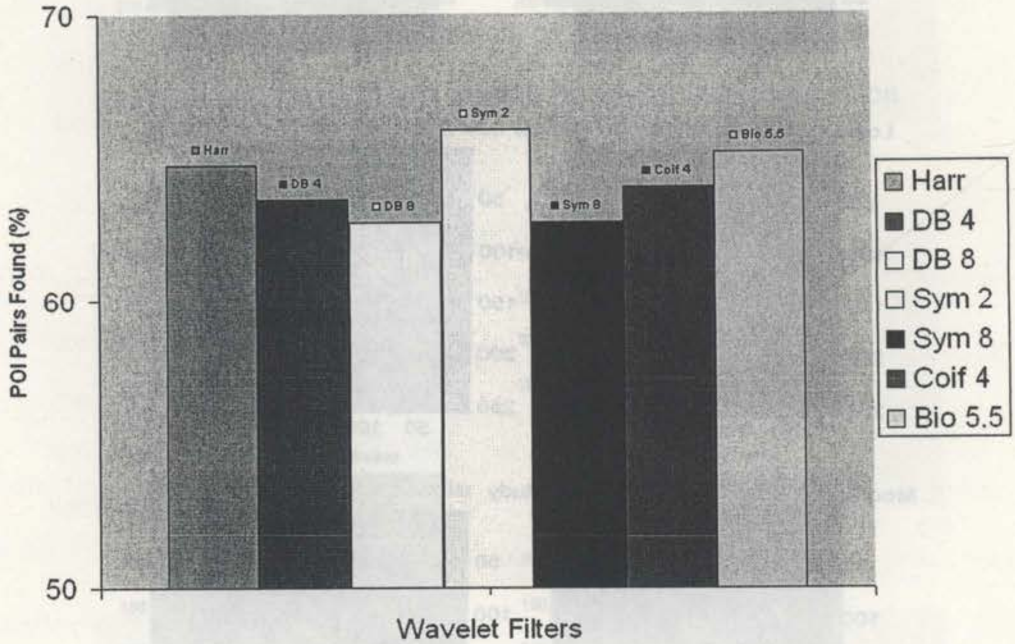

Figure 9-8 Comparison of POI Detection Performance Based on Different Wavelet Decomposition

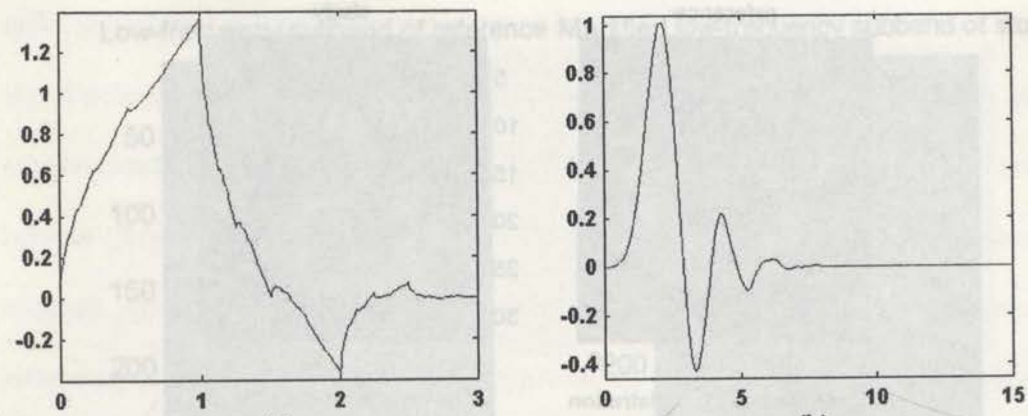

(a) (b)

Figure 9-9 Decomposition Filters for Low-frequency Domain of Different Wavelets
(a) DB 2 "sharp and narrow" filter; (b) DB 8 smooth filter

Figure 9-9 illustrates the decomposition filters of low order wavelet (DB2) and high order wavelet (DB8) for low-frequency domain.

9.3.4 Experiments on CT Abdominal Images

Experimental results are presented in this section to demonstrate the performance of the proposed algorithm in coping with nonlinear deformations in clinical tomographic images. To validate the proposed approach, clinical CT abdominal data (512*512) are used to monitor the changes over medical examinations over different time intervals. These changes may include both rigid and nonlinear distortions, Figure 9-10.

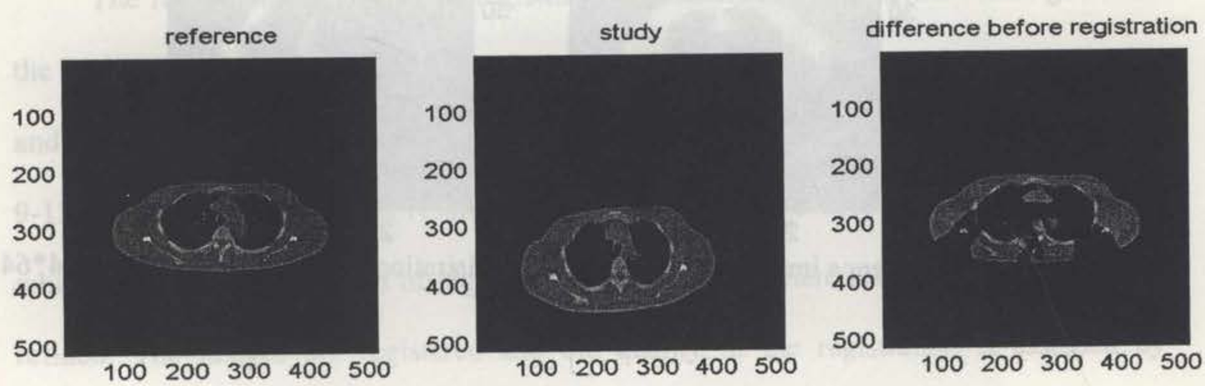

Figure 9-10 CT Abdominal Data for Experiments

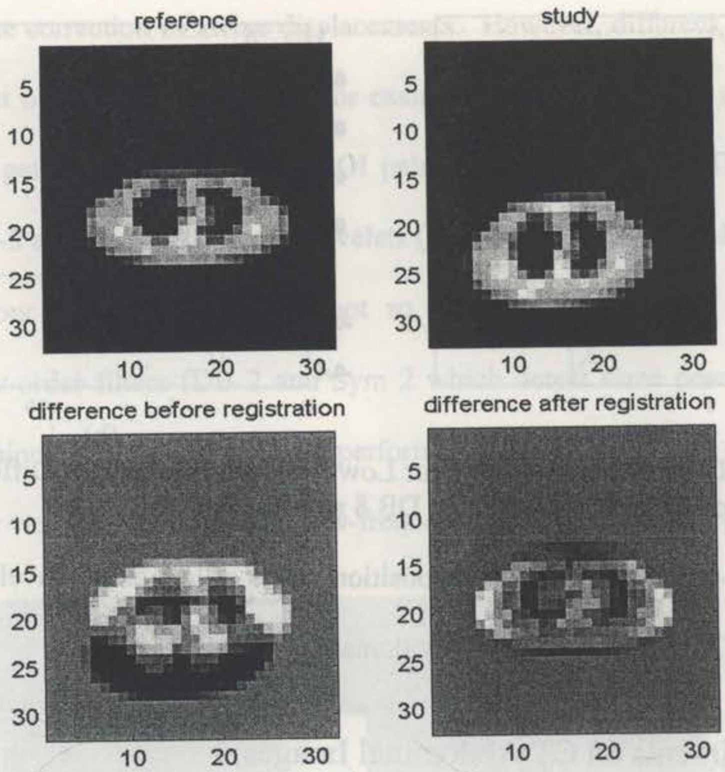

Figure 9-11 Lowest Resolution Level (Level 4 of 32*32) of Registration Pyramid
The 1st row is low-frequency subimages of reference and study; the 2nd row is the difference images before and after registration procedure is carried out.

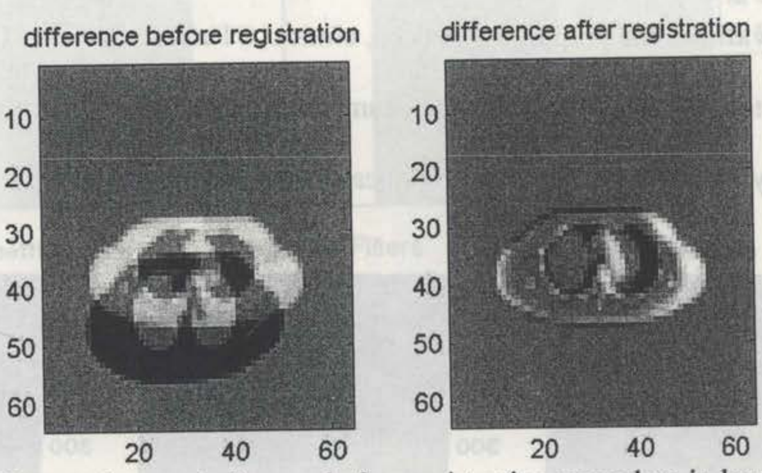

Figure 9-12 Difference images before and after registration procedure in level 3 of 64*64

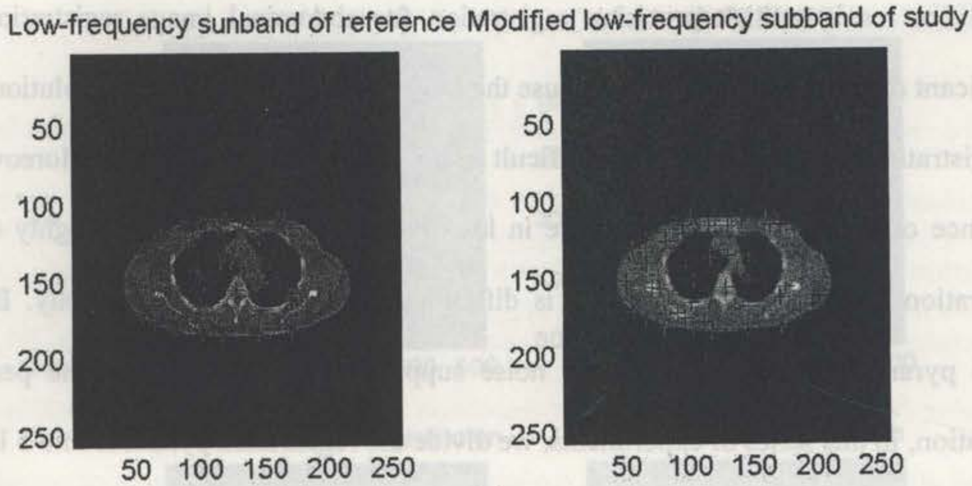

(a)

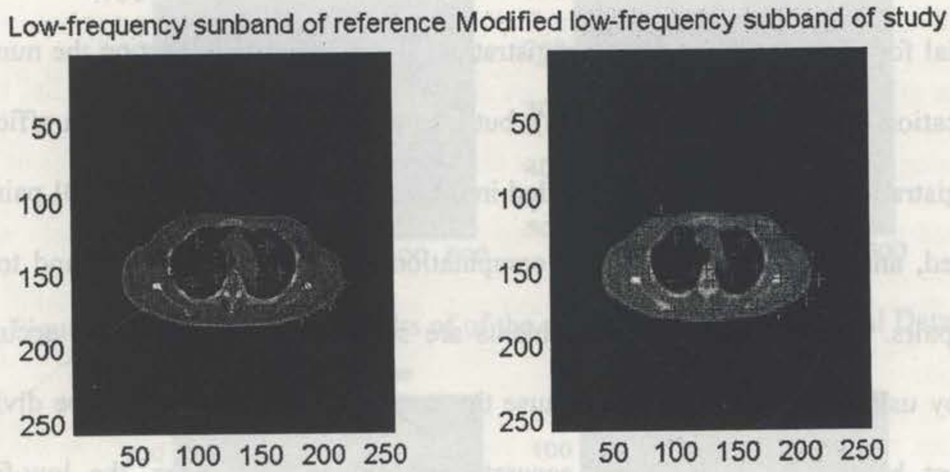

(b)

Figure 9-13 POI Pairs Selected by Using Different Size Blocks
(a) POI pairs found using blocks of 5*5; (b) POI pairs found using blocks of 7*7.

The results of low resolution registration hierarchy are used as the initial guess for the high resolution hierarchy by keeping the rotation and scaling parameters unchanged and multiplying the translation parameters by 2. From the results in Figure 9-11 and Figure 9-12 we know that the lowest resolution registration level provides good initial estimation which assists the registration of higher registration levels where the registration is further refined. The images are registered and the quality of the registration is assessed by comparing the transformed ones with the original ones.

The number of registration pyramid levels is one of important issue in our approach. Rough level division, which means no sufficient hierarchies in the registration pyramids, would not result in high precision registration for abdominal image registration with significant displacements. Firstly, because the large displacements in high resolution levels of registration pyramids make it is difficult to get accurate affine features. Moreover, the existence of the large amount of noise in low-frequency domain of the roughly divided registration pyramids would make it is difficult to select POI pairs correctly. Because subtle pyramid division can help in noise suppression and accurate affine parameter estimation, in this series of experiments, we divide the registration pyramids into 5 levels.

Block size is critical in the procedure of accurately selecting POI pairs which are essential for the point-based elastic registration. It not only has impact on the number and the location of POI pairs (Figure 9-13), but also influences the computation efficiency of the registration. If the images are divided into blocks of small size, more POI pairs can be obtained, and correspondingly, more computation time is needed to find and to register these pairs. However, when displacements are significant, we cannot get accurate POI pairs by using very small blocks because the corresponding features may be divided into different blocks. In order to get accurate and enough POI pairs, the low-frequency subimages of the lowest resolution level (32*32) are divided into blocks of 3*3 or 4*4 in our experiments on abdominal images.

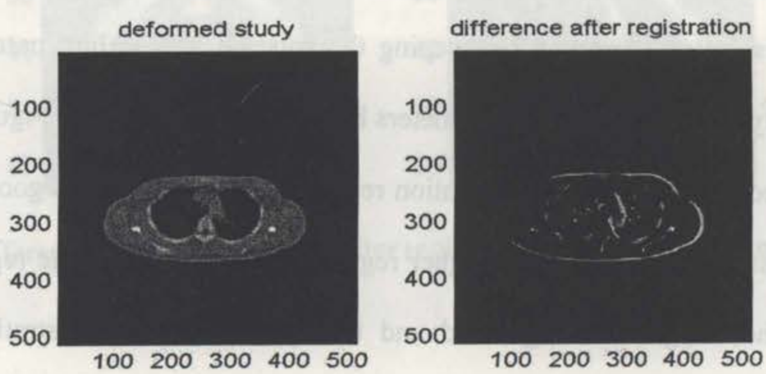

Figure 9-14 Registration Result after the Whole Registration Procedure

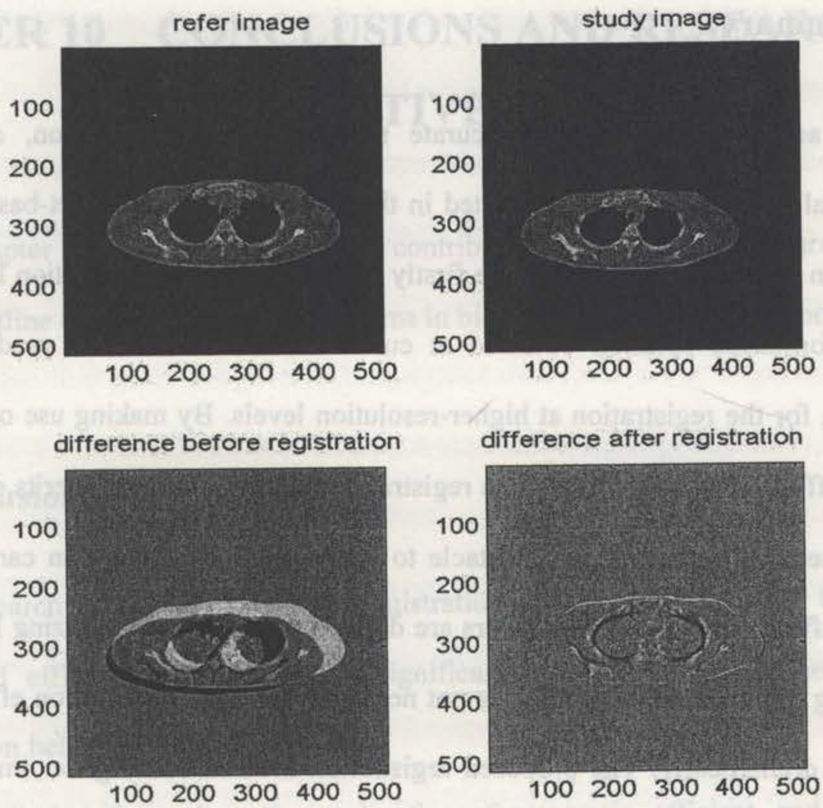

Figure 9-15 Registration Results of of the same person CT abdominal Data

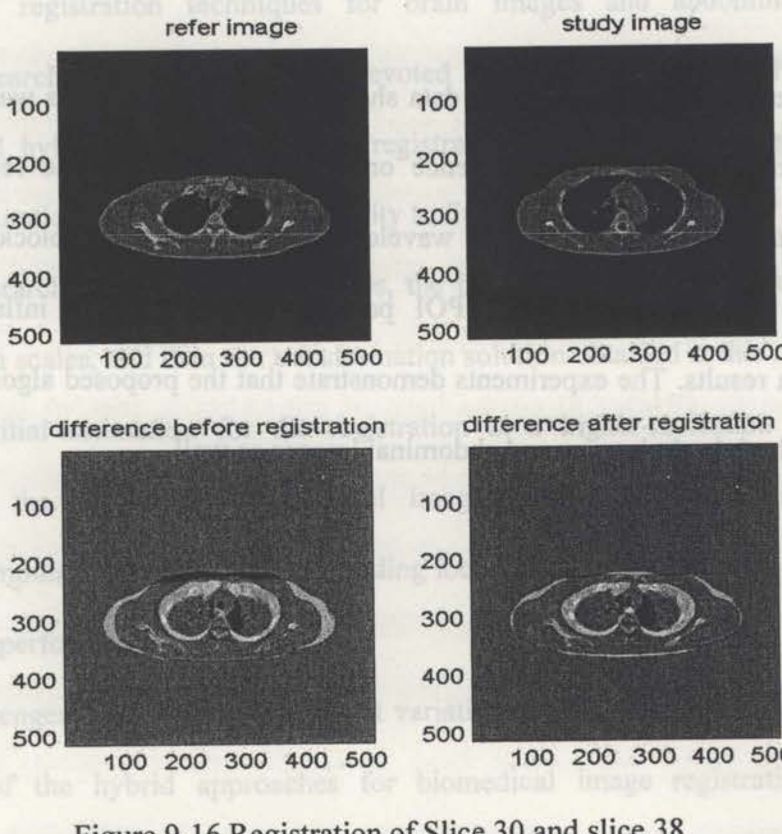

Figure 9-16 Registration of Slice 30 and slice 38

9.4 Summary

To achieve efficient and accurate medical image registration, a non-iterative hierarchical method has been presented in this chapter. In the wavelet-based hierarchical registration procedure, the images are firstly registered at lower-resolution levels, and then the transformation solution obtained at current resolution level is used as the initial estimation for the registration at higher-resolution levels. By making use of automatically selected affine-invariance features as registration feature space, the merits of wavelets can be exploited while the inherent obstacle to wavelet-based registration can be overcome. Because affine registration parameters are derived directly by minimizing MSE, the time-consuming optimization procedure is not necessary, and the registration efficiency can be improved dramatically. The proposed registration method can register images with both affine displacements and elastic distortions, and high registration precision can be achieved.

Our experiments on different data show that Poisson noise, as well as the different wavelets, has no significant influence on the non-iterative affine registration results. However, the selection of different wavelets and the variation of block size have strong impact on the determination of POI pairs and therefore will influence the elastic registration results. The experiments demonstrate that the proposed algorithm can be used to register both brain images and abdominal images as well.

CHAPTER 10 CONCLUSIONS AND RESEARCH PERSPECTIVES

This chapter will summarize our main contributions, suggest a few future research trends, and outline our future research concerns in biomedical image registration area.

10.1 Conclusion

The research on biomedical image registration is carried out with the belief that automatic and efficient registration will significantly benefit healthcare service and improve human being's life quality.

This thesis has focused on the exploration of automatic, efficient, and non-rigid medical image registration techniques for brain images and abdominal images. Especially, research efforts have been devoted to hierarchical biomedical image registration and hybrid biomedical image registration that have advantages of both increased computation efficiency and the ability to find better solutions.

In the hierarchical registration methods, the images are first registered at coarse, lower-resolution scales, and then the transformation solution obtained at this resolution is used as the initial estimation for the registration at a higher-resolution scale. The advantages of the hierarchical biomedical image registration approaches include accelerating computation efficiency and avoiding local minima, and therefore, improving the registration performance.

The challenges created by inter-subject variations in the organ structures promote the research of the hybrid approaches for biomedical image registration. Hybrid registration approaches, combining the intensity-based algorithms with landmark-based methods and making use of the merits of both these methods, have potential to achieve automatic and high performance biomedical registration results.

1. To improve the registration accuracy without significant additional computational cost needed, an elastic registration based on image intensity has been described in Chapter 4.
2. To fully make use of both intensity information and structural information of the images, two hybrid automatic image registration approaches have been presented in Chapter 5. By making use of automatically selected landmarks in the elastic registration procedures, these registration methods can be used to register multimodal medical images.
3. Not only devote our research energies and enthusiasm to brain image registration, we also realize the important role of abdominal image registration in improving human being's life quality. However, abdominal image registration is more complex and challenging task because of more complex and involuntary movements of organs. By using the traditional optimization searching methods, it would be difficult to achieve efficient registration results. The intensity-based registration approaches would not be able to generate optimal results, especially for the case of multimodality image registration. In our research, an efficient and elastic registration method has been proposed (in Chapter 6) on the basis of automatically selected feature points and active contours. The method can be applied to intra-subject registration, inter-subject registration, monomodality image registration, and multimodality image registration.
4. Wavelets provide a flexible image analysis and processing mechanism by representing the image information in multiresolution and different frequencies. Wavelets have been widely used in image processing areas, including image reconstruction, image compression etc. However, the application of wavelets in

medical image registration has not been investigated extensively. To explore its application in hierarchical medical image registration, intensity (coefficient) based registration method (Chapter 8) on the basis of steerable wavelet decomposition has been presented, which can register both brain images and abdominal CT images as well. Besides, the hybrid and hierarchical registration method has been applied to bioinformatics to register the gel protein images.

5. To facilitate practical clinical applications and avoid being trapped in local minimal by traditional optimization methods, an efficient non-iterative hierarchical registration method has been proposed (Chapter 9) by deducing the registration parameters directly from MSE. On the basis of automatically selected affine-invariance image features, the inherent obstacle of MRA to registration can be overcome. The method not only can correct rigid distortions but also can register the images with non-rigid displacements.

10.2 Future Challenges

Duncan and Ayache [DUN 2000] presented an excellent prospective of challenges ahead in medical image analysis area. In this section, we summarize a few of the many possible and potential research trends in the biomedical image registration area.

1. Precise and efficient biomedical image registration is not only a big challenge, but also provides exciting opportunities to improve the quality and safety of diagnostic and medical decision making, treatment monitoring, and healthcare support. Although the more advanced imaging system, the PET scanner containing a CT scanner, has been developed, there is still a need for multi-dimensional, multimodality image registration techniques to assist the analysis of temporal changes and the integration

of necessary information from different imaging modalities.

2. The applications of multimedia techniques, for example, electronic patient records and medical images, greatly push the advance of e-health and telemedicine. As an important component and technique of e-health and telemedicine, accurate and efficient biomedical image registration will play a more and more important role in remote diagnosis, patient monitoring, teleradiology, and overcoming the barriers of distance in health care service.
3. Although the existing image-based virtual human can provide the healthcare professionals with a quality of anatomical information and knowledge, there is a need to produce virtual humans with both anatomical and functional information and knowledge. Hence, whole-body multimodality image registration needs further efforts to support the virtual human projects which are essential in surgery simulation and virtual and augmented reality in medicine.
4. The multimodality biomedical image registration will be more and more important in medical diagnosis, surgery planning as well as intraoperative navigation, and in the future, biomedical image registration will play a more essential role in helping people to discover the mysteries of the human body and its complicated functions.

10.3 Future Work

This thesis has concentrated on the research of automatic and elastic registration for brain images and abdominal images. However, multimodal deformable organ registration needs further exploration and investigation. Furthermore, in order to benefit clinical safety and facilitate clinical decision making, automatic registration, especially for the deformable organs such as heart, lung, and liver, is highly desirable.

Our future research work will target at solving the following aspects:

1) Elastic registration approaches for the integration of deformable organ information from multiple imaging modalities.
2) Automatic approaches for the registration of heart images, lung images, and liver images. Hybrid methods, combining similarity measures with morphological information may provide possibilities for elastic registration.
3) The validation of the registration performance is particularly important. Although a wide variety of registration approaches have been proposed, objective validation of these methods is not well established. Image databases may in the future provide a source for the objective comparison of different registration methods.

Although it has attracted considerable researchers, biomedical image registration is not widely applied in routine clinical practice. With continuous developments of medical imaging techniques and their applications in clinical areas, biomedical image registration will remain a challenge in the future. With ever-increasing growth of medical datasets with higher resolution, higher dimensionality, and wider range of scanned areas, the demand for more efficient biomedical image registration will increase and there is a long way to go in the research of biomedical image registration.

BIBLIOGRAPHY

[ACK 2001]

Ackerman, M.J., Yoo, T., & Jenkins, D. (2001). "From data to knowledge-the Visible Human Project continues," Medinfo, 10 (2), pp.887-890.

[ALP 1990]

Alpert, N. M., Bradshaw, J. F., Kennedy, D. & Correia, J. A. (1990). "The principal axes transformation - A method for image registration," J. Nucl. Med., 31, pp.1717-1722.

[AUD 2000]

Audette, M., Ferrie, F. & Peters, T. (2000). "An algorithm overview of surface registration techniques for medical imaging," Medical Image Analysis, 4(4), pp.201-217.

[AYA 1993]

Ayache, N., Guéziec, A., Thirion, J., Gourdon, A., & Knoplioch, J. (1993). "Evaluation 3D registration of CT-scan images using crest lines," In Wilson, D.C. & Wilson, J.N. (Eds.), Mathematical methods in medical imaging, 2035, pp.60-71. Bellingham, WA: SPIE Press.

[BAJ 1989]

Bajcsy, R. & Kovacic, S. (1989). "Multiresolution Elastic Matching," Computer Vision, Graphics, and Image Processing, 46, pp.1-21

[BAN 2000]

Bankman, I. (2000). Handbook of medical imaging: processing and analysis. Academic Press.

[BES 1992]

Besl P.J. & MaKey, N.D. (1992). "A method for registration of 3-D shapes," IEEE Trans, PAMI, 14(2), pp.239-256.

[BOO 1989]

Bookstein, F. L. (1989). "Principal warps: Thin-plate splines and the decomposition of deformations," IEEE Trans. Patt. Anal. Mach. Intell., 11(6), pp.567-585.

[BOR 1988]

Borgefors, G. (1988). "Hierarchical chamfer matching: a parametric edge matching algorithm," IEEE Transactions on pattern analysis and machine intelligence, 10, pp.849-865.

[BRO 1992]

Brown, L.G. (1992). "A survey of image registration techniques," ACM Computing Surveys 24(4), pp.325-376.

[CHE 1987]

Chen, C., Pellizari, C.A., Chen, G.T.Y., Cooper, M.D., & Levin, D.N. (1987). "Image analysis of PET data with the aid of CT and MR images," Information processing in medical imaging, pp.601-611.

[CHR 2001]

Christensen, G.E. & Johnson, H. (2001). "Consistent Image Registration," IEEE Trans. Med.imag., 20, pp.568-582.

[CHR[1] 1996]

Christensen, G.E., Kane, A.A., Marsh, J.L., & Vannier, M.W. (1996). "Synthesis of an individual cranial atlas with dysmorphic shape," Mathematical methods in biomedical image analysis, pp.309-318. Los Alamitos, CA: IEEE computer society press.

[CHR 1996]
Christensen, G.E., Miller, M.I., Vannier, M. & Grenarder, U. (1996). "Individualizing neuroanatomical atlases using a massively parallel computer," IEEE Computer, 29(1), pp.32-38.

[COL 1995]
Collignon, A., Maes, F., Delaere, D., Vandermeulen, D., Suetens, P., & Marchal, G. (1995). "Automated multimodality image registration using information theory," In Bizais, Y & Barillot, C., & Di Paola, R. (Eds.), Information Processing in Medical Imaging, (pp. 263-274), Ile de Berder, France.

[CAN 1986]
Canny, J. F. (1986) "A computional approach to edge detection", IEEE Trans. Pattern Analysis and Machine Intelligence", 8(6): 679-698, 1986.

[COH 1993]
Cohen, I. and Cohen, I. (1993). "Finite-element methods for active contour models and balloons for 2-D and 3-D images," IEEE Pattern Anal. Machine Intelligence, vol.15, pp.1131-1147, Nov. 1993.

[COL 2003]
Cole-Rhodes, A. A., Johnson, K. L. , LeMoigne, J. and Zavorin, I. (2003) "Multiresolution registration of remote sensing imagery by optimization of mutual information using a stochastic gradient," IEEE Transactions on Image Processing, vol. 12, no. 12, pp.1495-1511, Dec. 2003.

[COL 1995]

Collignon, A., Vandermeulen, D., Suetens, P., & Marchal, G. (1995). "3D multi-modality image registration using feature space clustering," In Ayche, N. (Ed.) Computer Vision, Virtual Reality, and Robotic Mechine, 905, of Lecture Notes in Computer Science, (pp.195-204). Berlin: Springer-Verlag.

[COL 1994]

Collins, D.L., Neelin, P., Peters, T.M., & Evans, A.C. (1994). "Automatic 3D intersubject registration of MR volumetric data in standardized Talairach space," Journal of computer assisted tomography, 18(2), pp.192-205.

[DAU 1988]

Daubechies, I. (1988) "Orthogonal bases of compactly supported wavelets," Commun. Pure Appl. Math., vol.41, pp. 909-996, 1988.

[DAU 1994]

Daubechies, I. (1994) "Ten lectures on wavelets," CBMS, SIAM, 61, pp.194-202, 1994.

[DAV 1996]

Davatzikos, C. A., Prince, J. L., & Bryan, R. N. (1996). "Image registration based on boundary mapping," IEEE Trans. Med. Imag., 15, pp.112–115.

[DEY 1999]

Dey, D., Slomka, P.J., Hahn, L.J., & Kloiber, R. (1999). "Automatic three-dimensional multimodality registration using radionuclide transmission CT attenuation maps: a phantom study," J. Nucl. Med., 40(3), pp.448-455.

[DUN 2000]

Duncan, J.S. & Ayache, N. (2000). "Medical image analysis: progress over two decades and the challenges ahead," IEEE Transactions on Pattern and Machine Intelligence, 22(1), pp.58-106.

[DUN 2001]

Dunn, M.J., Gorg, A. (2001) "From protein sequence to function", In S.R. Pennington, M. J. Dunn (Eds.) *Proteomics,* BIOS Scientific Publishers, Oxford, pp.43-63, 2001.

[EDW 1995]

Edwards, P.J., Hawkes, D.J., Hill, D.L.G., Jewell, D., Spink, R., Strong, A., & Gleeson, M. (1995). "Augmented reality in the stereo operating microscope for otolaryngology and neurosurgical guidance," Medical robotics and computer assisted surgery, pp.8-15. Wiley.

[FIT 2001]

Fitzpatrick, J.M. (2001). "Detecting failure, assessing success," In Hajnal, J.V., Hill, D.L.G., & Hawkes, D.J.E. (Eds.), Medical Image Registration, (pp. 117-139). CRC Press.

[FIT 2000]

Fitzpatrick, J.M., Hill, D.L.G. & Maurer, C.R. (2000). Handbook of medical imaging, (pp. 375-435). Bellingham, WA: SPIE Press.

[FIT 1998]

Fitzpatrick, J.M., West, J. B. & Maurer, C. R. (1998). "Predicting error in rigid-body point-based registration," IEEE Trans. Med. Imag., 17, pp.694-702, 1998.

[GEF 2004]

Gefen, S., Tretiak, O., Bertrand, L., Rosen, G. D. and Nissanov, J. (2004) "Surface alignment of an elastic body using a multiresolution wavelet representation," IEEE Transactions on Biomedical Engineering, vol. 51, no. 7, pp.1230-1241, July 2004.

[GRI 1995]

Grimson, W.E.L. (1995). "Medical applications of image understanding," IEEE Expert, pp.18-28.

[GUÉ 1993]

Guéziec, A. (1993). "Large deformable splines, crest lines and matching," International conference on computer vision, pp.650-653. Los Alamitos, CA: IEEE computer society press.

[GUÉ 1992]

Guéziec, A. & Ayache, N. (1992). "Smoothing and matching of 3-D space curves," In Robb, R.A. (Ed.), Visualization in Biomedical Computing, 1808, Proc. SPIE, (pp. 259-273). Bellingham, WA: SPIE PRESS.

[HAJ 1995]

Hajnal, J., Saeed, N., Soar, E., Oatridge, A., Young, I., & Bydder, G.(1995). "Detection of subtle brain changes using subvoxel registration and subtraction of serial MR images," J. Comput. Assist. Tomogr., 19(5), pp. 677-691.

[HAN 2003]

Handels, H. (2003). "Medical image processing: new perspectives in computer supported diagnostics, computer aided surgery and medical education and training," Year Book of Medical Informatics, pp.503-505.

[HEI 1997]

Heieh, J. W., Liao, H. Y. M., Fan, K.C., Ko, M. T. and Hung, Y. P. (1997) "Image registration using a new edge-based approach," Computer Vision and Image Understanding, vol. 67, no. 2, August, pp. 112-130, 1997.

[HEL 2001]

Hellier, P., Barillot, C., Memin, E., & Perez, P. (2001). "Hierarchical estimation of a dense deformation field for 3-d robust registration," IEEE Transactions on Medical Imaging, 20, pp.388-402.

[HIL 2001]

Hill, D. L. G., Batchelor, P. G., Holden, M. H. & Hawkes, D. J. (2001). "Medical image registration," Phys. Med. Biol., 46(1), pp.1-45.

[HIL 2000]

Hill, D. L. G. et al. (2000). "Sources of error in comparing functional magnetic resonance imaging and invasive electrophysiology recordings," Journal of Neurosurgery, 93, pp.214-223.

[HIL 1998]

Hill, D. L. G. et al. (1998). "Measurement of intraoperative brain surface deformation under a craniotomy," Neurosurgery, 43, pp. 514-528.

[HIL 1993]

Hill, D. L. G., Hawkes, D. J., Haarison, N. A. & Ruff, C.F. (1993). "A strategy for automated multimodality image registration incorporating anatomical knowledge and imager characteristics," Proc. 13th int. Conf. Information Processing in Medical Imaging; In Barrett, H. H. and Gmitro, A. F. (Eds.), Lecture Notes in Computer Science, (pp. 182-196). New York: Springer-Verlag.

[HOH 1993]

Hoh, C.K., Dahlbom, M., Haaris, G., Choi, Y., et al. (1993). "Automated iterative three-dimensional registration of positron emission tomography images," J. Nucl. Med., 34(11), pp.2009-2018.

[HOL 2000]

Holden, M. et al. (2000). "Voxel similarity measures for 3d serial MR image registration," IEEE Transactions on Medical Imaging, 19, pp.94-102.

[HTTP]

http://kr.expasy.org.

[KAP 1999]

Kapoutsis, C. A., Vavoulidis, C. P. and Pitas, I. (1999) "Morphological Iterative Closest Algorithm," IEEE Transactions on Image Processing, vol. 8, no. 11, Nov 1999.

[KAS 1988]

Kass, M., Witkin, A., & Terzopoulos, D. (1988). "Snakes: active contour models," Int. J. Comp. Vision, pp.321-331.

[KIM 1997]

Kim, B., Boes, J.L., Frey, K.A., & Meyer C.R. (1997). "Mutual information for automated unwarping of rat brain autoradiographs," NeuroImage, 5, pp.31-40.

[KIN 2004] King, P., S. Mitra and B. Nutter. (2004). An Automated, Segmentation-Based, Rigid Registration System For Cervigram/Spl Trade/ Images Utilizing Simple Clustering and Active Contour Techniques. 17th IEEE Symposium on Computer-Based Medical Systems. Proceedings. pp. 292-297.

[KOV 1998] Kovacic, S., and Bajcsy, R. "Multiscale/Multiresolution Representation," Brain Warping, W. Toga, ed., pp. 45-65, Academic Press, 1998.

[LEE 2003] Lee, Z., Nagano, K.K., Duerk, J.L., Sodee, D.B., & Wilson, D.L. (2003). "Automatic registration of MR and SPECT images for treatment planning in prostate cancer," Acad. Rodiol, 10, pp.673-684.

[LEH 1999] Lehmann, T.M., Gönner, C., & Spitzer, K. (1999). "Survey: interpolation methods in medical image processing," IEEE Transactions on Medical Imaging, 18(11), pp.1049-1075.

[LES 1999] Lester, H. & Arridge, S.R. (1999)."A survey of hierarchical non-linear medical image registration," Pattern Recognition 32, pp.129-149.

[LIA 1996]

Liang J. and Parks, T. W. (1996). "A translation-invariant wavelet representation algorithm with applications," IEEE Trans. Signal Processing, vol. 44, pp. 225-232, Feb. 1996.

[LIK 2001]

Likar, B. & Pernus, F. (2001). "A Hierarchical Approach to Elastic Registration Based on Mutual Information," Image and Vision Computing 19, pp.33-44.

[LIN 1994]

Lin, K. P. & Huang, S. C. et al. (1994). "A general technique for interstudy registration of multifunction and multimodality images," IEEE Trans. Nucl. Sci., 41, pp.2850-2855.

[MAE 1997]

Maes, F., Collignon, A., Vandermeulen, D., Marchal, G. & Suetens, P. (1997). "Multimodality image registration by maximisation of mutual information," IEEE Transaction on Medical Imaging, 6(2), pp.187-198.

[MAE 1999]

Maes, F., Vandermeulen, D. & Suetens, P. (1999). "Comparitive evaluation of multiresolution optimisation strategies for multimodality image registration by maximisation of mutual information," Medical Image Analysis, 3(4), pp.373-386

[MÄK 2002]

Mäkelä, T., Clarysse, P., Sipilä, O., Pauna, N., Pham, Q.C., Katila, T. & Magnin, I.E. (2002). "A review of cardiac image registration methods," IEEE Transaction on Medical Imaging, 21(9), pp.1011-1021

[MAI 1996]

Maintz, J.B.A., van den Elsen, P.A. & Viergever, M.A. (1996). "Evaluation of ridge seeking operators for multimodality medical image registration," IEEE Trans, PAMI, 18(4), pp.353-365.

[MAI 1998]

Maintz, J.B.A. & Viergever, M.A. (1998). "A Survey of Medical Image Registration," Medical Image Analysis, vol. 2(1), pp.1-36.

[MAL[1] 1989]

Mallat, S. (1989) "A theory of multiresolution signal decomposition: The wavelet representation," IEEE trans. Pattern Anal. Machine Intell., vol. PAMI-11, pp. 674-693, 1989.

[MAL 1989]

Mallat, S. (1989) "Multiresolution approximations and wavelet orthonormal bases of Ĺ(R)," Trans. Amer. Math. Soc., vol.315, no.1, pp.69-87, 1989.

[MAL 1998]

Mallat, S. (1998) "A Wavelet Tour of Signal Processing," Academic Press, San Diego, 1998.

[MAL[1] 1992]

Mallat, S. and Hwang, W. L. (1992) "Singularity detection and processing with wavelets," IEEE Trans. Inform Theory. 38: 617-643, 1992.

[MAL 1992]

Mallat, S. and Zhong, S. (1992) "Characterization of Signal from Multiscale Edges," IEEE Transactions on Pattern Analysis and Machine Intelligence, Vol.14, no. 7, pp. 710-732, July 1992.

[MAU 1995]

Maurer, C.R., Aboutanos, G.B., Dawant, B.M., Gadamsetty, S., Margolin, R.A., Maciunas, R.J., & Fitzpareick, J.M. (1995). "Registration of CT and MR images using a combination of points and surfaces," In Loew, M.H. (Ed.), Medical imaging: image processing, 2434, pp.109-123, Bellingham, WA: SPIE Press.

[MAU 1993]

Maurer, C. R. & Fitzpatrick, J. M. (1993)."A review of medical image registration," In Maciunas, R. J. (Ed.), Interactive Image guided Neurosurgery, 17-44. Parkridge, IL: American Association of Neurological Surgeons.

[MAU 1998]

Maurer, C. R., Maciunas R. J., & Fitzpatrick, J. M. (1998). "Registration of head CT images to physical space using a weighted combination of points and surfaces," IEEE Trans. Med. Imaging 17, pp.753-761.

[MCI 1995]

McInterney, T. & Terzopoulous, D. (1995). "A dynamic finite element surface model for segmentation and tracking in multidimensional medical images with application to cardiac 4D image analysis," J. Comp. Med. Imag. & Graph., 19(1), pp.69-83.

[MCL 2002]

McLeish, K., Hill, D.J.G., Atkinson, D., Blackall, J.M., & Razavi, Reza. (2002). "A study of motion and deformation of the heart due to respiration," IEEE Transactions on Medical Imaging, 21(9), pp.1142-1150.

[NEL 1965]

Nelder, J.& Mead, R.A. (1965). "A simplex method for function minimization," Comp. J., 17, pp.308-313.

[NIX 2002]

Nixon, M. and A. Aguado. (2002). "Feature Extraction and Image Processing," Elsevier Newnes. Oxford.

[O'CO 1998]

O'Connor, M.K., Kanal, K.M., Gebhard, M.W., & Rossman, P.J. (1998). "Comparison of four motion correction techniques in SPECT imaging of the heart: a cardiac phantom study," J. Nucl. Med., 39, pp.2027-2034.

[PAL 1995]

Pallotta, S. et al. (1995). "Application of a surface matching image registration technique to the correlation of cardiac studies in positron emission tomography by transmission images," Phys. Med. Biol., 40, pp.1695-1708.

[PEL 1989]

Pellizari, C.A., Chen, G.T.Y., Spelbring, D.R., Weichselbaum, R.R., & Chen, C.T. (1989). "Accurate three-dimensional registration of CT, PET, and/or MR images of the brain," Computer assisted tomography, 13(1), pp.20-26.

[PEN 1998]

Penny, G.P., Weese, J., Little, J.A., Desmedt, P., Hill, D.L.G., & Hawkes, D.J. (1998). "A comparison of similarity measures for use in 2D-3D medical image registration," IEEE Transactions on Medical Imaging, 17, pp.586-595.

[PIE 2000]

Pielot, R., M. Scholz, K. Obermayer, E. D. Gundelfinger and A. Hess. (2000). "Warping with Optimized Weighting Factors of Displacement Vectors - A New Method to Reduce Inter-individual Variations in Brain Imaging," Proceedings of the 4th IEEE Southwest Symposium Image Analysis and Interpretation. pp. 264 - 268.

[PLU 2001]

Pluim, J.P.W., Maintz, J.B.A., & Viergever, M.A. (2001). "Mutual information matching in multiresolution contexts," Image and Vision Computing, 19(1-2), pp.45-52.

[POW 1964]

Powell, M.J.D. (1964). "An efficient method for finding the minimum of a function of several variables without calculating derivatives," Comput.J., 7, pp.155-163.

[RIV 2003]

Riva, G. (2003). "Review paper: medical applications of virtual environments," Year Book of Medical Informatics, pp.159-169.

[ROH 2000]

Roche, A., Malandain, G., & Ayache, N. (2000). "Unifying maximum likelihood approaches in medical image registration," International Journal of Imaging Systems and Technology, 11, pp.71-80.

[ROH 1998]

Rohr, K. (1998). "Image Registration Based on Thin-plate Splines and Local Estimates of Anisotropic Landmark Localization Uncertainties," Proc. MICCAI'98, LNCS 1496, pp.1174-1183. Springer-Verlag.

[ROH 2000]

Rohr, K. (2000). "Elastic Registration of Multimodal medical images: A Survey," Auszug aus: Kunstliche Intelligenz, Heft, pp.11-17.

[ROH 2003]

Rohlfing, T. & Maurer, C.C. (2003). "Nonrigid image registration in shared-memory multiprocessor environments with application to brains, breasts, and bees," IEEE Transactions on Information Technology in Biomedicine, 7(1), pp.16-25.

[ROS 1998]

Rosenman, J.G., Miller, E.P., Tracton, G., & Cullip, T.J. (1998). "Image registration: an essential part of radiation therapy treatment planning," International Journal of Radiation Oncology, Biology, Physics, 40, pp.197-205.

[RUB 1996]

Rubinstein, R., Karger, H., Pietrzyk, U., Siegal, T., Gomori, J.M., & Chisin, R., (1996). "Use of 201 thallium brain SPECT, image registration, and semi-quantitative analysis in the follow-up of brain tumors," European journal of radiology, 21, pp.188-195.

[SAM 2001]

Samani, A., Bishop, J., Yatte, M.J., & Plewes, D.B. (2001). "Biomechanical 3-D finite element modeling of the human breast using MRI data," IEEE Transactions on Medical Imaging, 20(4), pp.271-279.

[SIM 1992]

Simoncelli, E. P., Freeman, W. T., Adelson, E. H. and Heeger, D. J. (1992) "Shiftable multiscale transforms," IEEE Trans. Inform. Theory, vol. 38, pp. 587-607, Feb. 1992.

[SUB 1999]

Subsol, G. (1999). "Crest lines for curve-based warping," Brain Warping, (pp.241–262). San Diego, CA: Academic.

[SUB 1998]

Subsol, G., Thirion, J.-P., & Ayache, N. (1998). "A scheme for automatically building three-dimensional morphometric anatomical atlases: application to a skull atlas," Medical Image Analysis, 2(1), pp.37-60

[TEZ 1991]

Terzopoulos, D. & Metaxas, D. (1991). "Dynamic 3D models with local and global deformations: deformable superquadrics," IEEE Trans. PAMI, 13(7), pp.703-714.

[THÉ [1] 2000]

Thévenaz P., Blu, T., & Unser, M. (2000). "Image interpolation and resampling," In Bankman, I. (Ed.). Handbook of medical imaging: processing and analysis, (pp. 393-418) Academic Press.

[THÉ 2000]

Thévenaz P. & Unser, M. (2000). "Optimization of mutual information for multiresolution registration," IEEE Transaction on Image Processing, 9(12), pp.2083-2099.

[THI 1996]

Thirion, J.P. (1996)."New feature points based on geometric invariants for 3D image registration," International journal of computer vision, 18(2), pp.121-137.

[THI 1998] Thirion, J.P. (1998). "Image matching as a diffusion process: An analogy with Maxwell's demons," Med. Image Anal., 2, pp.243–260.

[THO 1996] Thompson P. & Toga, A.W. (1996). "A surface-based technique for warping three-dimensional images of the brain," IEEE Transaction on Medical Imaging, 15(4), pp.402-417.

[TSA 2002] Tsai D. and Chiang, C. (2002) "Rotation-invariant pattern matching using wavelet decomposition," Patter Recogn. Lett., vol.23, pp.191-201, 2002.

[TUR 2000] Turner, R. & Ordidge, R.J. (2000). "Technical challenges of functional magnetic resonance imaging: the biophysics and technology behind a reliable neuroscientific tool for mapping the human brain," IEEE Engineering in Medicine and Biology, 42-54.

[UME 1991] Umeyama, S. (1991) "Least-squares of transformation parameters between two point patterns," IEEE Transactions on Pattern Analysis and Machine Intelligence, vol. 13, No. 4, pp.376-380, April 1991.

[UNS 2003]

Unser, M., Aldroubi, A., and Laine, A. (2003) "Guest Editorial: Wavelets in Medical Imaging," IEEE Transactions on Medical Imaging, vol. 22, no. 3, pp. 285-288, March 2003

[VAN 1993]

van den Elsen, P. A., Pol, E.J.D. & Viergever, M.A. (1993). "Medical Image matching— a Review with classification," IEEE Eng.Med.Biol., 12, pp.26-39.

[VAN 1995]

van den Elsen, P.A. Mainze, P.B.A, Pol, E.J.D. & Viergever, M.A. (1995). "Automatic registration of CT and MR brain images using correlation of geometric features," IEEE Transactions on medical images, 14(2), pp.384-398.

[VAN 1994]

van Herk, M.& Kooy, H.M. (1994). "Automatic three-dimensional correlation of CT-CT, CT-MRI, and CT-SPECT using chamfer matching," Medical Physics, 21(7), pp.1163-1177.

[VES 2001]

Veeser, S., Dunn M.J., and Yang G-Z. (2001). "Multiresolution image registration for two_dimensional gel electrophoresis," Proteomics 2001, 1, pp.865-870.

[VIO 1995]

Viola P. & Wells, W.M. (1995). "Alignment by maximization of mutual information," 5th International Conference on Computer Vision, pp.16-23.

[WAN 2001]

Wang, H.S., Feng, D., Yeh, E., and Huang, S. C. (2001). "Objective assessment of image registration results using statistical confidence intervals," IEEE Transactions on Nuclear Science, 48, pp.106-110.

[WEL 1996]

Wells W. M., Viola, P., Atsumi, H., Nakajima, S., & Kikinis, R. (1996). "Multi-modal volume registration by maximization of mutual information," Med. Image Anal., 1(1), pp.35–51.

[WON 1995]

Wong, S., Knowlton, R., Chew, M., & Huang, H. (1995). "Integrating multidimensional imaging, multimodality registration, and multimedia database for epilepsy diagnosis," SPIE-Med. Imag., pp.2431

[WOO 2000]

Woods, R.P. (2000). "Validation of registration accuracy," In Bankman, I. (Ed.). Handbook of medical imaging: processing and analysis, (pp. 491-497). Academic Press.

[WOO 1998]

Woods, R.P., Grafton, S.T., Cherry, S.R., & Mazziotta, J.C. (1998). "Automated image registration: I.General methods and intrasubject, intramodality validation," J.Comp. Assist. Tomogr., 22(1), pp.139-152.

[WOO 1993]

Woods, R.P., Mazziotta, J.C. & Cherry, S.R. (1993). "MRI-PET registration with automated algorithm," J.Comp. Assist. Tomogr., 19(4), pp.536-546.

[XIA 1995]

Xiao, H. & Jackson, I.T. (1995). "Surface matching: application in poat-surgical/post-treatment evaluation," In Lemke, H.U., Inamura, K., Jaffe, C.C., & Vannier, M.W. (Eds.), Computer assisted radiology, (pp. 804-811). Berlin: Springer-Verlag.

[XU 1998]

Xu, C. and Prince, J. (1998). "Snakes, shapes, and gradient vector flow," IEEE Trans. Image Processing, vol.7, pp. 359-369, Mar. 1998.

[XUE 2004]

Xue, Z., Shen, D. and Davatzikos, C. (2004) "Determining correspondence in 3-D MR brain images using attribute vectors as morphological signatures of voxels," IEEE Transactions on Medical Imaging, vol. 23, no.10, pp. 1276-1291, Dec. 2004.

[YOU 2000]

You, J. and Bhattacharya, P. (2000) "A wavelet-based coarse-to-fine image matching scheme in a parallel virtual machine environment," IEEE Transactions on Image Processing, vol. 9, no. 9, pp.1547-1559, Sep. 2000.

[ZIT 2003]

Zitová, B. & Flusser, J. (2003). "Image registration methods: a survey," Image and Vision Computing, 21, pp.977-1000.

[ZHU 2002]

Zhu, Y. M. (2002). "Volume image registration by cross-entropy optimization," IEEE Transactions on Medical Imaging, 21(2), pp.174-180.